

REAL-TIME MOTION CAPTURE FOR ANALYSIS AND PRESENTATION WITHIN VIRTUAL ENVIRONMENTS

ANDREW BROWNRIDGE

A thesis submitted in partial fulfilment of the requirements of
the Manchester Metropolitan University for
the degree of Doctor of Philosophy

Department of Engineering & Technology
School of Engineering
the Manchester Metropolitan University

June 2014

Table of Contents

Abstract.....	iii
Declaration.....	iv
Acknowledgements.....	v
List of Figures	vi
Nomenclature and Abbreviations	x
1 Introduction to Thesis	1
1.1 Aim	2
1.2 Objectives.....	2
1.3 Context.....	3
1.4 Overview of Thesis	3
2 An Introduction to Motion Capture	6
2.1 Overview of Motion Capture	6
2.2 Motion Capture Methods	7
2.3 Motion Capture in the Performing Arts.....	9
2.4 Motion Analysis and Performance Development.....	10
2.5 Summary	12
3 Corrective Coaching	13
3.1 Stages of Learning	13
3.2 The Role of Feedback.....	14
3.3 Frequency of Feedback	16
3.4 The Guidance Hypothesis	18
3.5 Presentation of Feedback	20
3.6 Biomechanics	21
3.6.1 Qualitative Analysis.....	21
3.6.2 Quantitative Analysis	22
3.6.3 Predictive Analysis Method	24
3.7 Conclusion.....	24
3.8 Summary	24
4 Measurement of Human Motion in Performance	25
4.1 Experimental Motion Capture Process	25
4.1.1 Recording General Ballet Movements with Motion Capture Equipment.....	27

4.1.2	Motion Capture Recording of Fault Conditions in Ballet	30
4.2	Results and Discussion of Motion Capture for Analysis of Ballet Movement and Gestures	33
4.3	Summary	44
5	Augmented Performance.....	45
5.1	The Uncanny Valley.....	45
5.2	Application of Motion Data to a Character Avatar	46
5.3	Results and Discussion of Virtual Character Animation.....	49
5.4	Summary	52
6	Body Scanning	53
6.1	Scanning Process.....	53
6.2	Constructing a Polygonal Mesh from the Scan Data	55
6.3	Rigging the Character for Animation	60
6.4	Animating the Character	65
6.5	Conclusion.....	66
6.6	Summary	67
7	Analysis of Recorded Character Motion	68
7.1	Matrix Composition in Maya.....	68
7.2	Rotations and Matrices	70
7.3	Summary	75
8	Fault Analysis and Isolation.....	76
8.1	Methods	76
8.2	Results from Direct Analysis of Motion Data	83
8.3	Discussion on Direct Analysis of Motion Data	88
8.4	Results and Discussion of Analysis with Avatar Application	93
8.5	Summary	98
9	Conclusion of Thesis and Contribution to Knowledge	99
9.1	Further Work and Application	100
10	References	102
11	Appendices.....	111
11.1	Vectors	111
11.2	Matrices	114

Abstract

This thesis describes motion capture methods with an application for real-time recording of extreme human movement. A wireless gyroscopic sensor based system is used to record and evaluate misalignments in ankle position of ballet dancers in a performance environment. Anatomic alignment has been shown to contribute to dance related injuries, and results of this work show that subtle variations in joint rotation can be clearly measured. The workflow has been developed to extract performance analysis data for fault detection in order to assist augmented feedback methods for the prevention of injury and improved performance. Infra-red depth sensing technology, commonly used in garment design, has been used to produce a representation of a scanned human subject and a workflow established to utilise this character avatar for animation using motion capture data. The process of presenting a visually acceptable representation of an overall performance in addition to the numerical evaluation of specific joint orientation provides a significant contribution to knowledge.

Declaration

No portion of the work referred to in this thesis has been submitted in support of an application for another degree or qualification at this, or any other university, or institute of learning.

Date: _____

Signed: _____

Acknowledgements

I would like to thank Dr. Peter Twigg, my director of studies, for his invaluable support and direction throughout the whole of my studies. I would also like to thank Prof. Steve Hawley for his contribution to the exposure of my work, Dr. Stephen Sigurnjak for his technical guidance, and Dr. Simeon Gill for allowing the time and assistance with use of the body scanner.

Thanks also go to The Northern Ballet School and the dancers who offered their time and expertise to the research and Leona Wing Yee So for her patience through gesture demonstrations.

Lastly, I would like to thank my partner, family and friends for their faith, encouragement and patience during my research.

List of Figures

4.1	Male dancer from the Northern Ballet School - front profile in calibration cube
4.2	Female dancer from the Northern Ballet School - front profile in calibration cube
4.3	Female dancer from the Northern Ballet School – performing in studio wearing IGS-190 motion capture suit
4.4	Real-time representation of female dancer from the Northern Ballet School – performing in studio
4.5	Gesture of relevé – First position
4.6	Gesture of relevé – Demi-pointe
4.7	Gesture of relevé – en Pointe
4.8	Gesture of relevé – en Pointe – correct position
4.9	Gesture of relevé – en Pointe – exaggerated fault of sickle
4.10	Gesture of relevé – en Pointe – exaggerated fault of winged
4.11	Representation of male dancer from the Northern Ballet School – demonstrating motion fully leaving ground
4.12	fCurves close up of animation curve showing correct alignment on right foot whilst in demi-pointe
4.13	Full motion recording animation curve of rotation on X-axis from right foot whilst in demi-pointe
4.14	fCurves close up of animation curve showing exaggerated sickle alignment on right foot whilst in demi-pointe
4.15	Full motion recording animation curve of rotation on X-axis from right foot whilst in demi-pointe
4.16	fCurves close up of animation curve showing exaggerated winged alignment on right foot whilst in demi-pointe
4.17	Full motion recording animation curve of rotation on X-axis from right foot whilst in demi-pointe
4.18	fCurves close up of animation curve showing correct alignment on left foot whilst en pointe
4.19	fCurves close up of animation curve showing correct exaggerated sickle on right foot whilst en pointe

4.20	fCurves close up of animation curve showing correct exaggerated winged on right foot whilst en pointe
4.21	Comparison of full animation curves from previous three figures
4.22	fCurves close up of animation curve showing correct alignment on left foot whilst in first position
4.23	fCurves close up of animation curve showing correct exaggerated sickle on right foot whilst in first position
4.24	fCurves close up of animation curve showing correct exaggerated winged on left foot whilst in first position
4.25	Comparison of full animation curves from previous three figures
4.26	Human subject demonstrating first position
4.27	Human subject demonstrating demi-pointe
4.28	Human subject demonstrating en pointe
4.29	Virtual representation of human subject demonstrating first position
4.30	Virtual representation of human subject demonstrating demi-pointe
4.31	Virtual representation of human subject demonstrating en pointe
5.1	Curve of emotional response demonstrating the uncanny valley
5.2	Virtual character animated using motion data within a virtual environment
5.3	Knight model to be used for character animation
5.4	Virtual character animated using motion data within a virtual environment
5.5	Photograph taken at the 'Possession' exhibition at Bangkok Art and Culture Centre
6.1	Comparison of six subjects all classified as size 12
6.2	Visual output of .bin and .rdb scan files
6.3	MeshLab .wrl file import
6.4	MeshLab .obj file import
6.5	ZBrush import of MeshLab converted .wrl to .obj file
6.6	ZBrush import of scan software output .obj file
6.7	Separated parts of the combined mesh
6.8	Accompanying UV layout of the face
6.9	Character with skeletal hierarchical system of joints
6.10	Script output placing locators at joint positions specified by the scan measurements

6.11	Script output placing joints at joint positions specified by the scan measurements
6.12	Script output placing joints at joint positions specified by the scan measurements with 'clear selection' applied after each joint placement
6.13	Demonstration of default skin weighting
6.14	Demonstration after adjusted skin weighting
6.15	Character avatar animated using motion capture data
7.1	Visual description of perpendicular axes and planes
7.2	Visual description of the 'dot product' of two vectors
7.3	Example of object axes compared to world axes when rotated 90° around the Y-axis
8.1	Hierarchical joint nodes placed from .bvh file in MotionBuilder schematic view
8.2	Hierarchical joint nodes placed from .bvh file in MotionBuilder perspective view
8.3	Direct .fbx file import to Maya
8.4	Joint display when converted to decimetres on .fbx file import to Maya
8.5	Adjusted joint display: Scale 0.1; Joint Radius 0.3
8.6	'Create Reference Node' option in MotionBuilder
8.7	Visualisation of Local rotation axis in Maya
8.8	Default local rotation axis orientation on joint creation
8.9	Maya graph editor showing animation curves for X, Y and Z axis rotation values for the right foot joint
8.10	Example alignment of lower leg joints
8.11	Example misalignment of lower leg joints
8.12	Motion data example of misalignment on Z-axis
8.13	Fault in foot alignment shown on the Z-axis rotation
8.14	Comparison of full animation curves from Z-axis Euler angle rotation values of the right foot joint in correct position, exaggerated sickle and exaggerated winged whilst in first position
8.15	Comparison of full animation curves from Z-axis Euler angle rotation values of the left foot joint in correct position, exaggerated sickle and exaggerated winged whilst in first position
8.16	Comparison of full animation curves from Z-axis Euler angle rotation values

	of the right foot joint in correct position, exaggerated sickle and exaggerated winged whilst in demi-pointe
8.17	Comparison of full animation curves from Z-axis Euler angle rotation values of the left foot joint in correct position, exaggerated sickle and exaggerated winged whilst in demi-pointe
8.18	Comparison of full animation curves from Z-axis Euler angle rotation values of the right foot joint in correct position, exaggerated sickle and exaggerated winged whilst en pointe
8.19	Comparison of full animation curves from Z-axis Euler angle rotation values of the left foot joint in correct position, exaggerated sickle and exaggerated winged whilst en pointe
8.20	Full body visualisation of the demonstration of en-pointe in 'correct' position
8.21	The default local axis orientation for the skeleton created for the avatar rig
8.22	The result of the script aligning local rotation axes to world axes
8.23	The result of the process aligning local rotation axes so that the Y-axis of the horizontal joint chains point upwards, and the Z-axis of the vertical joint chains point to the side of the character

Nomenclature and Abbreviations

.bin	File type associated with depth sensing information
.bvh	File type associated with motion capture data
.fbx	File type associated with three dimensional modelling applications
.obj	File type associated with object meshes in 3D modelling applications
.rbd	File type associated with point cloud data
.wrl	File type associated with point cloud data
3D	Three Dimensional
Animation curve	The graphical representation of a value over time of an attribute associated with animation
Avatar	An incarnation, embodiment, or manifestation of a person or idea
Calibration cube	Cube used to calculate limb length of a subject to be recorded using the IGS-190 motion capture suit
Euler angles	Three angles introduced by Leonhard Euler to describe the orientation of a rigid body
fCurves	Animation curve editor in Autodesk's MotionBuilder software
First position	The legs are externally rotated, and heels are together
IGS-190	Inertial Gyroscopic System motion capture suit by Animazoo
Local space	Uses the origin and axes of the object's parent node in the hierarchy of objects
Mesh	Surface made up of polygons
Node	Object within Autodesk's Maya that stores configurable characteristic information from the dependency graph database
Perpendicular	At an angle of 90° to a given line, plane, or surface
Perspective	Three dimensional view showing everything within the scene
Pointe	Position of the foot in which the dancer stands on the toes
Polygon	A plane determined by a closed loop of edges
Relevé	A rise or spring onto the toes (demi- or full pointe)
Rig	Hierarchical set of interconnected bones used to animate an object mesh
Schematic	Two dimensional view omitting details not relevant to the view
Script	A program written for a special runtime environment that can interpret and automate the execution of tasks which could alternatively be executed

	one-by-one by a human operator
Sickle	The turning of the foot inward (inversion)
Skin weighting	The process of determining the amount a vertex will be affected by a joint bound to the mesh
UV	Axes used to map a three dimensional model to a two dimensional representation
Vertex	A point that describes the corner or intersection of a geometric shape
Winged	The turning of the foot outward (eversion)
World space	The coordinate system for the entire scene

1 Introduction to Thesis

Work presented within this thesis has contributed to the following publications:

BROWNRIDGE, A. 2011. *Chapter 21*, [video] 'The Anthony Burgess Archive' exhibition. Manchester: International Anthony Burgess Foundation, 9 June.

HAWLEY, S., TWIGG, P. & BROWNRIDGE, A. 2011. Motion Capture: Art, Technology & Collaboration. *Consortium on Applied Research and Professional Education*. Utrecht, NL: CARPE.

BROWNRIDGE, A., TWIGG, P. & SIGURNJAK, S. 2013. Measurement of Human Motion in Performance. *The Journal of the Institute of Measurement and Control*, 46 (1), 21-25

BROWNRIDGE, A. 2013. *Actor*, [video] 'Possession' exhibition. Bangkok: Bangkok Arts and Cultural Centre, 14 March – 26 May.

BROWNRIDGE, A., TWIGG, P. 2014. Body Scanning for Avatar Production and Animation. *International Journal of Fashion Design, Technology and Education*, 7 (2). *In press*.

This thesis describes motion capture methods with an application for real-time recording of extreme movement, performance analysis, and reproduction within a virtual environment. A wireless gyroscopic sensor based system is used to record the extreme human movements of ballet dancers in order to establish a suitable workflow to investigate the detection of misalignments in ankle position. Anatomic alignment, poor training and technical errors have been shown to be contributing factors to dance related injuries. Results from work presented here show that subtle variations in joint rotation can be clearly measured and could be used to develop fault detection and isolation possibilities for injury prevention and improved performance.

It is anticipated that the end user of such analytical applications would not be of a technical discipline such as engineering, and instead would be a performer or a coach. Work presented in this thesis describes a workflow developed to produce a visually acceptable representation of a subject that can be used to visualise a performance through the animation of a realistic virtual human using motion capture technologies. Infra-red depth sensing technology, commonly used in garment design, is used to produce a representative avatar of a scanned human subject. Several methods of constructing a clean polygonal character mesh from the scan data are investigated and discussed. The preparation of the resulting character mesh for

animation involves rigging techniques, such as a skeletal hierarchy and skin weighting, used within 3D animation and are optimised using Python scripts developed for this specific task. It is established that measurement data extracted by software that accompanies the body scanner can be used to place joints and assist the rigging process.

A process for the visual analysis of an overall performance in addition to the numerical evaluation of specific joint orientation has been proposed and validated in order to deliver augmented feedback to a performer.

1.1 Aim

The aim of this work is to deliver visual and technical augmented feedback within a virtual environment of a performance using analysis of real-time motion capture data.

1.2 Objectives

- Review recent motion capture technologies and their use within performance.
- Review augmented feedback theories and the use of technology to present feedback.
- Test and evaluate sensor based motion capture equipment for extreme movement, such as performed in ballet.
- Test, evaluate and develop data capture workflow for real-time recording and presentation of motion capture data.
- Investigate the suitability of the skeleton rig for application by the BVH file (format recorded by motion capture processes) and consider alternatives to the basic hierarchy.
- Investigate the analysis of rotation values of specific joints which are associated with dance related injury.
- Explore the theory of the 'uncanny valley' in terms of modelled human motion by application of unadulterated motion data to a virtual character.
- Examine the use of depth sensing technology to produce a character avatar.
- Evaluate the suitability of a character avatar representative of a human subject for animation using a retarget workflow of motion capture data.
- Determine the necessary mathematical techniques involved in order to extract accurate and readable numerical analysis of motion capture data.
- Establish a method of presenting pertinent and valuable augmented feedback to a performer encouraging improved performance and injury prevention.

1.3 Context

Currently, motion capture is a technology heavily invested in by the film industry and has been used in the production of films such as Avatar, Happy Feet, Pirates of the Caribbean, A Christmas Carol, and Lord of the Rings. It is also a technology that is used in prosthetics such as artificial limb development, immersive environments such as video games, and biomechanics such as gait analysis.

Sensor based motion capture, whilst still in its infancy, is gaining popularity due to its increasing ability to free the user from constraints during performance, which have in the past been a concern with exoskeletal methods and cabling, and its ability to offer real time visualisation of the performance. Up until recently, sensor based motion capture data was not particularly useful due to the inaccuracies of the sensory system and the post processing required, meaning that it was not a real time solution. Latest developments such as the Animazoo IGS-190 have offered the ability to record accurate motion data in real time, and this is currently being taken advantage of through use in television and sporting applications.

Recent examples of how a sensor based system has been used include an interactive children's show at Europa Park, Germany, and The Dragon Tower experience at Warwick Castle, England. An example of motion capture used within sports is a project to analyse and adapt running technique in athletes which was part funded by the Swedish National Centre for Research in Sports (CIF). Motion capture technologies are also used to present augmented performance such as at Melbourne Ballet Company where movements are used to create 3D graphics.

Future planned developments in sensor based motion capture include collaboration between Animazoo and UbiSense, to integrate positional data through an ultra-wideband radio based system. Animazoo are also working with DynamiXYZ, a company providing facial motion capture, to deliver a more comprehensive motion capture system.

1.4 Overview of Thesis

Chapter 1

Chapter 1 highlights the contribution to knowledge through references to conference presentation, international exhibitions and journal publications. Further to this, it provides an introduction to the work and its context within current research and industry practice and gives an overview of the thesis by chapter.

Chapter 2

This chapter provides an introduction to the general area of motion capture and the technologies and methods used. Particular attention is given to the application of motion capture within the performing arts, motion analysis and performance development.

Chapter 3

This chapter introduces the theories of skill learning and retention and looks at the effect of feedback in the development of those skills. Technologies used to analyse a performance and present feedback are described.

Chapter 4

Work presented in this chapter analyses the IGS-190 motion capture suit to establish a suitable workflow for extreme human movements such as ballet. Results show that subtle variations in joint rotation can be clearly measured and could be used to develop fault detection and isolation possibilities for injury prevention and improved performance.

Chapter 5

Investigations were carried out to determine the level of comfort the viewer instinctively feels with the movement and form of what is presented. The phenomenon of the 'uncanny valley' was explored and exhibitions were presented to establish the perception of a wider audience.

Chapter 6

A workflow was developed, as described in this chapter, to produce a virtual character representative of a human subject for animation using motion capture. Different software and techniques were investigated to find the most efficient and appropriate method.

Chapter 7

This chapter provides an explanation of the necessary mathematical theories needed to analyse motion capture data for the purpose of error detection and performance development. A script is developed to convert the transformation matrices held in Maya to Euler angles that are more easily understood to an end user.

Chapter 8

The theories described in Chapter 7 are validated and used to determine whether the orientation of a movement is desirable. The level of fault, or misalignment, is extracted from the motion data and plotted in simple to read graphs.

Chapter 9

This final chapter concludes the thesis, outlining the contribution to knowledge and suggesting areas for future development of the research.

2 An Introduction to Motion Capture

For work presented here, it is proposed that motion capture techniques are used to record, classify and analyse human motion for specific applications within real-time virtual environments. The applications written here being for performance analysis and the prevention of injury resulting from extreme movement (Motta-Valencia, 2006) which is associated with sport and performing arts such as ballet (Hiller et al., 2004).

Through a review of current and past literature, the extent at which motion capture technologies are used, in which disciplines and to what purpose, shall be discussed. Problems that have been previously encountered and whether any resolutions have been made to these problems shall serve as a foundation to the methodologies and hypotheses, and the potential relationships between different areas of research shall be identified.

2.1 Overview of Motion Capture

Man has always had a compelling urge to make representations of the things he sees in the world around him (Thomas and Johnston, 1981). In the late 1800's, new inventions seemed at last to make it possible to capture that elusive spark of life (Beckerman, 2003). Eadweard Muybridge (Stillman and Muybridge, 1882) and Etienne-Jules Marey (Marey, 1879) conducted independent studies of human and animal motion by shooting multiple photographs of moving subjects over a short period of time, developing devices to graphically record locomotion and movement (Webster, 2005).

In the early 1900's, cartoonist Max Fleischer used this idea to create the rotoscope (Fleischer, 1917), which allowed animators to trace characters over photographs of live performers.

The second incarnation of performance animation in entertainment officially started in the mid 1980's, when Robert Abel used it to create 'Brilliance'. This commercial marked the birth of motion capture for animation in three dimensions (Menache, 2000). During the 1980's, mainstream character animation in 3D was born and 'Preview', by Wavefront Technologies, became the first commercially available package for computer animation (Waters, 2003).

Motion capture developed as a photogrammetric analysis tool in biomechanics research in the 1970s and 1980s (Orr and Shelton, 1997) and expanded into different industries as the technology matured.

The main markets that benefit from motion capture today are medicine (Corazza et al., 2006), sports (Ohgi, 2006), entertainment (Okada et al., 2006), and law/surveillance (Kiryati et al., 2008). There are smaller markets that are also taking advantage of the technology; for example, motion capture equipment is used to help design ergonomic environments (Ma et al., 2011). Additional uses include automobile safety tests where the motion of crash test dummies is captured and analysed (Rosenhahn et al., 2008).

2.2 Motion Capture Methods

There are a number of markets that benefit from motion capture technology for the recording of a person's movement. Within these markets, O'Rourke (2003) and Parent (2008) acknowledge two broad approaches that are commonly used.

The first approach uses *electromagnetic* sensors placed at the joints that transmit their positions and orientations back to a central processor where the motion is recorded or viewed. The sensors necessitate either cables or wireless transmission to communicate with the central processor. The former requires that the subject be 'tethered' with some kind of cabling harness, whereas the latter requires that the subject carries a power source such as a battery pack (Parent, 2008). The advantage of electromagnetic sensors is that the three-dimensional position and orientation of each sensor can be recorded and displayed in real time, regardless of posture of the actor. The drawbacks relate to the range of the electromagnetic field, the restricted movement of the subject resulting from the instrumentation required and the global positioning of the subject.

The second approach makes use of reflective markers to triangulate the 3D position of a subject between one or more cameras calibrated to provide overlapping projections. This *optical* approach requires no cables, so potentially permits greater freedom of movement within the studio range of the cameras for the actor. As a network of cameras determines the location of each marker, the global positioning of the subject is easily determined. Depending on the posture of the actor however, many of the reflective markers may be hidden from the view of some of the recording cameras and this occlusion can create problems in the acquisition of data (O'Rourke, 2003). A disadvantage of the optical approach is that it does not provide real-time feedback and the data can be error prone and noisy. Because orientation information is not directly generated, more markers are required than with magnetic trackers.

Beckerman (2003) goes further to split these two broad approaches into sub-categories. Electro-magnetic motion capture can include *mechanical exoskeletal systems* that directly

track body joint angles. These systems are typically rigid structures made up of metal or plastic rods linked together with potentiometers that articulate at the joints of the body. *Magnetic systems* on the other hand, calculate position and orientation by the relative magnetic flux of three orthogonal coils on both the transmitter and each receiver. The relative intensity of the voltage or current of the three coils allows these systems to calculate both range and orientation by meticulously mapping the tracking volume. The markers are not occluded by non-metallic objects but are susceptible to magnetic and electrical interference from metal objects and electrical sources in the environment that affect the magnetic field. *Inertial systems* are based on miniature inertial sensors, biomechanical models and sensor fusion algorithms. The motion data from the inertial sensors is often transmitted wirelessly to a computer where the motion is recorded or viewed. Most inertial systems use gyroscopes to measure rotational rates that are translated to joints of a skeleton in associated software. Inertial systems are capable of capturing the full six degrees of freedom of body motion in real-time (Beckerman, 2003).

Optical motion capture systems are generally defined by the way in which the markers are identified. *Passive optical systems* use markers coated with a retro-reflective material to reflect light back to the camera's lens. The markers are usually attached directly to the skin, or to a full body spandex/lycra suit designed specifically for motion capture. The camera's threshold can be adjusted so only the bright reflective markers will be sampled, ignoring skin and fabric. The centroid (geometric centre) of the marker is estimated as a position within the two-dimensional image that is captured. Providing two calibrated cameras see a marker, a three-dimensional fix can be obtained. Typically, a system will consist of around 6 to 24 cameras. *Active optical systems* triangulate a marker's relative position by illuminating multiple LEDs that are then identified through computer software. Rather than reflecting light back that is generated externally, the markers themselves are powered to emit their own light. Since Inverse Square law provides $1/4$ the power at 2 times the distance, this can increase the distances and volume available for capture since the light travelling from the active markers is half of the distance of that of the reflective markers. *Semi-passive imperceptible marker systems* do not specifically rely on an illumination device to be tracked; instead, they rely on tags with photo sensors to be detected. The traditional approach, based on high-speed cameras, can be reversed using specially built multi-LED infrared projectors to encode the space optically. Instead of retro-reflective or active LED markers, the system uses photosensitive marker tags to decode the optical signals. By attaching tags with photo sensors to scene points, the tags can compute not only their own locations of each point, but also their

own orientation, incident illumination and reflectance. These markers can be embedded within clothing as to track movement and can be unobtrusive to the wearer.

The type of motion capture system used in a study will essentially depend on a number of factors. The nature of the movement to be recorded and the requirements of the actor will have a significant influence on the choice of system. Considerations will be made to the size of the available capture volume, the effect of the equipment on the motion of the actor and the required accuracy of the joint orientations. The cost of the motion capture session will also have an important bearing on the choice of system used. What the initial budget for the project is, whether the project will be a one-off or the system will contribute to future projects and what return there will be on the investment, will all be factors that ultimately dictate the system choice.

2.3 Motion Capture in the Performing Arts

Meador (Meador et al., 2004) describes a cross-departmental project where it was attempted to deliver a public performance combining real-life performers on stage with virtual performers in a virtual environment driven by real-time motion capture. The Gypsy 3 electromechanical motion capture suit was used in this project, which utilises 43 potentiometers to record joint rotations. This particular suit utilises an exoskeleton and it was described that the range of motion was limited to a 50-foot radius using batteries, or 25 feet using corded A/C power.

It was described in the report that although there were advantages of the Gypsy suit, such as the cost, quick setup and portability, it did suffer from motion data drift, noise and limitation of the actor's motion due to the mechanics of the suit.

Motion drift was described as a constant problem and it was said that noise and jerkiness was often seen in the virtual character's performance. The report identifies the orientation trackers that make up the suit as the cause of the drift problem.

A similar investigation by John Haag (2009) using inertial motion capture technology for live performance identifies some very similar problems. Foot drop and foot slide are identified in this report, which relate closely to the 'drift' described in the previous investigation. Similarly, a problem with relative positioning is identified. He suggests that the accuracy of the data relies upon the accuracy of the actor measurements. Haag also suggests that "highly vigorous, acrobatic or contorted actions may not record accurately" and actions such as jumping and

climbing up stairs are difficult to record accurately. Similar to the investigation by Meador, Haag identifies the suit having significant amounts of hardware attached as being a problem. However, he describes this as a restriction for costuming rather than the motion of the actor. Haag does identify a number of positive outcomes from the investigation, some of which echo those identified by Meador. The portability and ease of set-up was mentioned, as was the ability to operate in real time. Another positive outcome that Haag describes is the range of the suit, which contradicts the problem that Meador encountered. Haag tells that he was able to operate over distances of up to 200 meters. The above authors also disagree on the complexity of the virtual environment that can be used within the performance. Meador claims that the production had a very two-dimensional feel to it and that the simplicity of the scene imagery lacked artistic depth. Haag argues that multiple characters, complex effects and elaborate 3D environments could be used.

In a similar investigation to Haag, a cross disciplinary group (Andreadis et al., 2010) produced a live performance against a virtual environment combining live actors with a virtual character driven by an actor using an inertial motion capture suit. The motion data was mapped to the digital character with Autodesk's MotionBuilder software. Like Haag and Meador, Andreadis describes the problem of lower positional accuracy and positional drift, which was compounded over time or due to electromagnetic interference. The positive outcomes of the investigation by Andreadis were that real time interaction between the avatar and real actors was achieved and they agreed with Haag that a complex virtual environment with visual effects was able to be created to enhance the live performance.

2.4 Motion Analysis and Performance Development

There have been a number of investigations into using motion capture technology to analyse and improve performance across a range of sports, the teaching of new motor skills and technique development.

Linden (Linden et al., 2011) describes a study conducted on novice violin players where vibrotactile feedback was given in real time. The feedback was based upon the player's bowing action compared to a target trajectory, where the deviation was deemed a fault. The motion data was recorded using inertial measurement units on an Animazoo Lycra jacket. The conclusions of the study were positive, as results suggest that the students who received the real-time feedback continued to show improved bowing technique when no longer receiving the feedback. The study group was small however (eight participants) and only consisted of six

sessions, therefore the effectiveness of the approach and its usability in a long term, real teaching setting is not known.

Aguinaldo (Aguinaldo and Chambers, 2009) uses an optical system to analyse the effects of valgus load on baseball pitching related elbow injury. The study shows that the pitching technique has a significant correlation with elbow valgus torque. Aguinaldo uses a much larger test group than Linden, analysing the throw of sixty-nine baseball pitchers. Due to the optical approach used, there is no real-time feedback. Techniques that appear to be associated with elbow injury resulting from elbow valgus torque are identified, however methods to minimise the effect are not.

Brodie (Brodie et al., 2008) uses a combination of 13 inertial sensors and a global positioning system to track the movement of an alpine ski racer. The purpose of the study is to provide useful design parameters to ski equipment engineers in order to reduce knee anterior cruciate ligament injuries and to provide a visual biomechanical analysis of an athlete, enhancing the experience of the television audience. It is stated that “the validity of the captured data is confirmed by agreement between computed kinematics presented in animated form and video images.” Like Aguinaldo, it is shown in the study that technique has an effect on performance, in this case the time taken to complete the course, although Brodie also describes the condition of the snow at differing times of day as an influence. As only two ‘runs’ were recorded in the investigation, both at different times of the same day, it is difficult to tell how much of an influence technique had on the performance. Brodie also fails to mention how the captured data might show a relationship with associated knee injury.

A study investigating training methods to reduce anterior cruciate ligament injury (ACL injury) in female athletes (Myer et al., 2006) made use of camera based motion capture technologies to test the effects of the balance and plyometric training on resultant lower limb kinematics. The setup (Motion Capture Corporation, California USA), similarly used and validated in an earlier study (McLean et al., 2003), consisted of eight high-speed Eagle cameras with each subject instrumented with 37 retro-reflective markers tracked using EVaRT software and an optimal capture volume was reported to be 4.5 x 2 x 2.5 metres. The study group consisted of eighteen 14-17 year old females after exclusions and reported significant changes in lower extremity coronal plane mechanics, resulting in the subjects landing with reduced valgus motion and subsequently reducing the risk of injury. The study reported that both training groups received feedback in different ways and as such it is difficult to determine to what extent training and feedback method had on the results.

2.5 Summary

This chapter indicates that there is a strong link between technique and the quality of a performance and injury resulting from poor technique. Results from work reviewed here shows that there is a desire to utilise motion capture technology to visualise and give feedback on movement in order to develop good technique and contribute to performance enhancement.

Researchers report that there are difficulties with existing methods of motion capture in the production of a visually pleasing performance; these difficulties are common and vary dependant on the technology used.

The review of literature indicates that development of motion capture methods to produce a visually acceptable representation of motion data in a virtual real-time environment, which can be used for the classification and analysis of human motion for performance analysis, would provide a clear contribution to knowledge.

3 Corrective Coaching

This chapter introduces the theories that underpin the learning of skills and the role in which feedback plays in the development of those skills. The frequency, timing, and presentation of feedback are shown to be important factors in the learning and retention rates of an observed skill. As one of the objectives of the work presented within this thesis is to detect error in technique with a view to prevent injury to a performer and assist the development of good technique, it is of great importance to understand the theories that support this objective.

The review and evaluation of literature in this chapter shall serve as the foundation for the methods of analysing and presenting the augmented feedback of motion from a performing subject.

3.1 Stages of Learning

Sequential and relatively distinct phases in the learning of motor skills have been identified and are important when considering feedback (Fitts and Posner, 1967, Luft and Buitrago, 2005, Schmidt and Wrisberg, 2008).

Learners confronted with an entirely unfamiliar task are considered to be in the *cognitive stage* of learning; their challenge being to become competent of the skill. Learners think about what they are trying to do and about strategies that might help achieve it. This process demands a lot of attention and prevents learners from processing other information such as the elements of proper form. Gains in performance through this stage tend to be large and occur rapidly; this indicates that people quickly discover and use more effective strategies of demonstrating the skill. Instructions, demonstrations, and other types of verbal and visual information are particularly beneficial for learners in this stage (Schmidt and Wrisberg, 2008).

Having solved most of the strategic or cognitive challenges and having achieved a general idea of how to perform the skill, the learner enters the *motor stage*. Several factors noticeably change during the motor stage, most of which are associated with a shift in their focus to refining the skill by organising more effective movement patterns (Nourrit et al., 2003).

Learners perform more consistently as their strategies for skill refinement become more sophisticated and their movements become more established. They are more efficient in producing their movements; at times appearing to perform almost effortlessly. As learners discover regularities in the environment, their anticipation and timing develop, making their

movements appear smoother and less rushed. In addition, performers begin to monitor their own feedback and become proficient in detecting their own errors (Liu and Wrisberg, 1997). With practice, learners begin to pay more attention to relevant feedback information, both proprioceptive (e.g., joint position) and exteroceptive (e.g., vision and audition), which allows them to detect performance errors.

This stage generally lasts considerably longer than the cognitive stage and instructional assistance and feedback become less important. When feedback is provided, it is most effective when precise; targeting the aspects of the movement which the learner is attempting to refine, and suggests ways of attaining success (Schmidt and Wrisberg, 2008).

After extensive practice, some learners are able to produce their actions almost automatically with little or no attention and are considered to be in the *autonomous stage*. These highly skilled performers have developed capabilities to control action for increasingly long periods (e.g., in dance). As a result, they do not have to think about every component of the skill when they are performing.

Learners in the autonomous stage demonstrate increased automaticity in their sensory analysis of environmental patterns (Schmidt and Wrisberg, 2008). This capability frees the best performers to engage in higher-order cognitive activities, such as split second shifts in strategy during a basketball game or spontaneous adjustments in the form or style of a movement in dance or figure skating.

During the autonomous stage, self-confidence increases and the learner becomes highly developed in detecting errors in movement.

3.2 The Role of Feedback

Behaviourism is a theory that centres on behaviour modification through stimulus-response and selective reinforcement (Armour, 2011); increasing the probability that a desired behaviour will occur again in similar circumstances. For over a century, researchers have examined the role of feedback in the learning of motor skills (Thorndike, 1914, Thorndike, 1932).

Feedback is available from various sensory systems as a natural part of performing a skill; such as *proprioceptive* and *tactile* feedback from the sensory receptors in the muscles, joints, vestibular apparatus, and skin, *visual* feedback from the eyes and *auditory* feedback from the ears. All of these physiological systems provide performance-based feedback that informs the

learner about the success of the task. The value of these sensory feedback sources depends on the specific characteristics of the situation. The term *task-intrinsic feedback* shall be used to describe this type of sensory feedback. An important advantage of the term task-intrinsic feedback is its acknowledgement of the skill-specific nature of sensory feedback sources associated with performing sport skills. People don't usually monitor this type of feedback unless someone directs their attention to it or asks them to perform an act that is dependent on the feedback (Schmidt and Wrisberg, 2008). One way instructors might do this is to ask learners to describe, or estimate, what they felt when they moved. Another way might be to ask the performer, immediately after the movement, how effective the action was in terms of achieving the desired outcome.

Another type of feedback, which may or may not be available to the learner, comes from information that is not inherent to the task such as from a coach, teacher, trainer or training device. This latter type of feedback adds to the natural sensory feedback and can be provided in a variety of ways such as in auditory, visual, or tactile form. This second type of feedback will be referred to as *augmented feedback* (others have used terms such as external and extrinsic feedback); the word augmented referring to adding to or enhancing the task-intrinsic feedback.

Researchers who study the acquisition of motor skills and practitioners who teach or coach sports skills can profit considerably from knowing about these two types of feedback (Magill and Anderson, 2012).

When augmented feedback is given to a learner it can function in at least three ways. One is to facilitate the learning of a new skill by providing performance-based information that allows the learner to determine what they should continue or not continue to do. Another function is to enhance the performance of well-learned skills by providing information that allows the learner to determine how to improve performance in specific contexts and situations. Furthermore, augmented feedback functions as motivation to continue to practice a skill or to continue to participate. These three functions demonstrate that augmented feedback can serve multiple roles in any learning or performance situation (Magill and Anderson, 2012).

Recently, researchers have increasingly directed their attention to the effects of *knowledge of results* (KR) (Wulf and Shea, 2004). KR is augmented feedback provided to the performer after the action is completed (Schmidt and Wrisberg, 2008), which indicates something about the

degree to which the performer achieved the desired movement outcome or environmental goal (Adams, 1971, Adams, 1968).

This source of information is thought to serve as a basis for error correction and is viewed as integral to achieving more effective performance as practice continues, guiding the performer to the correct response. Early accounts of the role of KR concluded that it was one of the most important learning variables and that learning did not occur in its absence (Bilodeau et al., 1959, Bilodeau and Bilodeau, 1958). Practice without KR was thought to weaken the memory of the action and cause performance to lose direction to the goal. The reason for this is that the memory of the action was thought to develop through combining the experience of a task with the KR received. That is, the more trials with KR an individual has performed, the stronger the trace of schemata was assumed to be and, eventually, the ability to detect errors without KR (Wulf and Shea, 2004). According to this view, learning was optimised when KR was provided more frequently, with shorter delay or more precisely (Adams, 1971, Schmidt, 1975, Thorndike, 1927). Recently, these ideas have been questioned, and researchers have suggested that a number of factors come into play when feedback is or is not provided during the learning of motor skills.

In recent years, researchers have tended to make a distinction between *knowledge of performance* (KP) and KR. KP refers to augmented feedback providing information about the quality of the movement (Schmidt and Wrisberg, 2008), or the ‘nature of the movement produced’ (Schmidt and Lee, 1999 p. 415), whereas KR refers to the ‘result produced in terms of the environmental goal’ (Schmidt and Lee, 1999 p. 415). Even though there might be situations where KR and KP serve specific and differential functions in the learning process (Brisson and Alain, 1996, Brisson and Alain, 1997), in general, both types of augmented feedback are considered to affect the learning of motor skills and adhere to the same principles (Wulf and Shea, 2004).

3.3 Frequency of Feedback

There has been much research on the timing of feedback (Hattie and Timperley, 2007, Bennett and Cavanaugh, 1998, Kulik and Kulik, 1988), and the scheduling of augmented feedback has been studied more extensively than any other variable that influences performance and learning (Magill and Anderson, 2012).

At the start of the 20th Century, Edward Thorndike laid the groundwork for a simple but important principle, which he named “the law of effect”. It was the work of Thorndike that

gave the foundations to instrumental conditioning; where reward (positive reinforcement), punishment, escape (negative reinforcement) and omission were used to adapt an organism's behaviour (Rachlin, 1976).

Burrhus Frederic Skinner developed instrumental conditioning and brought about the operant learning theory; the process of acquiring the capability to behave in ways that produce desirable outcomes (Schmidt and Wrisberg, 2008). Through the process of operant conditioning, behaviour that produces a consequence with survival value becomes more likely to occur (Skinner, 1974). The behaviour is said to be strengthened by its consequences, and for that reason the consequences themselves are called 'reinforcers'.

Throughout the 20th Century, the understanding of how feedback affected motor skill learning was largely based on the law of effect and operant learning theory. Because Thorndike believed that learning involved the strengthening of the bond between a stimulus and a response, he assumed that feedback should be presented as often as possible. Furthermore, Thorndike proposed that if feedback was not presented after a movement attempt, and learners could not determine the outcome based on their own intrinsic feedback, the bond would not be strengthened at all on that attempt. Scientists discovered little that contradicted Thorndike's viewpoint, therefore a notion emerged that more feedback is better and it was assumed that feedback information that was more immediate, more precise, or more detailed would be most beneficial for learning.

In time though, scientists began to discover that more is not always better. Researchers began to realise that feedback frequency could be viewed in two ways. One way is in terms of absolute feedback frequency, which refers to the total number of times feedback is presented during a practice session. On the other hand, relative feedback frequency refers to the total number of times feedback is presented when compared to the number of repetitions. For example, if a performer attempts 300 repetitions of a movement and the instructor gives feedback on 100 of them, the absolute feedback frequency is 100 whereas the relative feedback would be 33%.

It is said that, in general, increasing the absolute frequency of feedback enhances learning (Schmidt and Wrisberg, 2008), although it is acknowledged that there are limitations to this rule. One study that contradicts this idea concluded that amount of practice has no significant effect, and that even minimal amounts of practice spread over several days is sufficient to facilitate the learning and retention of a motor skill (Savion-Lemieux and Penhune, 2005).

The results of studies examining the effects of various schedules of reinforcement show through retention tests that participants who receive intermittent reinforcement during practice continue to perform at higher levels when the reinforcement is withdrawn than participants who receive reinforcement after every attempt in practice. One effective way practitioners can provide intermittent reinforcement is by using a fading procedure, in which they gradually reduce the frequency with which they provide reinforcing feedback as they see learners becoming more adept at performing the task (Schmidt and Wrisberg, 2008).

Research has shown that practice attempts followed by no feedback can actually be beneficial for learning, even when participants cannot see or feel the outcome or determine the outcome on their own. One study (Winstein and Schmidt, 1990) found that participants who received augmented feedback after half (50% relative frequency) of their practice attempts performed as accurately as those who received feedback after every attempt (100% relative frequency). Furthermore, retention of the skill 10 minutes after practice performed in the absence of augmented feedback was about the same for both groups. Results such as these challenge Thorndike's assumption that movements followed by no feedback produce no learning. In the same study when participants were tested 2 days after practice, the group that received less frequent feedback during practice performed more accurately than the group that had received feedback after every attempt. This is further highlighted in the results of a study examining the learning of correct movement form (Weeks and Kordus, 1998). In this study it was found that 12-year-old children who received KP following 33% of their practice attempts of the soccer throw-in movement demonstrated significantly better movement form (based on eight biomechanical characteristics) than children receiving KP 100% of the time.

One explanation of this may be that when people don't receive feedback, they engage in various kinds of information-processing activities they do not engage in when they receive feedback (Schmidt and Wrisberg, 2008).

3.4 The Guidance Hypothesis

The guidance hypothesis was proposed following a comprehensive review of the KR literature (Salmoni et al., 1984). The hypothesis states that augmented feedback plays a major role in scaffolding the learning process by helping the learner discover how to accomplish the goal of the task. If scheduled inappropriately however, augmented feedback can become an essential part of the task and the learner can become dependent on the feedback preventing the learner from processing critical sources of task-intrinsic feedback or engaging in important

aspects of action planning that are essential to a successful outcome (Magill and Anderson, 2012).

Several aspects of scheduling have been shown to lead to a dependence on augmented feedback. Increased dependence occurs when the feedback is provided too quickly after a practice attempt (Swinnen et al., 1990), if it is provided concurrently during performance (Vander-Linden et al., 1993), if it is provided too frequently during practice or in a manner that is very easy to use (Winstein and Schmidt, 1990). It has also been shown that the likelihood of a learner to develop a dependence on augmented feedback can be reduced by delaying its provision over trials (Anderson et al., 1994), delaying it over trials and providing it in summary form (Lavery, 1962) or as an average (Young and Schmidt, 1992), or making the provision of augmented feedback contingent to the magnitude of errors made by the learner (Sherwood, 1988). Allowing learners to select the trials on which they receive augmented feedback (Patterson and Carter, 2010) or estimate their errors before receiving feedback (Hogan and Yanowitz, 1978) has also proved to be effective in minimising dependency.

The KR-delay interval is the amount of time that KR is delayed after a movement. For a long time (Lorge and Thorndike, 1935), scientists have always expected to find that increasing the KR delay degrades learning; one reason being due to instrumental learning research with animals. Delaying the reward from an animal's desired action has large effects on animal learning, and delaying the reward too much eliminates learning completely (Fantino and Logan, 1979, Tarpy and Sawabini, 1974). Scientists expected something like this for KR delay in human motor learning as well. A second reason is that because movement information is lost rapidly from memory (Adams and Dijkstra, 1966), learning should be less effective as the feedback delay from the associated movement is increased. This would seem to weaken the possibility for the learner to associate the method of producing the movement with its actual outcome; a concept critical to many early theoretical ideas about learning. However, more recent reviews (Salmoni et al., 1984) have shown that experiments examining the delay of KR in human motor learning have almost uniformly failed to show that increasing the KR delay has any effect at all (Schmidt and Lee, 1999).

In a study where participants attempted to learn a simulated batting task (Swinnen et al., 1990), one group received instantaneous feedback after each movement whereas another group received delayed feedback a few seconds after movement completion. The group receiving instantaneous feedback performed worse than the delayed feedback group on the second day of practice and on several retention tests administered over a 4-month period.

Research (Anderson et al., 2005) has indicated that learners pay closer attention to feedback, and explore the available intrinsic feedback more when KR is delayed than when it is given immediately after a movement. Moreover, asking participants to critique their movements before providing augmented feedback can enhance learning. A recent study (Chambers and Vickers, 2006) revealed that competitive swimmers who were questioned by the coach before receiving feedback during practice improved their short course (25m) times over the course of a season more than swimmers who were not questioned.

The relationship between task-intrinsic feedback and augmented feedback is a significant factor in the likelihood of a learner becoming dependent on augmented feedback. One study (Annett and Kay, 1957) noted that learners have a preference for using augmented feedback when it is available because it is typically presented in familiar scales (cm, inches, seconds), whereas no scale may initially exist for comparing task-intrinsic feedback to the goal of the task. A later study (Annett, 1961) suggested that errors on a retention test (after receiving augmented feedback) would be highest when the augmented feedback provided during practice was very informative and the intrinsic feedback was much less informative. Developing this idea, subsequent researchers suggested that dependence on augmented feedback would likely occur when augmented feedback was considerably easier to detect and interpret than intrinsic feedback (Armstrong, 1970, Lintern, 1980). This assertion has been validated in recent research (Anderson et al., 2001, Blandin et al., 2008, Maslovat et al., 2009).

Augmented feedback is most effective when it facilitates the learner's discovery of the critical sources of task-intrinsic feedback that are essential for controlling performance in the absence of augmented feedback (Magill and Anderson, 2012). Successful practitioners allow enough time for both intrinsic feedback processing and error evaluation before providing augmented feedback (Schmidt and Wrisberg, 2008).

3.5 Presentation of Feedback

Augmented feedback can be presented in many forms; ranging from the verbal feedback of a coach to sophisticated visual displays. Studies have reported the use of many different forms of augmented feedback that are presented to the learner in a multitude of different ways. As technology has improved and become more accessible, there has been an increase in augmented feedback involving computer-based technology. It is difficult to determine which parameters of non-verbal augmented feedback are likely to have the greatest influence on learning because the effectiveness of any parameter will be a function of what parameters of

the task need to be modified (e.g., spatial parameters, temporal parameters, coordination, movement scaling), as well as characteristics of the task and learner (Magill and Anderson, 2012).

Studies providing examples of technology-based augmented feedback can be found across a wide range of sports. These include; body segment alignment in gymnastics (Baudry et al., 2006), fluctuations in speed and hand propulsive force in swimming (Chollet et al., 1992), boat speed and the relation to oar position and torque in rowing (Spinks and Smith, 1994, Smith and Loschner, 2002), elbow and wrist motion in netball (Helmer et al., 2010), running technique in athletes (Eriksson et al., 2011), kinematic analysis of rifle stability while shooting (Mononen et al., 2003, Konttinen et al., 2004), bar path when performing a power snatch in weight lifting (Winchester et al., 2009, Rucci and Tomporowski, 2010), swing technique in golf (Bertram et al., 2007) and shooting skills in ice hockey (Feltz et al., 2008).

3.6 Biomechanics

Objective, accurate and pertinent data on performance is essential to aid coaches and practitioners in making informed judgements and decisions, and to provide players with the feedback necessary for skill learning and performance enhancement (Hughes and Franks, 2004).

Biomechanics offers methods by which the very fast actions that occur in sport can be recorded and analysed in detail. There are various reasons for undertaking such analyses; one is to understand the general mechanical effectiveness of the movement, another is the detailed description of the skill, and another is an analysis of the factors underlying successful performance. An important application of biomechanics within any sport is the definition and understanding of skills. Information derived from biomechanical analyses can help in the coaching process and, as a result, enhance the learning and performance of those skills (Lees, 2013).

In exercise and sports biomechanics, the three most common approaches to technique analysis are qualitative, quantitative and predictive biomechanical analysis methods (Koh and Tan, 2006).

3.6.1 Qualitative Analysis

Qualitative biomechanical analysis method is a systematic observation and introspective judgement of the quality of human movement so as to provide the most appropriate

intervention to improve sports performance (Knudson and Morrison, 2002). In other words, movement is observed and interpreted by the analyst depending on the required outcome. Observation models such as *phase analysis model*, *temporal analysis model* as well as *critical feature analysis model* form the basis for undertaking observation in qualitative analysis method. Breaking down a whole motion of performing a particular skill into phases provides a systematic part-by-part observation. Phase analysis can be broken down into a three-phase analysis (Barlett, 1999) or a four-or-more phase analysis (Lees, 1999), depending on the complexity of the particular skill and the needs of the analyst. Temporal analysis (Adrian and Cooper, 1995), unlike phase analysis, is more suited for rhythmic and timing activities such as dancing and has minimal application in most sports. Critical feature analysis (McPherson, 1990) uses specific features (key elements) that are considered as observable aspects, such as the back-swing observed in a tennis stroke, which is essential to the successful performance of that skill and will determine performance outcome.

One of the major criticisms of qualitative analysis methods is in its subjectivity. Based on the concept of 'spectator' analysis, verbal feedback using non-numerical descriptions such as "good shot", "poor pass", "too long" or "well done" is given continuously to evaluate performance. Such verbal feedback does convey some degree of information on the athlete's performance, but may lack clarity. Much of the feedback given fails to explain why the performance is either good or bad and as a result is inadequate to develop performance effectively. This subjectivity can be overcome if the evaluations are done using the templates model, where an evaluation of the observed performance is compared to benchmark performance indicators obtained through a coaching manual or to a performance by a better skilled athlete (Tidow, 1990, Hucklememkes, 1992). Any differences to either reference will be diagnosed as faults.

3.6.2 Quantitative Analysis

Advancements in technology capabilities have resulted in the ability to record, display and evaluate dynamic movements both kinematically and kinetically. Quantitative biomechanical analysis methods are similar to the qualitative analysis methods in terms of approach but are not subjective as they use a range of instruments to capture, observe and evaluate athlete's performance. Some examples of these instruments include high-speed cameras, force plates or force platforms, electromyography (EMG) and electro-goniometers.

The key component in using quantitative analysis method for technique analysis is the selection of key variables. The selection of key variables are based on the 'deterministic model'

(Hay and Reid, 1988) and are selected because they are thought to have some priority importance for the movement of a particular skill.

The selection of key variables is also made in reference to previous research and coaching articles. For instance, an investigation into the accuracy of qualitative analysis for the assessment of skilled baseball pitching technique (Nicholls et al., 2003) referred to data gathered in a previous study (Fleisig et al., 1999).

Quantitative analysis methods have provided insights into technical differences between good and average athletes. For instance, analyses provided (Takei et al., 2003) on gymnastics vaulting using the 'deterministic model' identifies the differences in techniques between high and low scoring vaults performed by elite male gymnasts.

Quantitative analyses have also enabled the identification of critical features of technique; for instance, kinematically analysing the *osoto-gari* leg sweep (Imamura and Johnson, 2003). The performance outcome of this study identified critical features in a judo leg sweep by emphasising the importance of using the sweeping leg in a sequential kinetic link motion rather than as a single rigid segment.

The integration of quantitative and qualitative methods of analyses can certainly advance the current status of coaching methods and help athletes achieve more technical competence with less training (Koh and Tan, 2006).

An alternative to giving either qualitative or quantitative KR is provided by the bandwidth-KR method (Sherwood, 1988). With this method, similar in some ways to the qualitative-KR methods first used by Trowbridge and Cason (1932), the nature of augmented feedback is determined by a bandwidth about the movement goal. In most studies using this method, qualitative KR in the form of "correct" or "right" is provided to the subject when the performance outcome lies within the boundaries of correctness as defined by the bandwidth. In contrast, specific KR that gives both the magnitude and the direction of error is provided when performance exceeds the bandwidth. This method is probably what many teachers and therapists do naturally; correcting relatively poor performance and reinforcing relatively good performance.

One consequence of bandwidth KR is that as the tolerance limits increase, the proportion of trials with error KR diminishes. As less frequent error KR (or augmented feedback) has also been associated with increased levels of learning, one question is whether the bandwidth effect essentially results in the same as a reduced KR frequency (Schmidt and Lee, 1999).

3.6.3 Predictive Analysis Method

Based on the examples of their application, both qualitative and quantitative biomechanical analysis methods rely on observation or recorded data from real movement that comment on the characteristics of technique that an athlete demonstrates.

Predictive biomechanical analysis method however uses simulation models of the human anatomical structure to mathematically calculate and predict an ideal sporting performance, thus allowing hypothetical questions to be investigated systematically (Lees, 2002).

3.7 Conclusion

It can be concluded from the review of literature on corrective coaching that it is important to be aware of the various forms of feedback available, and what benefits they bring, throughout the stages of learning. Feedback, in any form, should facilitate the learning process and, as a result, enhance the performance. Knowledge of performance or results should be provided to the performer, but not at a cost of the learner processing intrinsic feedback or engaging in action planning. Augmented feedback should scaffold the learning process without becoming essential to the learner. Instantaneous feedback has been shown to result in dependence upon feedback and low retention rates of a skill. Enough time should therefore be allowed before providing augmented feedback so that it facilitates the learner's discovery of critical sources of intrinsic feedback that are essential to controlling performance when augmented feedback is not presented.

3.8 Summary

This chapter has reviewed theories on skill learning and retention and the role of feedback within that process. Frequency, timing and depth of feedback as well as presentation methods have all shown to be important factors in determining the progression and retention rates of skill learning. Biomechanical technologies allow accurate quantitative analysis of performance which would not be possible by visual observation alone. The next chapter presents an investigation into novel motion capture methods to establish a workflow for measuring movement within a live performance for presentation of feedback.

4 Measurement of Human Motion in Performance

This chapter describes motion capture work applied to ballet gestures. A wireless gyroscopic sensor based system is used to record the movements of ballet dancers in order to establish a suitable workflow for extreme human movements and to investigate if such equipment is capable of detecting misalignments in ankle position. Results show that subtle variations in joint rotation can be clearly measured and could be used to develop fault detection and isolation possibilities for injury prevention and improved performance. The limits of the current techniques and some improvements are discussed for real-time performance feedback.

4.1 Experimental Motion Capture Process

From the literature review, it was evident that sensor based suits have previously been used for walk cycles, general everyday movement and gait analysis. There are few reported applications of such equipment for more extreme movements such as those demonstrated in ballet. Capturing such motions as performed in ballet, and the extreme nature of the ranges and positions of the dancers, required new workflow methods for recording and data processing.

In order to achieve the aim of the project, it was decided that the Animazoo IGS-190 inertial motion capture suit would be employed to capture the movement of the subject. The suit makes use of 18 small solid-state inertial sensors (gyros) to measure the rotations of the actor's joints in real-time. The subject required that they could perform in their usual environment in an unhindered way. The requirements of the equipment were to provide a representation of the subject in real-time and to record sufficient and accurate movement data for analysis. The IGS-190 suit was chosen for several factors:

- The suit base is elastane (Lycra) with small external gyros compact and lightweight enough to transport to any location. The suit is also comfortable and non-restrictive to the subject.
- The system uses wireless signal transmission with a range of around 50 m (although tests for work presented here achieved accurate wireless motion capture recording over distances of several hundred metres), which means the subject is not restricted by cables connecting to the signal receiver.

- A stand-alone driver for output to Biovision Hierarchical data file and integration with Autodesk's MotionBuilder for real-time visualisation is included in the system.
- The gyros accurately record the rotations of the subject's bones in real-time at a rate of up to 120 frames per second (fps).
- The gyroscopic sensor-based system means that there is no occlusion associated with camera-based systems, avoiding significant post-production and allowing real-time potential.
- Previous experience of staff in the School of Engineering at MMU indicates that the suit records very high precision and accurate data at various frame rates.

Prior to processing data taken from the subject for biometric analysis, the appropriate sampling frequency of the data must be determined. Human motion by its very nature is an analogue process with almost infinite points of data variation when measuring the kinematic, kinetic and temporal properties. Sampling the signal at 120 Hz (the highest sampling frequency available using the motion capture equipment) or 60 Hz with linear interpolation applied to the captured signal, provides an average variance of 0.36 mm and 0.63 mm respectively from the analogue signal.

When capturing human motions, sensors are used. Inherently these sensors, active, passive or camera-based, include a degree of error. In the case of the Animazoo system used to capture the subject's motions, the gyroscopic sensors provide an angular sensor resolution of 0.03° . This resolution is the lowest amount of rotation that the system can record per sample with the gyroscopes having a maximum angular rate of $1200^\circ/\text{s}$. Using the minimum measurable angles provided by the gyroscopes the translational data error of the resulting joint can then be determined as 2.87×10^{-6} cm in the X-axis and 0.0219 cm in the Y-axis for a limb 41.9 cm long and would provide a sufficiently high resolution dataset for further processing and analysis (using the average mean human upper leg length of 41.9cm for male subjects aged between 20 and 29 years of age defined by the findings of Fryar et al. (2012)). The measurements that can be obtained from the motion capture system will inherently have the above-mentioned errors, varying on the limb lengths of the individual subject. Larger errors will be present for longer limb length and less error for shorter limb length. The above error within the capture system is very low, however must be noted as any biometric measurements lower than this value are subject to inconsistency due to the hardware error present.

It would be predicted that as motions increase in speed, the level of translational error for both the maximum and average variation would increase. The percentage deviation of the

measurement signal from the analog signal due to the increasing duration between the samples would also increase. When determining the correct sampling frequency for a set movement, the time duration of the movement must be taken into consideration. The lower the applied sampling frequency, the higher the variance between the sampled and analog signal, and the higher the variation from distinct points with regards to the temporal difference between the sampling points. When gathering data suitable for biometric applications, where small interpersonal differences can provide the basis for classification, it is of great importance that these motions are captured at a sufficiently high frequency for classification to take place. It is recommended, wherever possible for the desired application, to capture the subject's motions at the highest possible frequency practical in order to reduce these losses.

The suit uses wireless transmission to send the motion data to a processing unit, which is attached to a laptop computer installed with software able to view and record the data in real-time. The wireless nature of the suit means that the subject is not restricted by connecting wires and the range of the suit is sufficient to encompass a large enough arena for the subject to perform. The bulkiest part of the suit is the power-pack which can be worn on either the front or rear of the subject's torso. This is held by a Velcro belt which is stretchy and adjustable to the comfort of the subject. The feedback provided by each of the subjects has been positive with each commenting that the suit did not restrict their usual movement. Invasive measurement is a vital factor when considering if the recording instrument interferes with the process in some way.

4.1.1 Recording General Ballet Movements with Motion Capture Equipment

An initial experiment would determine whether the IGS-190 motion capture suit would be capable of recording extreme motion, meeting the requirements of the subject and providing the data needed to fulfil the aims and objectives set out in the proposal.

The subject required that they could perform in their usual environment in an unhindered way, and it was required that the equipment would provide a representation of the subject in real-time and record sufficient and accurate movement data for analysis.

A Biovision Hierarchical (BVH) data file – a format originally developed by Biovision – provides skeleton hierarchy information in addition to the motion data; this is the industry standard file format for motion capture data. A header section describes the hierarchy and initial pose of the skeleton, and a data section follows which contains the motion data.

This experiment would also determine whether the number of sensors on the suit and the skeletal hierarchy information within the BVH data file would capture suitable data for analysis of extreme human movement.

The location for the initial experiment was the Royal Northern School of Dance. An experienced male and a female dancer volunteered to be the subjects. A dance studio within the school was arranged for a duration of 2 hours mid-afternoon. The equipment used was the Animazoo IGS-190 suit, a laptop computer with appropriate software and drivers installed, a compass, a calibration cube and a digital camera.

On arrival at the studio, the laptop and wireless receiver for the IGS-190 suit were connected to the nearest power source and the calibration cube was set up. The dancers were photographed in the calibration cube so that actor files could be created. Actor files are used to measure and record the limb length of the subject whose motion is to be recorded. This is achieved by loading the front and side profile photographs of the actor into a piece of software that accompanies the IGS-190 hardware, and aligning the joint location points appropriate to the BVH file format. This detailed procedure prescribed by Animazoo engineers, when strictly followed, allows for the accurate proportional motion recording of the subject to the BVH file. The direction of north was identified in order for a reference point to be set within the motion recording software on calibration.

The male subject was to be recorded first and was fitted with the IGS-190 suit (see figure 4.1). The suit was calibrated, north was set, and recording commenced.

Following the recording of a series of movements and routines by the male subject, the same procedure was followed with the female subject (see figures 4.2 and 4.3).

The motion data was viewed in real-time through Autodesk's MotionBuilder software and recorded to BVH files for later analysis. An image of the subject being recorded can be seen in figure 4.3, with the corresponding image taken from the view in MotionBuilder shown in figure 4.4. The two-hour session allowed for approximately 1 hour of direct motion capture, within which a substantial amount of data was recorded; this indicates that the logistical aspects of the IGS-190 suit make it an ideal choice for the circumstances of this experiment.



Figure 4.1: Male dancer (Liam) in the calibration cube

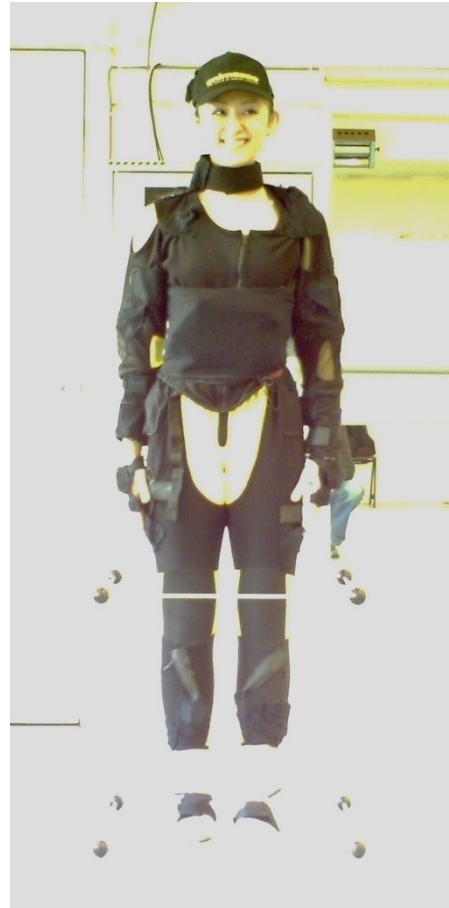


Figure 4.2: Female dancer (Nana) in the calibration cube



Figure 4.3: Female subject in studio

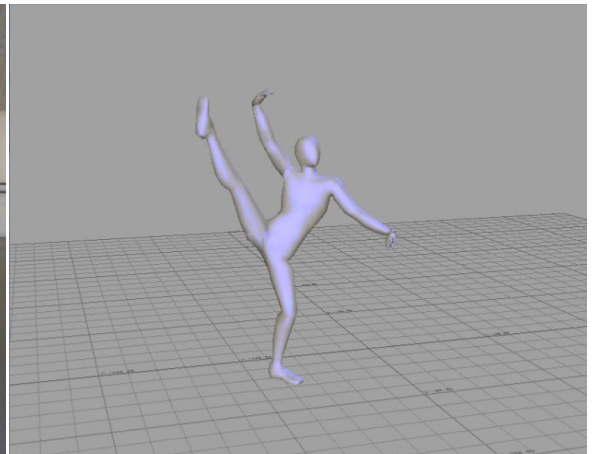


Figure 4.4: Real-time representation in MotionBuilder

Following the literature review, there was the hypothesis that there may be problems with foot slippage (skating) and the global positioning of the subjects. This experiment confirmed that there were some minor issues with foot slippage. Although the global positioning of the subject was generally very good when the subject had a point of contact with the floor, when

the subject's feet both left the floor during certain dance routines there were obvious problems. This is discussed in more depth later in the chapter.

4.1.2 Motion Capture Recording of Fault Conditions in Ballet

The next experiment was designed to discover whether the chosen setup detects, and to what extent, the subtle differences associated with good and poor technique. Those movements shown to result in injuries (Kadel, 2006) which may be immediate, such as stress fractures, tendon or ligament damage, or non-immediate that can lead to long term damage to the joint and the shortening of a dancer's career would be considered poor technique.

The experiment would record an experienced female ballet dancer in three different gestures of relevé: first position (see figure 4.5), demi-pointe (see figure 4.6) and pointe (see figure 4.7).



Figure 4.5: First Position



Figure 4.6: Demi-pointe



Figure 4.7: Pointe

The location for the experiment was a small office within the school of engineering at Manchester Metropolitan University, available for 1 hour. A competent female dancer volunteered to be the subject. The same set-up and calibration procedure was followed as described in the previous experiment.



Figure 4.8: Relevé en pointe - Correct position



Figure 4.9: Relevé en pointe - Exaggerated Sickle



Figure 4.10: Relevé en pointe - Exaggerated Winged

The gestures were captured in their correct positions (for example see figure 4.8), and then in fault positions both turning the sole of the foot outward (for example see figure 4.9) and inward (for example see figure 4.10).

In ballet terms the turning of the foot inward is known as sickle (in medical terms ‘inversion’) and the turning of the foot outward is known as winged (in medical terms ‘eversion’).

These positions, both correct and incorrect, were initially analysed post recording for fault detection; the degree of fault (sickle or winged) was of particular interest due to the potential damage this can cause to the dancer’s body. To do this, the motion data curves of the foot and ankle sensors were investigated. The subject required that the experiment could be carried out in a 1-hour session in a suitable environment, allowing for the correct supporting footwear to be worn. The requirements of the experiment were to record, in real-time, sufficient data to examine whether the degree of fault could be detected and isolated from the motion recording. The equipment used was the IGS-190 suit, a laptop computer with appropriate software and drivers installed, a compass, a calibration cube and a digital camera. The equipment was set up as in the previous experiment. The dancer reported that the IGS-190 suit had no restrictive effect on their movements and after a 5 minute familiarisation and warm-up routine, they were not aware of the presence of the equipment.

The gestures of relevé in first position, demi-pointe and pointe were recorded sequentially in order of correct position, position with sickle and winged position, and then saved to individual BVH files.

During the course of the experiment, it became clear that due to the placement of the sensors on the IGS-190 suit there would be a lack of appropriate detail around the foot setup. This is because the gyros placed upon the lower leg and the foot combine to give a rotation value for the ankle joint of the skeleton hierarchy, which is the last joint of the leg chain to record rotational data neglecting that there is a set of joints at the base of the toes. This is the fundamental difference between a ballet dancer being in the pointe or demi-pointe position. The neglected set of joints also represents the set of joints that is the middle section of the heel-to-toe roll in a walk cycle. This problem is discussed further in the following section.

4.2 Results and Discussion of Motion Capture for Analysis of Ballet Movement and Gestures

The initial experiment indicates that the Animazoo IGS-190 suit is capable of recording extreme human performance based movement. It also meets the criteria of the actors due to its portability and un-hindering usability; the suit fits into a small case, which, due to the materials it is made up of, is lightweight and easily transportable to wherever the location requires. A small team can set it up ready to capture within 20 minutes. Whilst such features might seem like a mere convenience, they are in fact vital for a realistic means of recording performers in a time constraint situation in their own environment. The conclusions made by Haag and Meador (Haag, 2009, Meador et al., 2004) about the portability and quick set up of the suit, which were presented in the literature review, are reaffirmed by this experiment.

The suit uses wireless transmission to send the motion data to a processing unit, which is attached to a laptop computer installed with software able to view and record the data in real-time. The wireless nature of the suit meant that the subject was not restricted by connecting wires, and the range of the suit was sufficient to encompass a large enough arena for the subject to perform. This contradicts the suggestion by Parent that “drawbacks relate to the range and accuracy of the magnetic field and the restricted movement resulting from the instrumentation required” (Parent, 2008), as a suitably large and unhindered environment allowed very pleasing results to be attained.

The bulkiest part of the suit is the power pack which can be worn on either the front or rear of the subjects’ torso. This is held by a Velcro belt, stretchy and adjustable to the comfort of the subject. The feedback provided by each of the subjects has been positive with each commenting that the suit did not restrict their usual movement; invasive measurement is a vital factor when considering if the recording instrument interferes with the process in some way.

The recorded motion data from the first session shows that the IGS-190 suit is capable of recording the extreme motion associated with ballet. The frame rate and accuracy of the data enabled the complete movement to be viewed and recorded in real-time with no jerkiness or lagging. This is contrary to what was reported by Meador, who stated that noise or jerkiness was often seen in the character’s performance, placing the blame on the mechanical parts being dusty, loose or not correctly aligned to the dancer’s body (Meador et al., 2004).

The study by Meador used the Gypsy 3.0 motion capture suit, which was an electro-mechanical system consisting of an exoskeleton made of lightweight aluminium rods following the motion of the performer's bones. Potentiometers (variable resistors), or 'pots', at the joints change voltage (varying resistance) based upon angular rotation of the rods. Due to the mechanical structure of these pots, it would go some way to explain the poor results from the study. Motion Capture technology has significantly improved since this 2004 study and the IGS-190 suit uses small inertial measurement units (IMUs) rather than mechanical pots. The IMUs use a combination of accelerometers and gyroscopes to record the motion data, which is a much more efficient and reliable method and eliminates the risk of mechanical misalignment.

Although there was some foot slipping, the captured motion was generally of high quality; the dancers had the opportunity to observe the basic motion captured on a laptop immediately afterwards and confirmed that the visualisation of the data accurately represented the performance. Problems were not encountered until the actor's whole body left the floor (for example see figure 4.11). These problems were similar to those identified by Haag (2009), who commented on jumping being difficult to record accurately. When there was no contact between the actor and the floor, the global positioning of the root node of the skeleton hierarchy was unpredictable. It would often over compensate the distance of the 'jump' and attempt to pull the skeleton back down to floor contact. This is clearly a problem that would need to be addressed in order for usable real-time results from the capture of all forms of ballet movement.

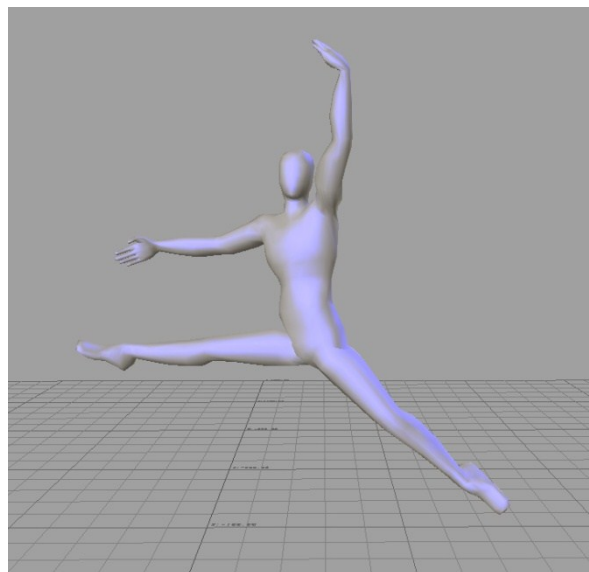


Figure 4.11: Male Subject leaving the ground

While the IGS-190 provides highly accurate local motion (limb motion data), it can only calculate the position of the root (which determines the global position of the actor). This is approximated by trigonometry; piecing together the rotational data from the legs in conjunction with limb lengths to provide calculated global motion data. The hip is the only node in the hierarchy that contains positional data on output. This explains why the global positioning of the actor can be unreliable, particularly during points where there is no floor contact such as jumps.

The IGS-190 suit offers the ability to incorporate a sonar system known as ExacTrax, which is currently available as a prototype system, in order to return absolute positioning of the actor's root node. This would potentially resolve the global positioning problem encountered in this experiment and further work is anticipated to establish this.

The results from the second experiment show that the accuracy of the rotation data for the joints, captured by the IGS-190 suit with customised settings, would enable the detection of minor movements and misalignment of bones associated with poor technique and injury. The anatomy of the ankle is quite complex. The tibia and fibula join each other to form a deep socket that meets the talus (a foot bone). These three bones form a hinge joint - the ankle joint. The subtalar joint is formed by the talus and the calcaneus (heel bone). The ankle joint and subtalar joint allow the full range of motion in the foot. Many ligaments (strong non-elastic tissues that connect bone to bone) reinforce the ankle. The Achilles tendon (tendons are elastic structures that connect muscle to bone) attaches the calf muscles to the calcaneus, allowing us to rise up on our toes. The posterior tibialis tendon that runs toward the back of the ankle attaches one of the smaller calf muscles to the underside of the foot. This tendon helps support the arch and allows the foot to turn inward.

The common ankle movements are as follows:

- **Dorsiflexion** is movement of the top of the ankle and foot toward the front of the shin bone.
- **Plantar flexion** is movement of the ankle and foot away from the shin bone – rising to demi-pointe or pointe in ballet.
- **Eversion** is turning the ankle and foot outward, away from the midline of the body – known as winged in ballet.
- **Inversion** is turning the ankle and foot inward, toward the midline of the body – known as sickle in ballet.

An independent study (Worthen and Hamill, 1997) states that each degree of misalignment in a dancer transmits force to the medial/lateral ankle structures (ligaments, bones, tendons and associated muscles), which are the most vulnerable to sprain.

It is stated in a study of the practice of classical ballet (Dixon, 2005) that if classical technique is to be performed efficiently, then classical stance and good alignment must be anatomically mastered. This is agreed in the teachings of Maggie Black; an internationally renowned ballet coach known for her anatomically based approach to ballet instruction (Zeller, 2009).

The following images show the variation of movement on the ankle joint in the X-axis. The graphs taken from MotionBuilder fCurves are mapped at 120fps and display values to a 100th of a degree, although the BVH file itself records the values to a 1,000,000th of a degree.

In order to take the data from the BVH file for analysis outside of MotionBuilder, a workflow has been devised. The BVH file is loaded up into the MotionBuilder viewer window and without any adaptation, the scene is saved to FBX file format. This enables the scene to be imported into Maya. Within Maya, this scene can be imported and the animation curves can be viewed in the Graph Editor, which is similar to the fCurves window in MotionBuilder. The major difference for the purpose of this report is that scripts can be run from the Script Editor window in Maya in MEL (Maya Embedded Language) or Python. With a script, it is possible to export plot data values of a given animation curve for analysis in other programmes.

The following Python script has been written in order to write the time/value data values of a selected curve to an XML file.

```
import maya.cmds as cmds
from xml.dom.minidom import Document

xmlDoc = Document()

root = xmlDoc.createElement('curveData')
xmlDoc.appendChild(root)

animCurves = cmds.keyframe(query=True, name=True, sl=True)

for c in animCurves:

    curveElement = xmlDoc.createElement('curve')
    curveElement.setAttribute('name', str(c))
    root.appendChild(curveElement)
```



```

keyTimes = cmds.keyframe(c, q=True, tc=True)
for t in keyTimes:

    frameElement = xmlDoc.createElement('frame')
    curveElement.appendChild(frameElement)

    value = cmds.keyframe(c, time=(t,), q=True, vc=True)[0]
    frameElement.setAttribute('time', str(t))
    frameElement.setAttribute('value', str(value))

file = open('C:/foldername/filename.xml', 'w')
file.write(xmlDoc.toprettyxml())
file.close()

```

The XML file format has been used due to its ability to be loaded into both Microsoft Excel and MathWorks MATLAB. The extraction of the data through this workflow will have many benefits to the further development of this investigation, besides the ability to display the data in clearer to read format. It offers the ability for the motion data to be analysed through principal component analysis, following which, it can be determined how the data can be analysed to provide the end user with real-time feedback with a view to corrective coaching.

Figures 4.12 and 4.13 show the subject demonstrating the position of demi-pointe with correct alignment. The subject rises to demi-pointe and holds the position with an average alignment of 53.8° in the x-axis. There is very little variance in the degree of rotation in this example whilst the subject is holding the position. This would be described as good technique and therefore injury preventative.

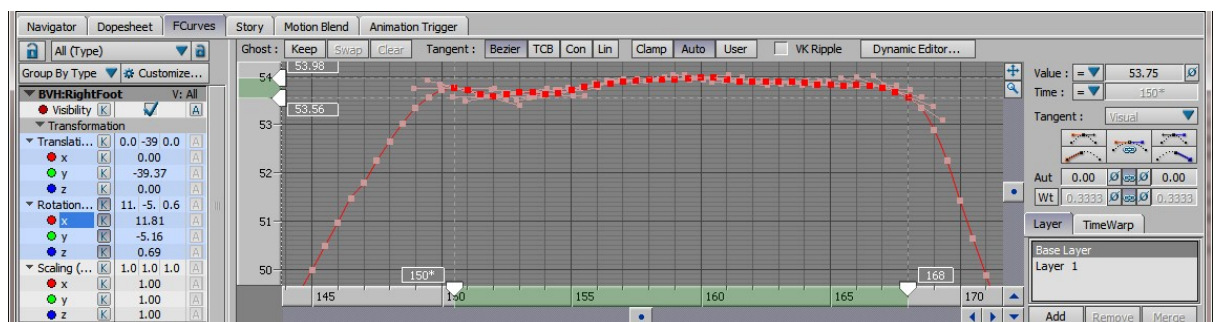


Figure 4.12: Subject in demi-pointe with correct alignment

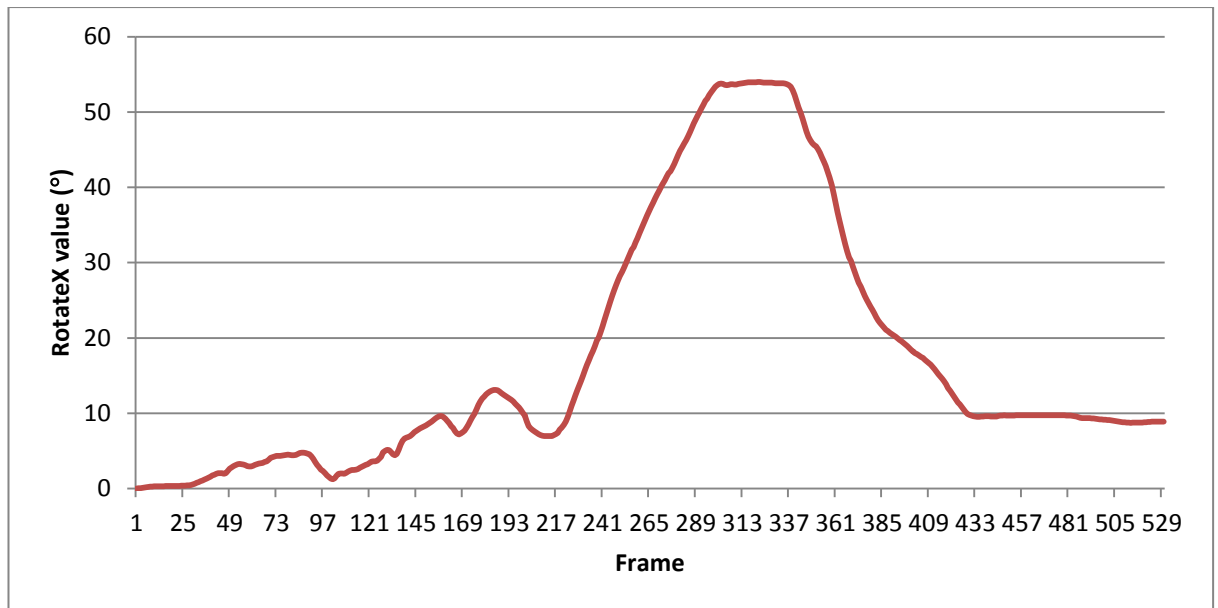


Figure 4.13: Subject in demi-pointe with correct alignment

Figures 4.14 and 4.15, show the subject initially rise into demi-pointe with the correct foot alignment and then roll into sickle, which is shown in the animation curve. When the subject initially rises, the rotation value for the right ankle joint is 47.2° . It then rolls to 46.2° before steadying off at an average of 46.6° and then rolling back down through 48.0° and into first position. This shows a maximum sickle of 1.8° , which would be considered poor technique and has the potential to cause musculoskeletal injury.

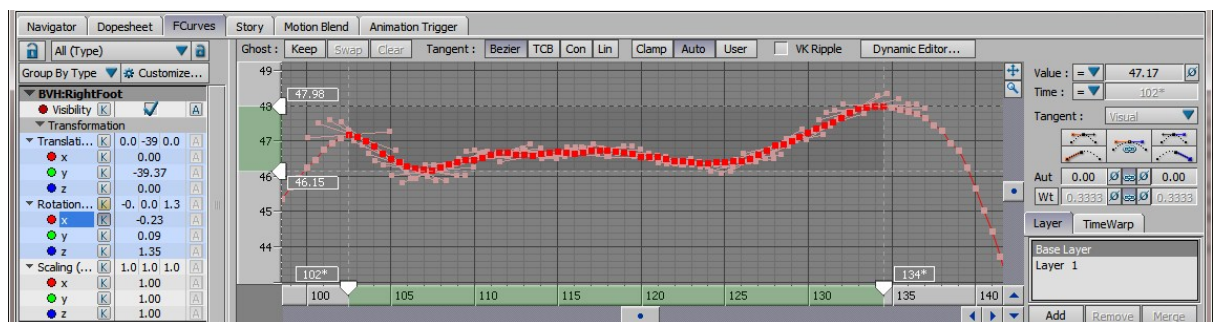


Figure 4.14: Subject in demi-pointe with sickle

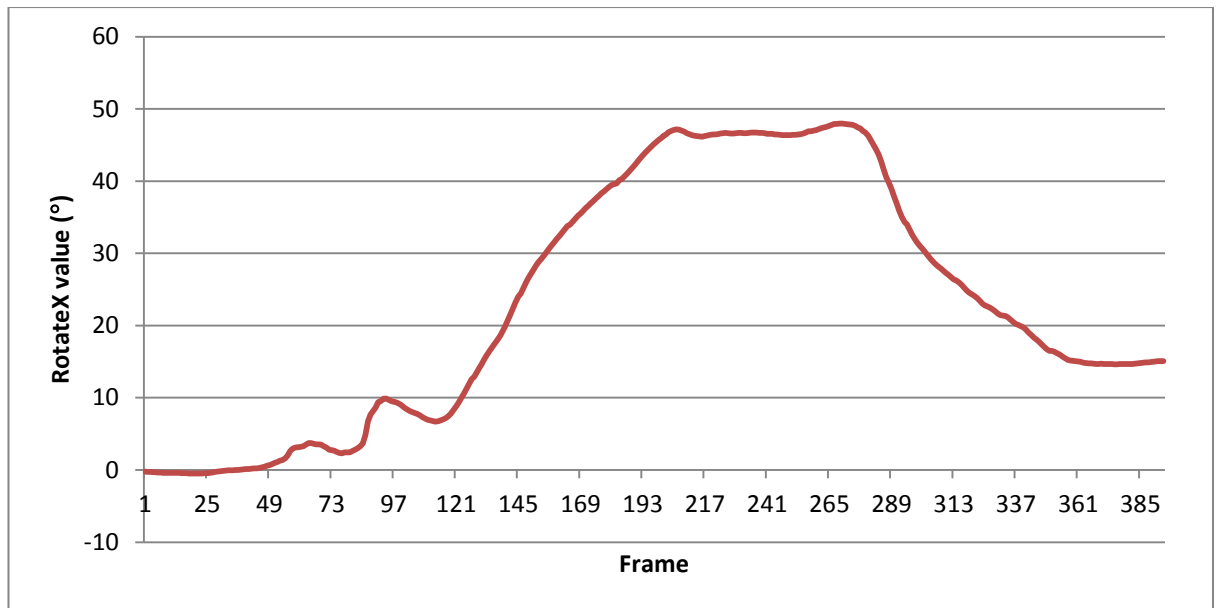


Figure 4.15: Subject in demi-pointe with sickle

Figures 4.16 and 4.17 show the degree of fault in the opposite direction (winged). They show the subject rise to demi-pointe at 50.4°, before rolling into a winged position at around 53.9° and then descending back to first position. The graph shows a maximum degree of variance of the position to be 3.5°, which again would be considered poor technique and indeed more likely to cause injury.

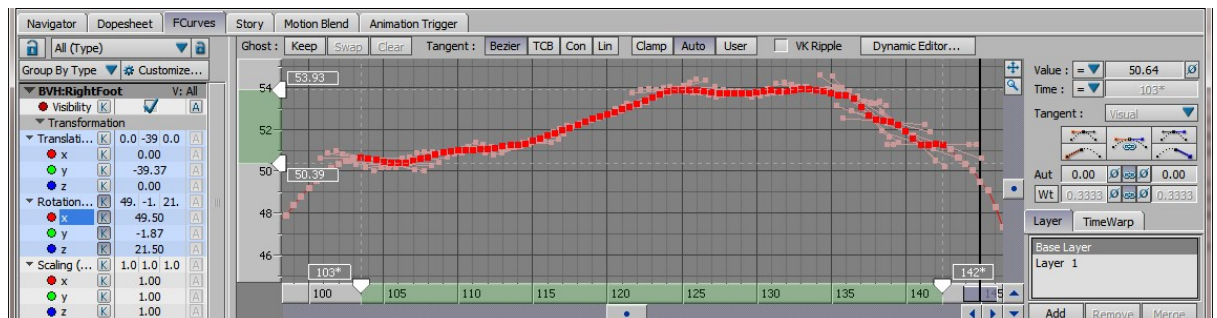


Figure 4.16: Subject in demi-pointe winged

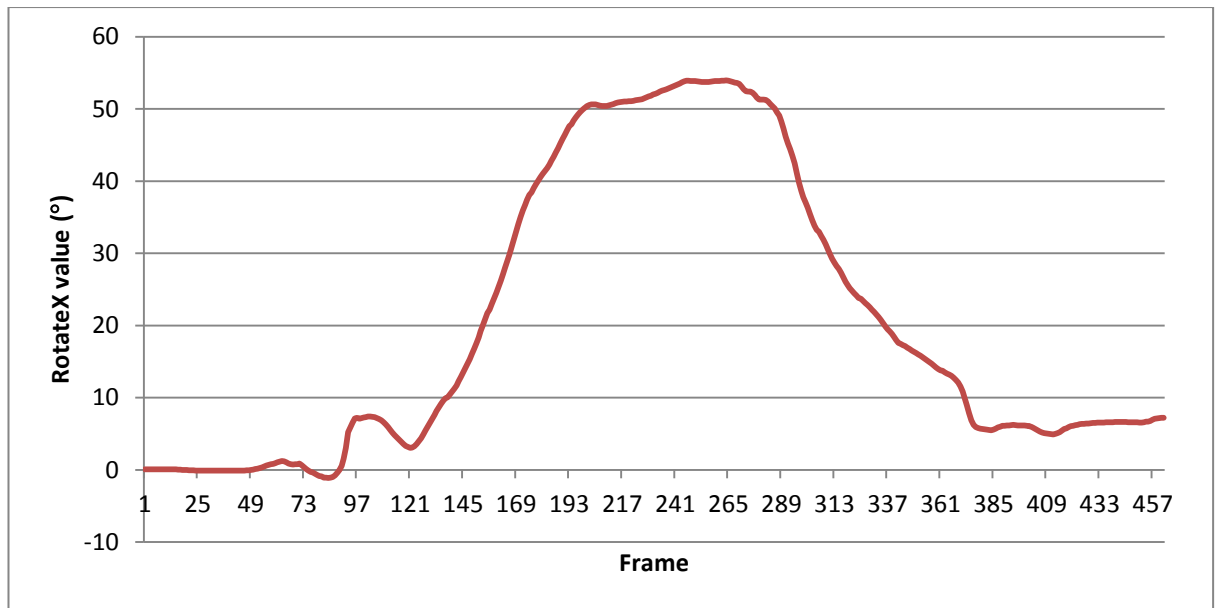


Figure 4.17: Subject in demi-pointe winged

The figures 4.18 through to 4.25 are from the gestures of relevé not described above from the right or the left foot, as specified in their titles, and provide further example of the degrees of sickle and winged fault associated with musculoskeletal injury in ballet dancers.

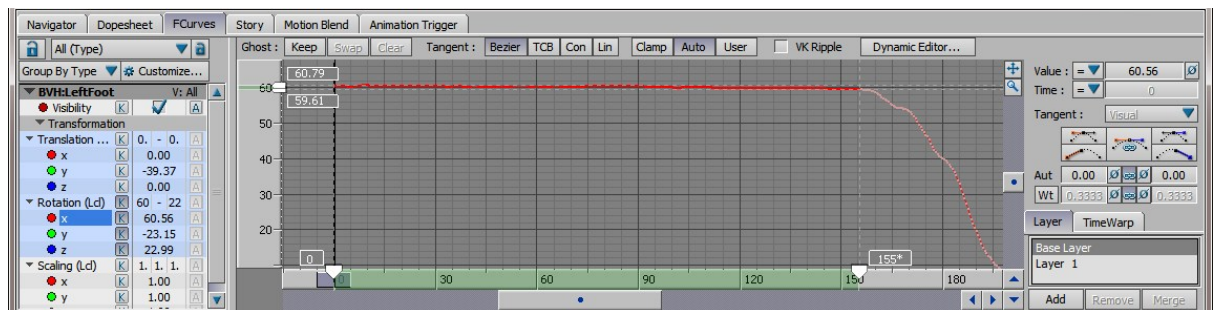


Figure 4.18: Subject en Ponte with correct alignment – left foot

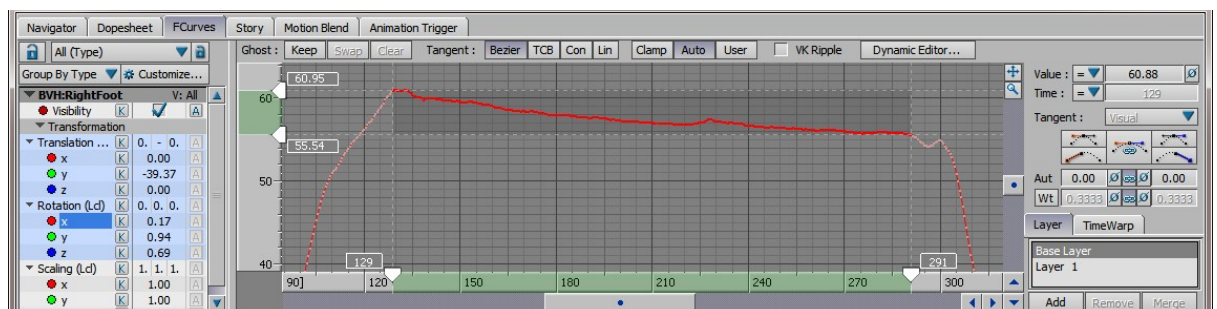


Figure 4.19: Subject en Pointe with sickle – right foot

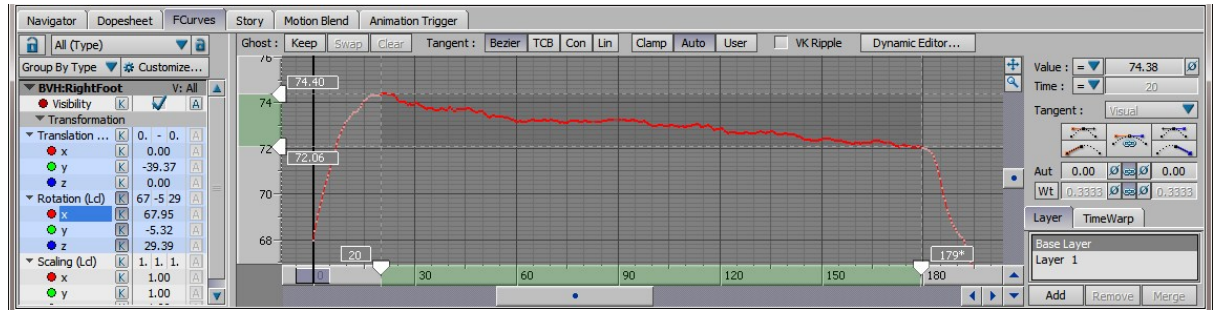


Figure 4.20: Subject en Pointe winged – right foot

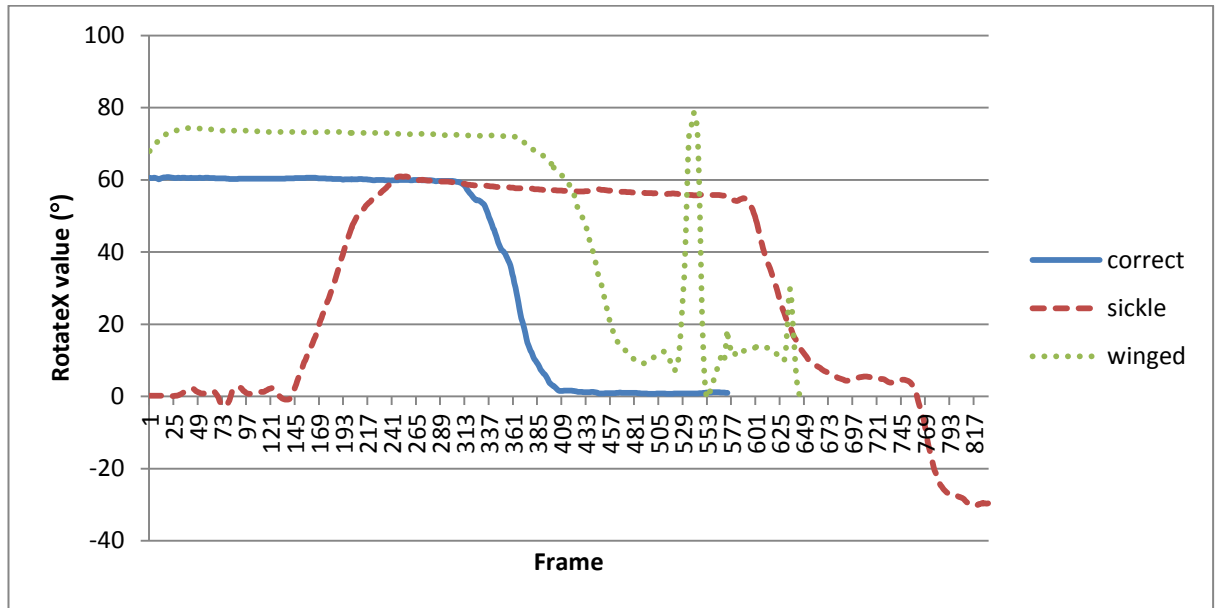


Figure 4.21: Subject en Pointe - animation curves

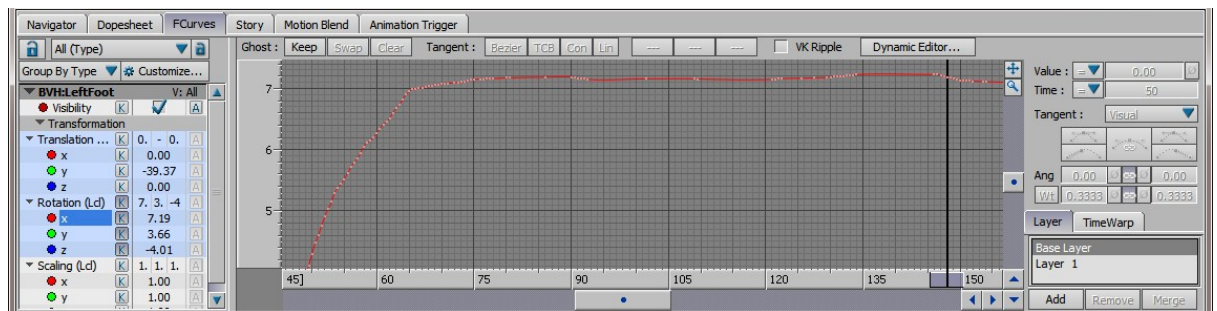


Figure 4.22: Subject in first position with correct alignment – left foot

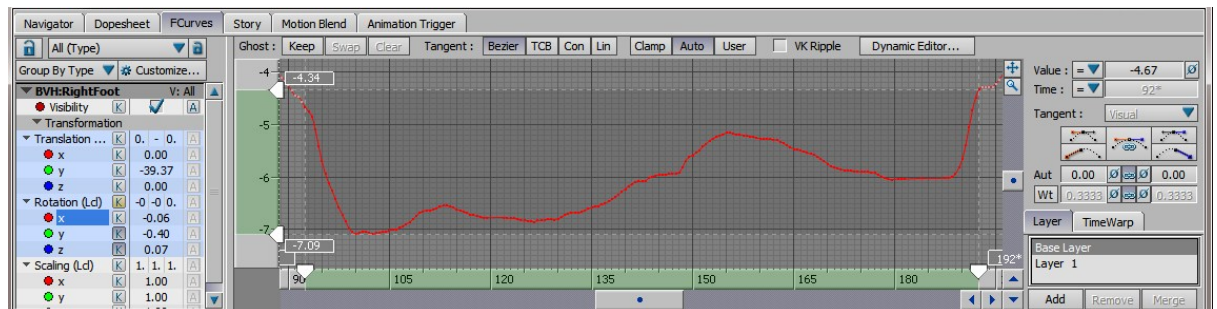


Figure 4.23: Subject in first position with sickle – right foot

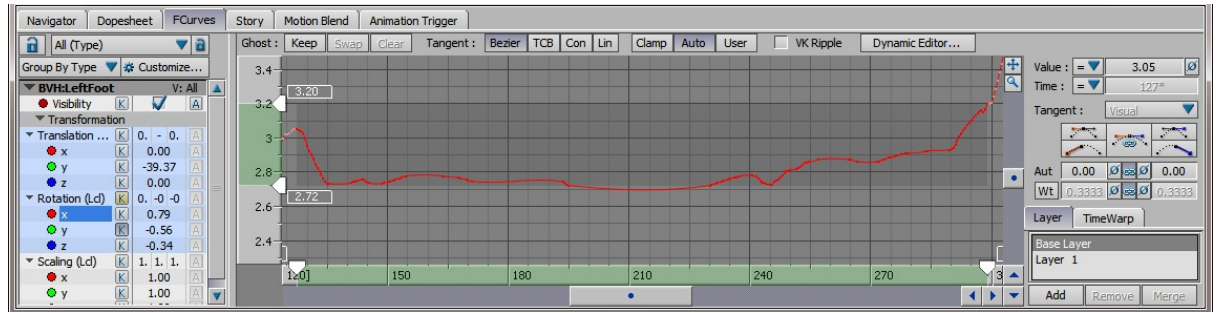


Figure 4.24: Subject in first position winged – left foot

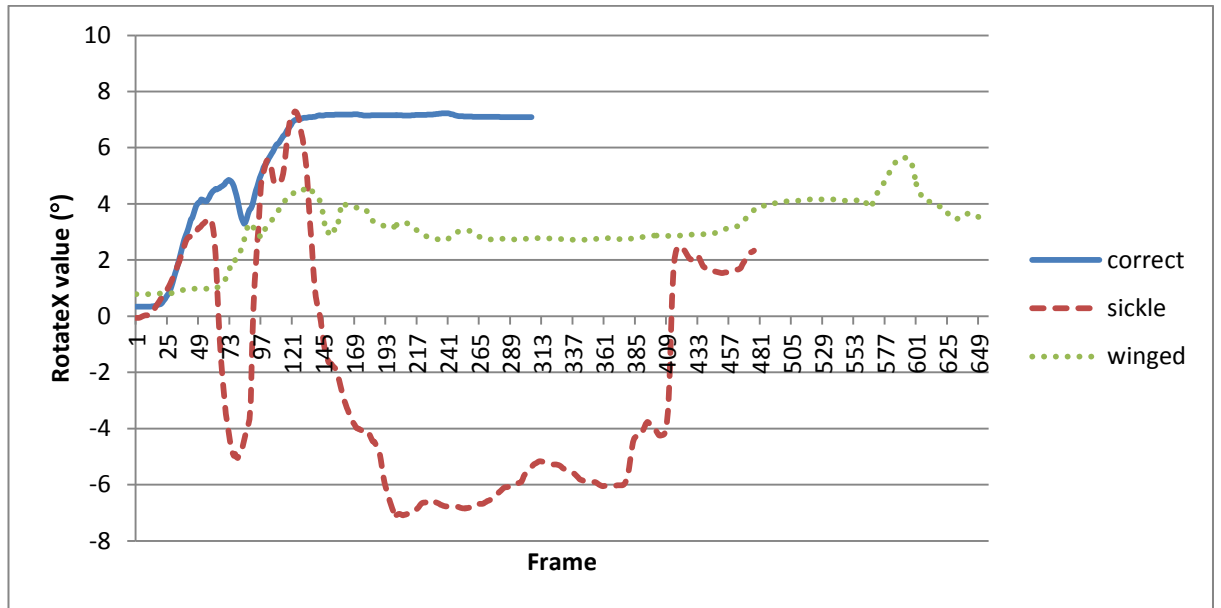


Figure 4.25: Subject in First Position - animation curves

The figures collectively show that the subtle changes in joint rotation that would affect performance, technique or injury, can be very accurately captured using the IGS-190 and can be identified mathematically from data curves and potentially from statistical models. This makes it possible for the technique of a ballet dancer, or any other performer or athlete to be recorded and analysed in order to identify where their technique can be enhanced.

It was shown in a study on lower extremity biomechanics that both plyometric and balance training can reduce lower extremity valgus measures (Myer et al., 2006). The ability of being able to identify winged or sickle positions in a dancer's technique as shown in this experiment would enable such training to be given.

Improving technique through corrective coaching may reduce the need for compensatory strategies triggered by limited lower limb extremities as was identified in a recent study (Steinberg et al., 2012). The identification and subsequent correction of poor joint alignment could therefore be used as a preventative measure to injury, as demonstrated by the very low

incidence of anterior cruciate ligament injuries among elite ballet and modern dancers (Liederbach et al., 2008).

Although the motion was captured in real-time for this experiment, feedback to the actor was not possible in real-time using this technique. It would require software to recognise changes in rotation values and assess whether there was fault in order for real-time feedback to be delivered. Further work is therefore planned to be carried out in order to develop these findings and incorporate a programme that will allow the real-time feedback of the subject's movement with a view to providing technique analysis and training.

It was clear from the second experiment that the motion data did not provide enough detail around the foot. Whilst the rotation values for the ankle were accurately recorded, this was the last joint with associated data values within the leg of the skeleton hierarchy.



Figure 4.26: First position – human subject



Figure 4.27: Demi-Pointe – human subject



Figure 4.28: Pointe – human subject

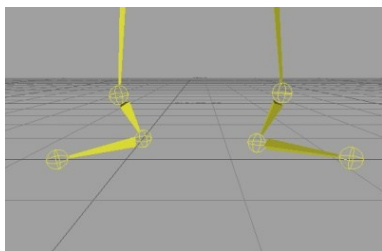


Figure 4.29: First position – virtual representation

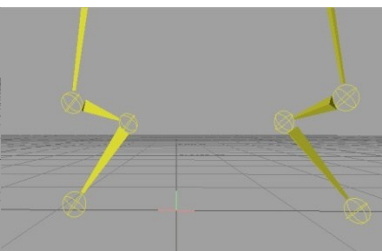


Figure 4.30: Demi-Pointe – virtual representation

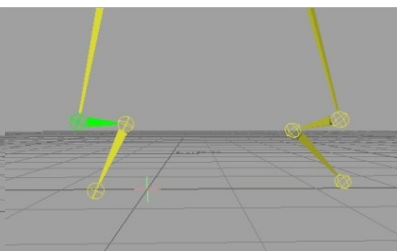


Figure 4.31: Pointe – virtual representation

As can be seen from figure 4.26 through to 4.31, the BVH data shows only the difference in the angle that the foot rises. The difference between demi-pointe and pointe positions in reality is clear from the set of joints at the base of the toes. In the current setup of the IGS-190 suit, the gyros placed at the lower leg and on the foot combine to give a rotation value for the ankle joint of the skeleton hierarchy, which is adequate for data recording for gait analysis. However, this forms the end of the joint hierarchy for the leg and neglects that there is a set of joints at

the base of the toes. As a result, this set of joints is not included in the header section of the BVH file and does not show on the reference skeleton hierarchy.

An additional sensor is to be considered for further testing to more accurately represent the anatomical alignment of the foot and produce more complete data for analysis. In addition, a reverse foot setup will be considered; a setup often used for manual animation of characters. This modification can be incorporated into the skeleton hierarchy to enhance the performance of the process and provide a more sophisticated rig for fault detection of ballet gesture.

4.3 Summary

This chapter has shown that a wireless gyroscopic sensor based system, namely the IGS-190 by Animazoo, can be used to record the extreme human movements such as displayed by ballet dancers. A suitable workflow has been established to detect misalignments in ankle position whilst performing gestures of relevé. Results have shown that subtle variations in joint rotation can be clearly measured and thus could be used to develop fault detection and isolation possibilities for injury prevention and improved performance. The limits of current techniques for real-time performance capture and suggestions for improvement were discussed. The next chapter shall introduce the application of recorded motion to a virtual character avatar.

5 Augmented Performance

Adding visual interest to a performance using CGI, or immersing a performer into a virtual environment has been the subject of much research and experimentation, see Azuma et al. (2001). Using motion capture to create a virtual performance (Haag, 2009), computer generated scenery on a live theatrical performance (Andreadis et al., 2010), and a virtual fashion show (Okada et al., 2006) have been the focus of previously mentioned articles. Further applications of immersive virtual environments are being researched; such as modelling human behaviour and reactions in dangerous environments (Kang et al., 2005), new educational approaches to scientific investigation (Lazoudis, 2011), and interactive museum experiences (Sparacino, 2004). The work in this chapter describes the translation of human motion recorded in real time applied to a virtual character within a virtual environment for the purpose of the presentation of augmented performance in arts and media.

5.1 The Uncanny Valley

When developing humanoid representation of real world performance, consideration must be given to the level of comfort and ease the viewer instinctively feels with the movement and form of the actor.

Japanese roboticist Doctor Masahiro Mori, while intending to provide an insight into human psychological reaction to robotic design, used the term 'the uncanny valley' to describe the negative response by a person observing something that is nearly human, but just enough off-kilter for it to appear eerie. The idea of the 'uncanny valley' (Mori, 1970) is that if one were to plot emotional response against similarity to human appearance and movement, there would not be a steady upwards curve. Instead, there would be a peak shortly before a completely human look, leading into a valley of strong negative response. Following the valley, a second peak is seen where resemblance to humanity is accomplished. The valley represents the point at which the person observing sees something nearly human, but just enough non-human for it to become sinister or repulsive. If an animation replicates our behaviour too exactly, it may lose the appeal of animation and become a dry simulation losing all visual and aesthetic interest. It has also been suggested that it is possible to overuse motion capture capabilities and to make an animated character too realistic (O'Rourke, 2003). Mori considers motion more important than appearance, though he does stress that both are affected by subtle nuances at least as much as by more striking factors.

The diagram below, figure 5.1, shows the curve of emotional response; the first peak representing the point where an individual sees something that is human enough to arouse some empathy, yet at the same time is not human enough to rouse a sense of wrongness. This first peak is followed by the 'uncanny valley' before rising again to the second peak which represents total acceptance.

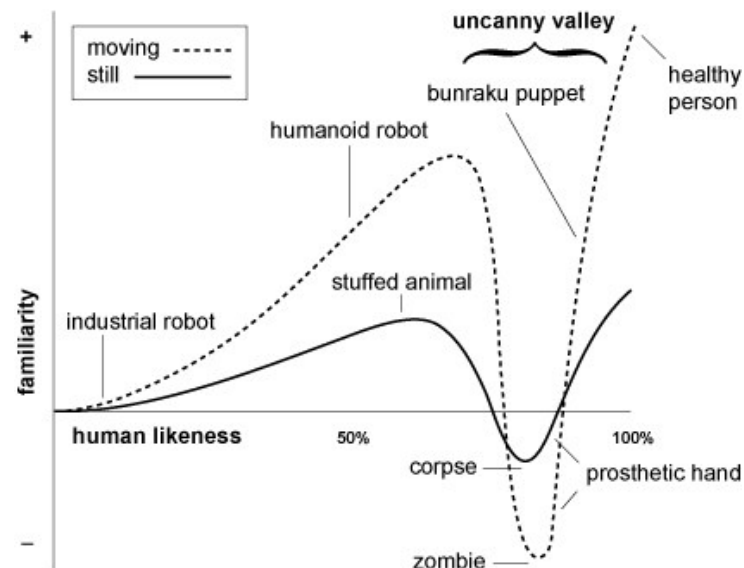


Figure 5.1: The uncanny valley (Ho and MacDorman, 2010)

The conclusion of Mori is that designers of robots or prosthetics should not strive overly hard to duplicate human appearance, but should be visibly artificial yet smart and stylish in appearance, putting it somewhere near the top of the first peak (Mori, 1970).

5.2 Application of Motion Data to a Character Avatar

An initial experiment was carried out to develop a workflow to apply pre-recorded motion data to a character avatar and immerse the character into a virtual environment. The motion recording of a male dancer from the Northern School of Dance was applied to a virtual character approximately matching his physical proportions using Autodesk's MotionBuilder and imported to a scene in Maya, see figure 5.2. The virtual environment was a night-time woodland scene in a fantasy world. The character was chosen based on the desire to have a non-human appearance, yet anatomically similar to the dancer's physical characteristics. A classical music audio track was added to the final rendered output video file. From carrying out this initial experiment, it became clear that motion data could be recorded, stored and later

used to create an animation directed by the creative influences of an individual or group to develop an augmented reality performance.



Figure 5.2: Virtual character animated using motion data within a virtual environment

A second experiment was subsequently arranged to explore the use of motion capture technology in an artistic scenario for the development of an augmented reality performance animation of an avatar within a virtual environment. The experiment was also expected to provide evidence of whether the ‘uncanny valley’ would have an effect on the viewer when the captured motion data was applied to a virtual character. It is anticipated that the end user of the performance analysis aspect of this research project will be from a performance or sports background, and therefore the final output is intended to be visually pleasing as well as effective as an analytical tool. The presentation of the data needs to be directed towards an athlete or an artistic viewer rather than an engineer or a scientist, hence the investigation into the visual acceptance of the reproduction of unadulterated human motion using a representative avatar.

A Clockwork Orange, written by Anthony Burgess and later filmed by Stanley Kubrick, offered a vision of Britain that was dystopian; blighted by gangs and ultra-violence. However, the film is based on the American version of the book, in which the redemptive chapter 21 is omitted. Burgess explained that when he first brought the book to an American publisher he was told that US audiences would never go for the final chapter, in which the lead character sees the

error of his ways, decides he has lost all energy and thrill from violence, and resolves to turn his life around. Professor Steve Hawley of the arts and media department at the Manchester Metropolitan University arranged a studio for two hours, late morning, for an actor to perform this omitted final scene. The motion of the actor would be recorded using the same techniques as used in the previously described experiments. The audio was to be recorded simultaneously and then combined with the render of the animated character post-production.

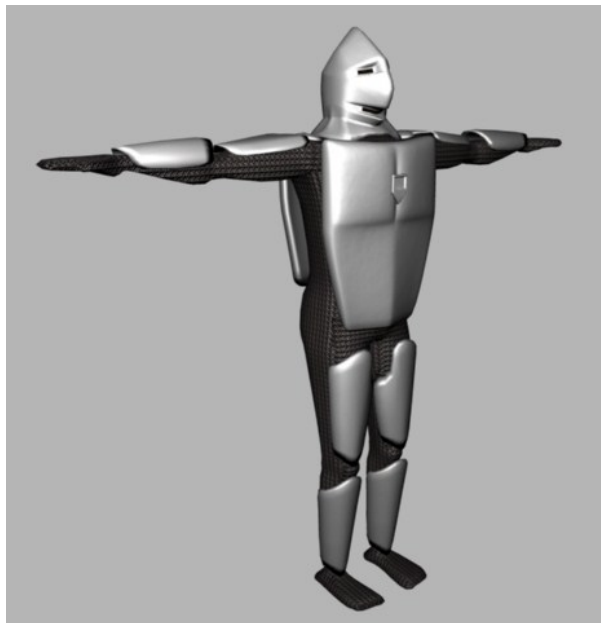


Figure 5.3: Knight model to be used for character animation

For artistic purposes, Prof. Steve Hawley decided upon a knight to be used as the virtual character for the experiment, and a character was subsequently modelled using Autodesk's Maya software (see figure 5.3).

The actor required that he could perform the scene unhindered by the equipment used to record his motion. The experiment required that the actor perform in a natural way and that there was a suitable reference point for which the sound could be synchronised with the rendered animation file. The inventory of equipment was the same used in the previous experiments and, on arrival at the studio, was set up as previously described. The only addition was the sound recording equipment, which was an omni-directional condenser microphone and digital audio recording device.

The motion recording commenced and was viewed in real-time using Animaview; proprietary software by Animazoo which although basic in appearance allows fast efficient real-time observations. At the start of the recording, a hand clap was accentuated by the actor in order

for the sound to be later synched to the motion recording. Following this, the actor played out the scene.

It was expected there would be some evidence of foot slipping and/or global positioning problems, and that the sound would synchronise with the rendered output without any problem. The experiment however, yielded some quite surprising results, highlighting a problem with the synchronisation of the sound with the rendered output that is discussed further in the results section.

5.3 Results and Discussion of Virtual Character Animation

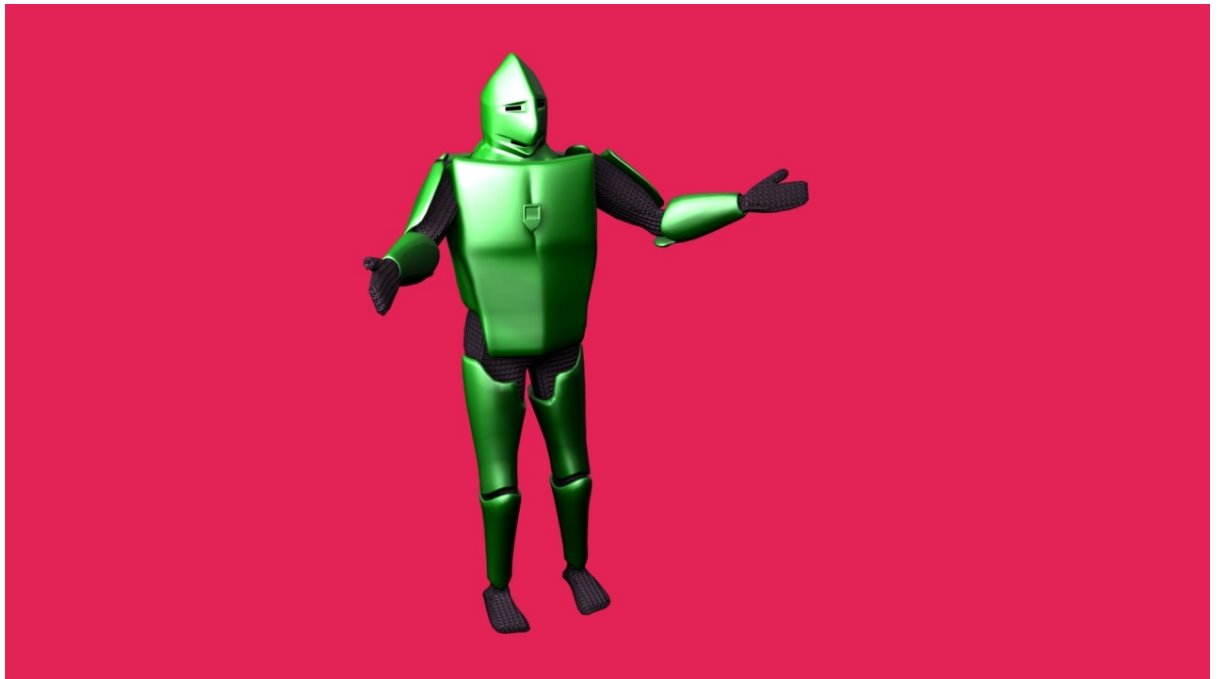
The initial experiment demonstrated that motion capture technology can be used effectively to animate an avatar within an augmented virtual reality performance. It shows that an actor or performer can perform the intended movement, which can be captured in real time and then stored and later applied to a virtual character within a virtual environment. The final experiment produced some quite unexpected results concerning the equipment performance and workflow. The purpose of the experiment was to explore the acceptance of a virtual character using human motion capture data and the effect of the uncanny valley for augmented reality performance.

In both experiments, the subjects were recorded at 120 fps, viewed live through Animaview and recorded to BVH file. The data that was captured was of high quality and when applied to the virtual character, aside from a little foot slippage and limb crossover, there were no unforeseen problems. The audio from the second experiment was recorded to an independent audio recorder through an omni-directional condenser microphone.

In order to gain an audience perception of the augmented reality performance, an initial black and white rendered video file was presented at an exhibition supported by the International Anthony Burgess Foundation. The video was seen by approximately 500 people, most of whom commented on the concept. Positive verbal feedback was given from the audience and there was no reported evidence of discomfort whilst viewing, as might be considered to be associated with the uncanny valley. This would suggest that, as the captured motion data was unadulterated and therefore accurate enough to have been accepted as true to life, the motion of the character would be beyond the uncanny valley, and that the character used for the animation was not life-like enough to go beyond the first peak and into the uncanny valley. As Mori suggests that motion is more susceptible to repulsion, in this experiment it was important that the motion and appearance of the character were at two distinct levels of

realism, so that the reaction of the viewer to the two elements could be suitably differentiated. As the animated character was well received by the audience, it can be accepted that this method of animation would be suitable for augmented performance.

Following the success of this exhibition, a higher resolution video file including colour to the knight and the background was presented at an international exhibition of contemporary art at the Bangkok Art and Culture Centre named 'possession'. A screen shot from the video file can be seen in figure 5.4 and a photograph taken from the exhibition can be seen in figure 5.5.



5.4: Virtual character animated using motion data within a virtual environment



5.5: Photograph taken at the 'Possession' exhibition at Bangkok Art and Culture Centre

The surprise came when attempting to synchronise the audio to the rendered video file. The hand-claps, which were obvious in both the audio and the video file, were co-ordinated but yet the two files did not stay in synch throughout the merged file. The audio file was noticeably shorter than the rendered video file, but yet this difference was at an inconsistent rate; the two files seemed to drift in and out of sync.

The original rendered video file was rendered at 24 fps, and it was considered that this may have been the issue with the timing; the conversion between the 120 fps that the motion was recorded at and the 24fps that the video was rendered at. A further two rendered video files were made, with each displaying the frame numbers at the bottom of the video. One was rendered at 30fps and the other was rendered at 25 fps. This however, still did not solve the problem, nor did it give any indication as to where the problem may lie.

It is planned that further experiments shall be carried out to investigate this problem, recording the motion at different frame rates, as well as looking at the render process and overall workflow. It is hoped that the cause of this unforeseen problem can be identified.

The application of unadulterated captured motion data to a virtual character did not display any signs of the 'uncanny valley' and was well received by the viewers. It is suggested that as the equipment setup records all movement (major and subtle), then the minor elements of chaotic and random movement that are part of realistic human motion, provide the viewer with a comfortable sense of acceptable human performance. It is anticipated that further work investigating the effects of presenting a more human-looking virtual character shall provide further discussion on the 'uncanny valley' theory.

5.4 Summary

This chapter has explored the phenomenon of the uncanny valley and investigated the perception of a virtual character, animated using unadulterated motion capture data and submersed within virtual environments. The audience perception was positive at two international exhibitions, and there was no evidence to suggest discomfort with augmented performance using this method. The next chapter will progress to produce a virtual character more alike to a real human subject using scanning methods.

6 Body Scanning

Work presented in this chapter describes a workflow developed to produce and animate a realistic virtual human for animation using motion capture. The production of the avatar uses infra-red depth sensing technology, commonly used in garment design, to produce a representative avatar of a scanned human subject. Several methods of constructing a clean polygonal character mesh from the scan data are trialled and discussed.

The preparation of the resulting character mesh for animation involves rigging techniques, such as a skeletal hierarchy and skin weighting, used within 3D animation and are optimised using Python scripts developed for this specific task. The report investigates how measurement data extracted by software that accompanies the body scanner can be used to place joints and assist the rigging process.

Motion capture data, pre-recorded using the IGS-190 inertial gyroscopic based suit, is successfully used to animate a representative avatar of a human subject in a realistic and natural way within a virtual 3D environment.

6.1 Scanning Process

In order to produce a mesh which accurately represented the actor, a body scanner was used; namely a [TC]² KX-16. The body scanner is a technology used commonly within the fashion industry for collecting measurements of the physique (Li and Li, 2010), which is then analysed for the purpose of garment design (Xu et al., 2002, Tyler et al., 2012), and sizing standards development (Loker et al., 2005, Wren, 2010). The non-contact, 3D measurement system is based on infrared depth sensing technology similar to that used in the Microsoft Kinect (Tong et al., 2012) and uses distance information from the depth sensor to produce a digital copy of surface geometry of the scanned object, similar to methods used for model reconstruction in archaeology (Doi et al., 2007). 3D images are taken of the body within seconds, generating a silhouette of the shape and an extensive list of actual body measurements; see figure 6.1.

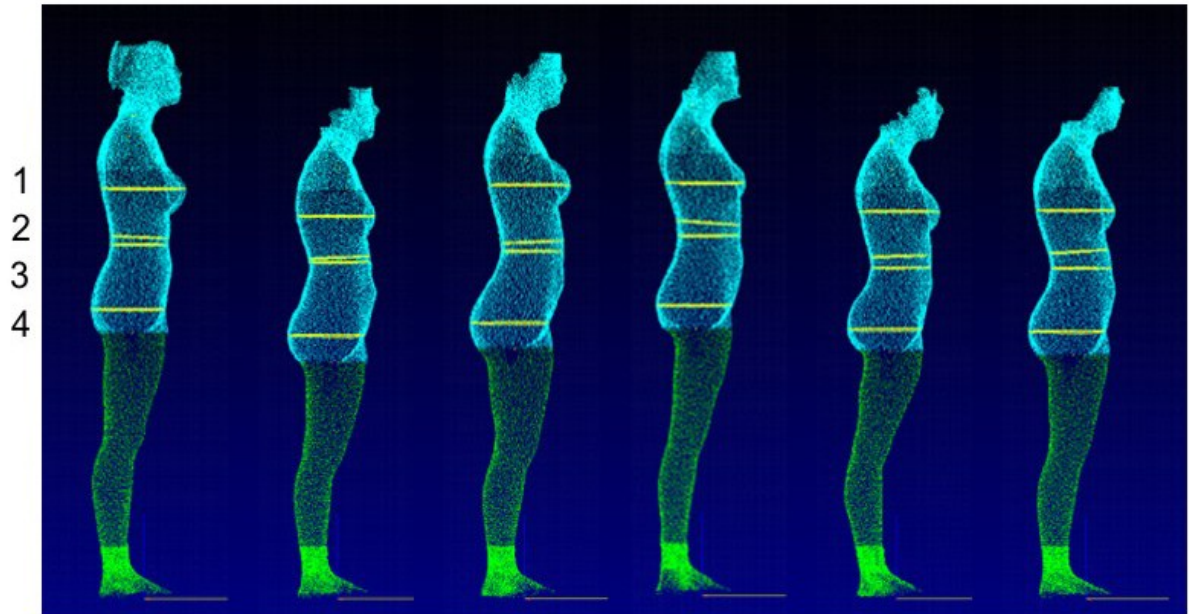


Figure 6.1: Scan data used for garment design (Tyler et al., 2012)
 Six subjects who would all be classified as size 12 from recent industry size specifications
 i.e. Measurements fall within range: Bust 89-93 cm, Waist 71-75 cm, Hip 96-100 cm.
 Subjects are between 19-22 years.
 Measurements shown are: 1. Bust, 2. Waist A (natural indent), 3. Waist B (small of back), 4. Hip

The test scanning session was planned for a midweek lunchtime and it was anticipated that it would take no longer than one hour to acquire the necessary data. Upon arrival at the scan site, it became apparent how compact the setup was. The scanner was no larger than a changing cubicle, and a desktop PC was connected to the side. The scanning process for taking measurements of the body requires the subject undresses down to underwear and that the underwear was of a neutral colour (grey, beige etc.). The subject to be scanned proceeded to change ready for the scan whilst the PC was booted. Three scans were taken in underwear, each taking eight seconds to complete. A further scan was taken in full clothing to examine whether the scan would produce a usable mesh for the animation of a clothed virtual character. Once the scan had completed after eight seconds, the data was immediately available for viewing; see figure 6.2. The scan data was available in a number of different file formats; .rbd (point cloud data), .wrl (VRML text data file), and .bin (depth scan image). The software also had a function that would use the scan data combined with a template polygon model of a human body to produce a smooth mesh based on the measurements taken from the scan. This was output in .obj file format.

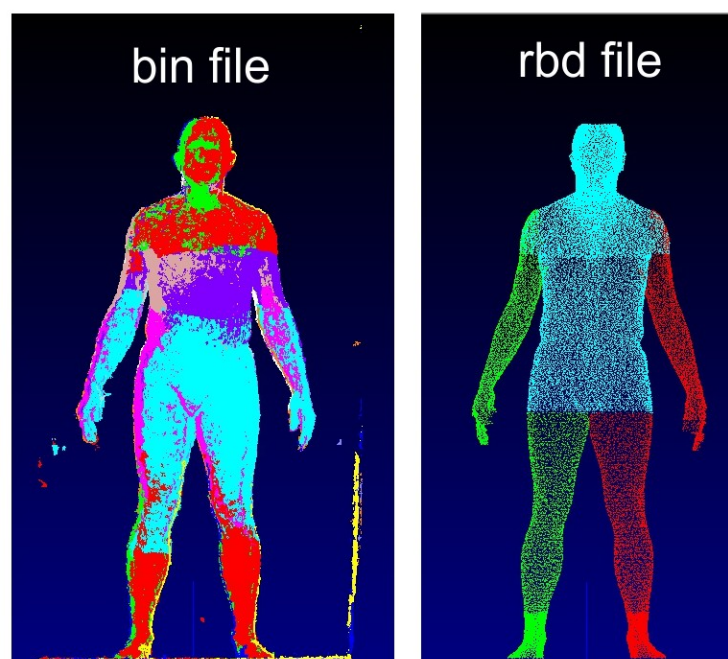


Figure 6.2: Depth scan image and point cloud data

The whole process took less than thirty minutes from arriving at the site to having the output files on a USB drive ready to take away. This process would be quicker with greater efficiency and experience of the workflow, and a large number of subjects could be scanned in a short period. The scanner itself can be made mobile with a setup and collapse time of only a few hours.

6.2 Constructing a Polygonal Mesh from the Scan Data

Once the scan data had been acquired, assessment was required to establish the most suitable method of producing a polygonal mesh that accurately represented the subject and could be animated by means of motion capture data with realistic deformation. A number of techniques were explored within a range of software using the different output files from the scan session.

The first attempt at reproducing a representative mesh of the subject used a piece of software called MeshLab. The software had the ability to import the .wrl and .obj file formats from the scan data acquisition; see figures 6.3 and 6.4. When importing the .wrl file format, the software takes the point cloud data points contained within the .wrl file (in coordinates in the X, Y and Z-axis) and joins the points together forming edges and polygonal faces. There are a number of tools within the software which can be used to attempt to 'clean up' the mesh such as removing duplicate or null faces, merging close vertices and flipping faces whose normals

are opposite to all of its adjacent faces. The software was found to be somewhat unreliable and had the tendency to crash when multiple operations were performed. It did however, have the ability to export the mesh to different file formats such as .ply, .obj and .u3d, which could be recognised by other software.

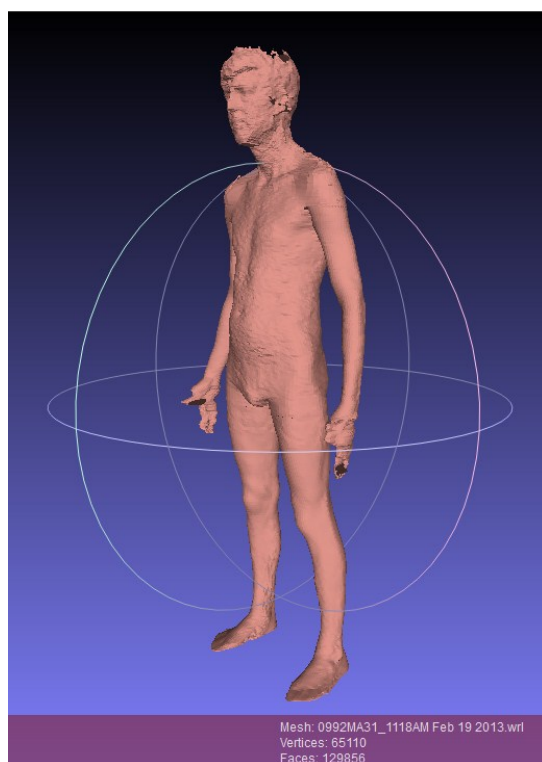


Figure 6.3: MeshLab wrf import

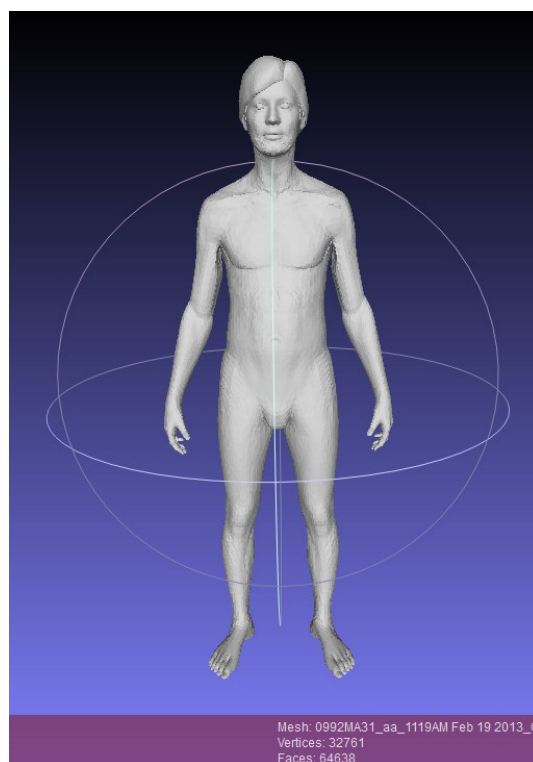


Figure 6.4: MeshLab obj import

The second piece of software that was used was Pixologic's ZBrush; this had the ability to import the .obj file from the data collected at the scan session and the .wrl file converted to the .obj file through MeshLab; see figures 6.5 and 6.6. ZBrush is a powerful sculpting tool used extensively for character creation. It was anticipated that the rather rough looking .wrl conversion could be smoothed using the tools within ZBrush, and that the inbuilt re-topologising plug-in 'QRemesher' would allow either mesh to be optimised for animation.

The smoothing of the converted .wrl data was a painstaking process, which required a great deal of skill and time, and was subject to deviation from the measurements taken from the scan of the subject. The results of this were less visually pleasing than the smoothed .obj file produced from the scanner software and, dependant on the artist that sculpts the converted .wrl file, is not as accurate a representation of the subject. In addition, this is a much longer process in contrast to the smoothed .obj file being available almost instantly from the scanner software.

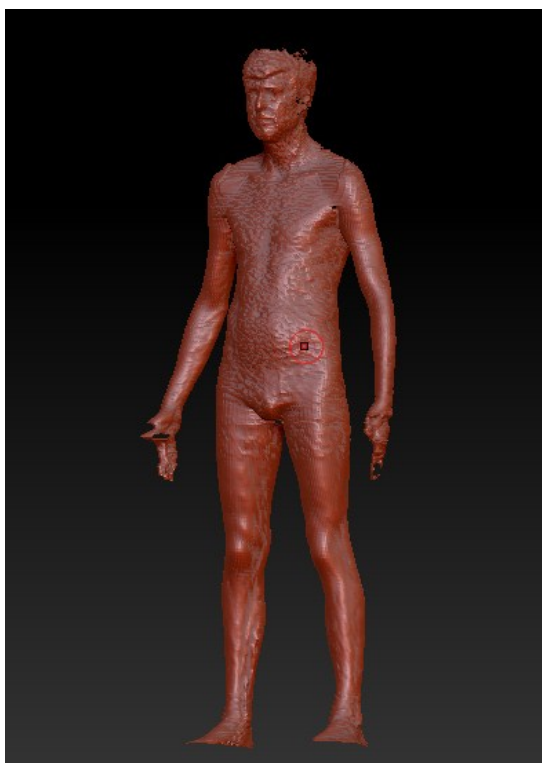


Figure 6.5: ZBrush wrl-obj import

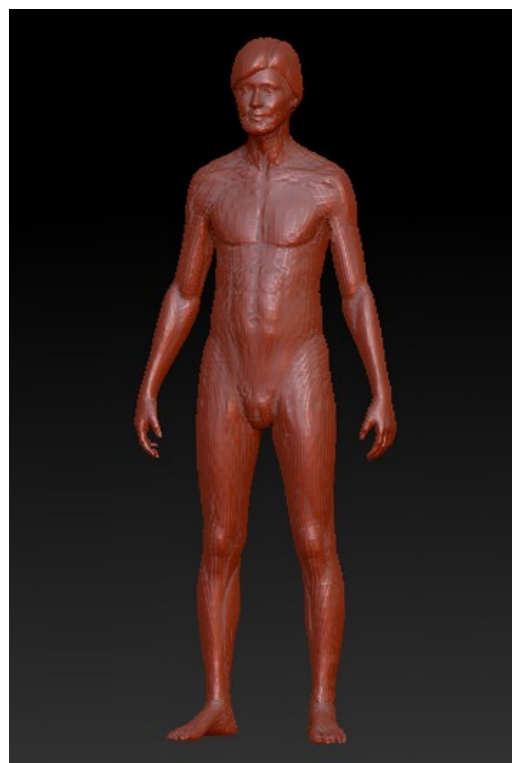


Figure 6.6: ZBrush obj import

It was concluded from this that the most suitable workflow for creating a representative polygonal mesh of a subject was to use the software supplied with the scanner. Although it lacks the subtle individual characteristics of the subject, it quickly produces a proportionally accurate representation. It would take a very skilled 3D artist a long time to produce a model that would contain the subtle individual characteristics of a subject and potentially at a cost of a less proportionally accurate model. This is not to say that this method does not have its issues. As it was evident from the .wrl import to MeshLab, there are problems accurately scanning the hands, feet and head. This can be explained because of the positioning of the sensors and their inability to capture the intricate details between the fingers and the limitations of scanning the base of the feet and top of the head. The software that creates the smoothed mesh from the scan data tackles this problem by using pre-made hands, feet and head models, and attaches these to the body mesh. This results in the head, hands and feet not being actual representations of the subject's relative surface geometry and there is a split in the combined mesh at the neck. The software also attaches a hairstyle to the mesh. The separated elements of the head and hairstyle from the neck split can be seen in figure 6.7.

In order to correct these issues, the mesh can be imported in the .obj file format into Autodesk's Maya software. There were minor surprising results in the import of the mesh to Maya. It appears that the global axis and scaling units differ in the scanner software and Maya,

as the character was imported sideways into Maya and was relatively very large. The character had to be resized and oriented to fit the Maya scene with rotations of -90° in the X and Y axis and scaling at 0.01 in the X, Y and Z (effectively scaling from millimetres to decimetres). The transformations were then frozen to give the mesh a clean history point from which to begin. As this would be an inconvenient, yet necessary step with the import of any character from a scanned .obj mesh, a work around was developed in the form of a MEL script (Maya Embedded Language). This script can be saved to the interface tool shelf within the software so the same collective operation can be carried out with the simple click of a button. The script is as follows:

```
#select by type geometry in scene
select `ls -geomtery`;
#perform transforms
rotate -90deg -90deg 0;
scale 0.01 0.01 0.01;
#freeze transforms to reset the origin point
FreezeTransformations;
#clear selection
select -clear;
```

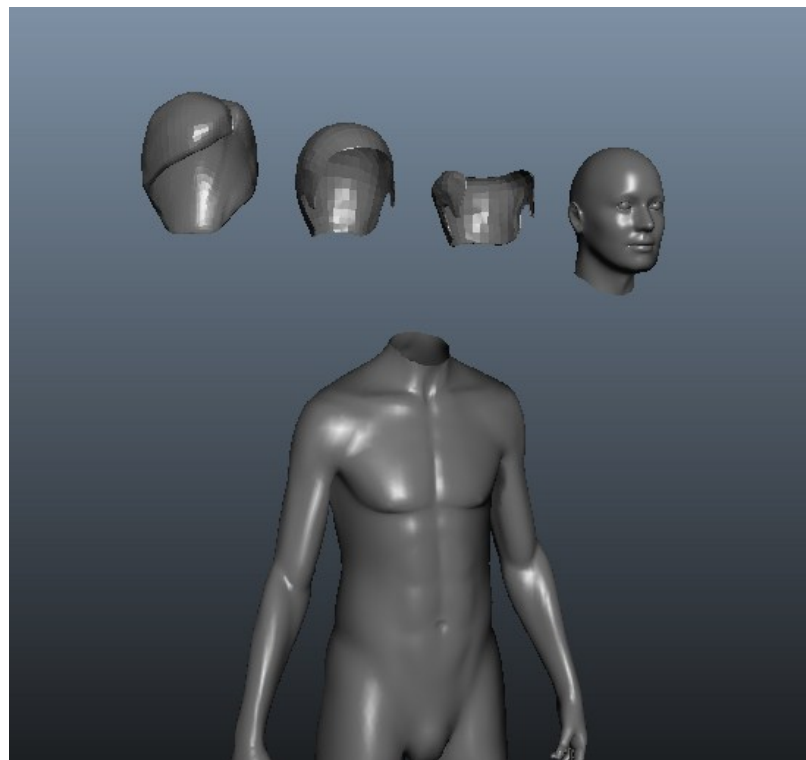


Figure 6.7: Separated parts of the combined mesh

The neck split can be stitched and the edges softened using a MEL script (see below) which merges all vertices at a specified distance apart and makes soft an edge if the angle between two owning facets is flatter (smaller) than the specified smoothing angle. Any further problematic geometry can then be corrected manually or by using the cleanup tool.

```
#select by type geometry in scene
select `ls -geometry`;
#merge vertices within close proximity with construction history off
polyMergeVertex -d 0.001 -am 1 -ch 0;
#smooth edge at a smoothing angle of 180 degrees
polySoftEdge -a 180 -ch 0;
#clear selection
select -cl;
```

Along with the smoothed polygonal mesh produced by the software, a UV map is also produced for the model; see figure 6.8. This is particularly useful for texturing the model. It can be quite an arduous task laying out a model's UV map, particularly on an organic model so complex. To have this UV map produced to compliment the model saves a lot of time and would enable a quick turnaround mapping a photograph of the subject to the virtual characters' mesh.

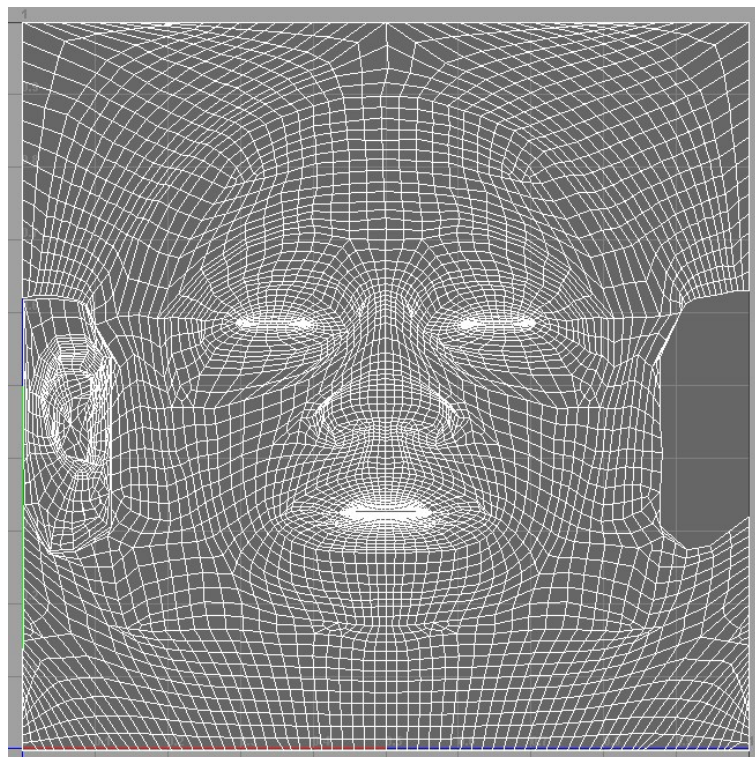


Figure 6.8: UV map of face

6.3 Rigging the Character for Animation

Once the character shell was complete, the next stage was to develop a rig with a joint hierarchy suitable for animation by motion capture. The conventional way of doing this is with the character in a 'T-pose', however, because of the way the body scanner worked it was necessary to do this with the character shell in a pose with the arms by its side. This resulted in a number of problems. When placing the joints for the arms and hands with the character in a T-pose, it is a simple process to view from the top orthographic view and work down the arms. The joints automatically snap to the base of the grid (Y axis at 0). Once the joint chain has been lined up from the top view with the arm, the joint chain can simply be translated up the Y-axis to fit into the geometry with minimal fuss. With the character's arms by the side of the body and not horizontal within the scene, this process was not possible and each joint had to be lined up within the geometry using a combination of the orthographic views and perspective view. This was rather a time consuming and intricate process, particularly for the fingers. The finished skeletal hierarchy can be seen in figure 6.9. The joints were named according to Autodesk's MotionBuilder naming convention so the characterisation process within that software would be straightforward.

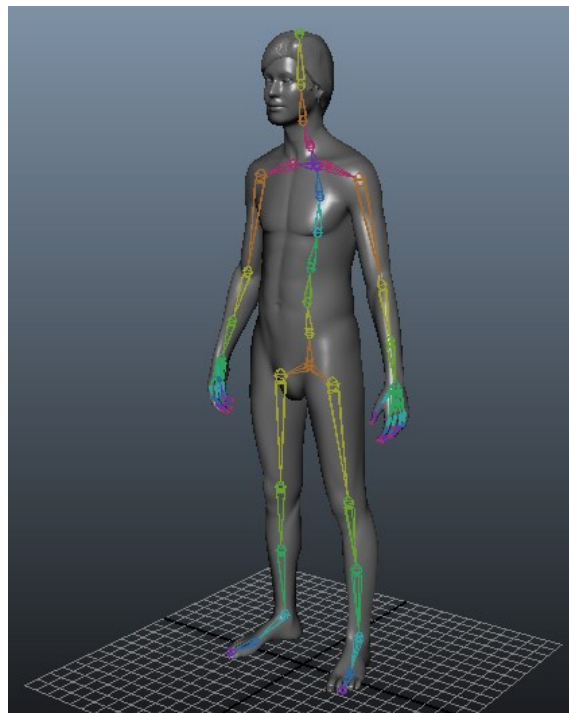


Figure 6.9: Skeletal rig

No motion data is recorded for the fingers in the current workflow; however, joints were added to the fingers in order to enable the possibility of adding secondary animation to the hands such as the flexing and curl of the fingers. This is not absolutely necessary for the investigation of joint alignment in the lower limbs of ballet dancers but the workflow was explored to determine the suitability for other sports or performing arts analysis in future research.

As part of the scanning process, the software that accompanies the scanner records a number of measurements of the subject. From these measurements, a number of joint locations are calculated and stored within a text file in the output folder of the scan. The first line of the text file reads "l_hip -15.22 127.56 952.51". Separated by a space, the first part is the name of the joint followed by the co-ordinates in units of centimetres in the order front, left, up.

Maya has the ability through Python scripting to read from a text file and use the data to place objects within the scene. It was considered that it might be possible to use this joints file to place the joints for the character rig. A script was written (see below) to initially place locators at each of the joint positions calculated by the scanner from the output text file.

```
{
    string $filename = "H:/My Documents/PhD/Scan Data/Scan Measurement
Data/0992MA31_aa_1119AM Feb 19 2013.joints";
    int $fileId = `fopen $filename "r"`;
    if (!`filetest -f $filename`) error "Specified File not Found!";
    while (!`feof $fileId`)
    {
        string $nextLine = `fgetline $fileId`;
        string $tokens[];
        while (size($nextLine) > 0)
        {
            string $cleanLine = strip($nextLine);
            tokenize $nextLine " " $tokens;
            string $name = $tokens[0];
            float $z = $tokens[1];
            float $x = $tokens[2];
            float $y = $tokens[3];
            spaceLocator -n $name -p ($x / 100) ($y / 100) ($z / 100);
            $nextLine = `fgetline $fileId`;
        }
    }
}
```

```

    }
}
fclose $fileId;
}

```

This script successfully placed locators within the Maya scene which lined up with the character mesh, seen in figure 6.10. It can be noted that the orientation axis and scaling differences between the software has been addressed within the script by reordering the ZXY from the scanner (front, left, up) to the XYZ order used in Maya and converting centimetres to metres by division of 100.

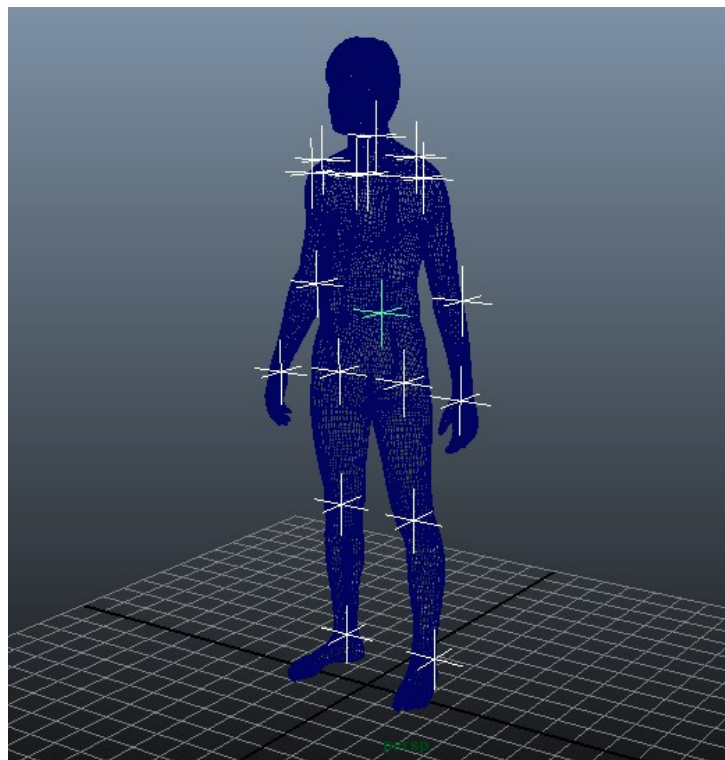


Figure 6.10: Locators places at joint positions

The script was then modified slightly, replacing 'spaceLocator' with 'joint', to place joints at the locations specified in the text file. A significant problem was encountered here, in that the joints were parented in the order that they were introduced (as is the case when constructing a joint chain in Maya). The script was again amended, and is shown below, to place the joints with no hierarchical chain by clearing the selection between creations (since creating a new joint leaves it selected, subsequent creations are parented to the previous one). The results of the former and latter mentioned scripts can be seen in figures 6.11 and 6.12 respectively.

```

{
    string $filename = " H:/My Documents/PhD/Scan Data/Scan Measurement
Data/0992MA31_aa_1119AM Feb 19 2013.joints ";
    int $fileId = `fopen $filename "r"`;
    if (!`filetest -f $filename`) error "Specified File not Found!";
    string $locators[] = {};
    while (!`feof $fileId`)
    {
        string $nextLine = `fgetline $fileId`;
        string $token[];
        while (size($nextLine) > 0){
            string $cleanLine = strip($nextLine);
            tokenize $nextLine " " $token;
            string $name = $token[0];
            float $z = $token[1];
            float $x = $token[2];
            float $y = $token[3];
            select -clear;
            string $j = `joint -n $name`;
            move ($x / 100) ($y / 100) ($z / 100) $j;
            $nextLine = `fgetline $fileId`;
        }
    }
    fclose $fileId;
}

```

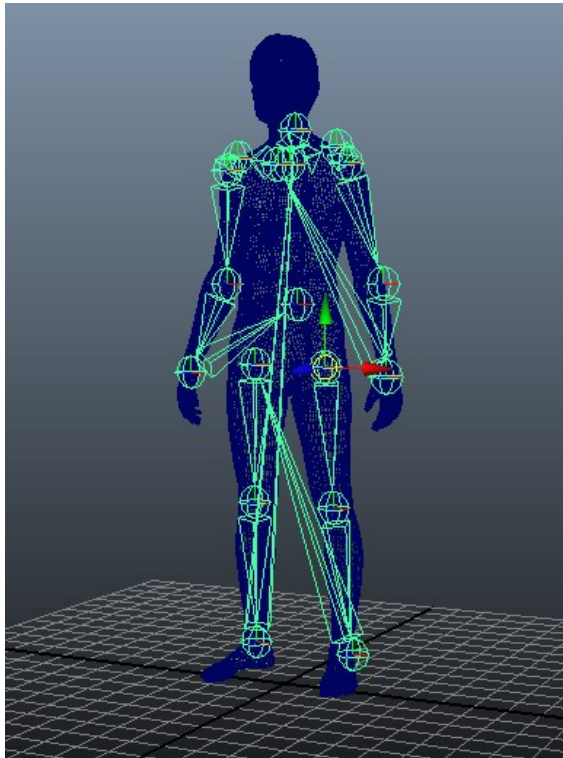


Figure 6.11: Chain of joints drawn

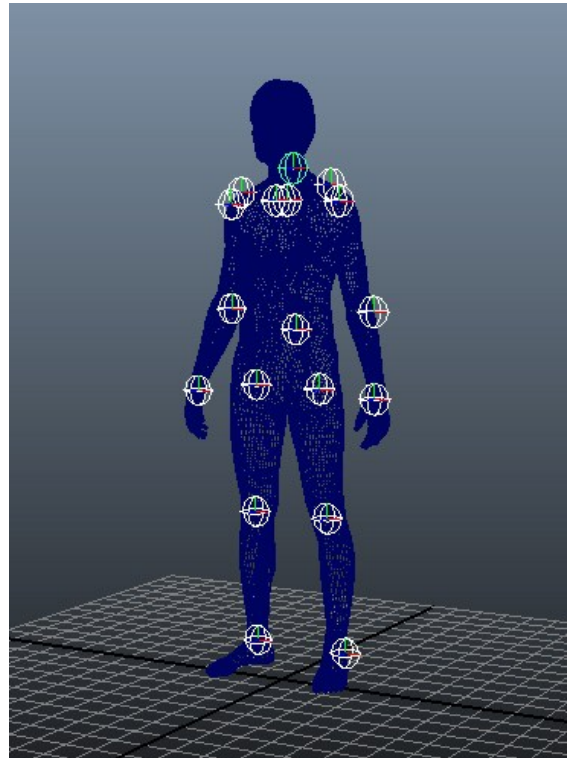


Figure 6.12: Individual joints placed

Although the scripts do not construct the ideal skeleton hierarchy for the purpose of animation through motion capture, they provide a good starting point for the placement of joints saving much time in the rigging process. Manual adjustments need to be made to the placement of some of the joints and a number of joints need to be added to complete the skeletal rig. The joints also need to be renamed to follow the MotionBuilder naming convention in order for the characterisation process to be straightforward.

Once the skeleton had been added to the mesh, it needed to be bound to the geometry in order for it to move and deform with the animation of the skeleton. A smooth bind operation with adjusted skin weighting was used for this process.

Usually skin weighting is a relatively straightforward process and although subject to the artists/animators preference, a usable bound mesh can be created with relative ease to produce visually acceptable results. Again, due to the character having its arms by the side rather than in a T-pose, this proved somewhat problematic. When the shoulder joint was rotated to move the arms up to the T-pose, it became evident that the close proximity of the arm and hand joints to the body had caused joint influence to be attached to the side of the torso of the character. As the arms moved up, the sides of the character followed, which is illustrated in figure 6.13. This had to be manually corrected using a combination of tools within

Maya (component editor and paint skin weights tool) and was once again a time consuming and intricate process. The skin weighting profile for the character can be saved to an xml data file with the weighting values corresponding to the vertex index. As the avatar is generated from a template mesh, subsequent avatars will share the same topology and the weighting values can be mapped onto a new character using this xml file. The mesh with corrected skin weighting can be seen in figure 6.14.

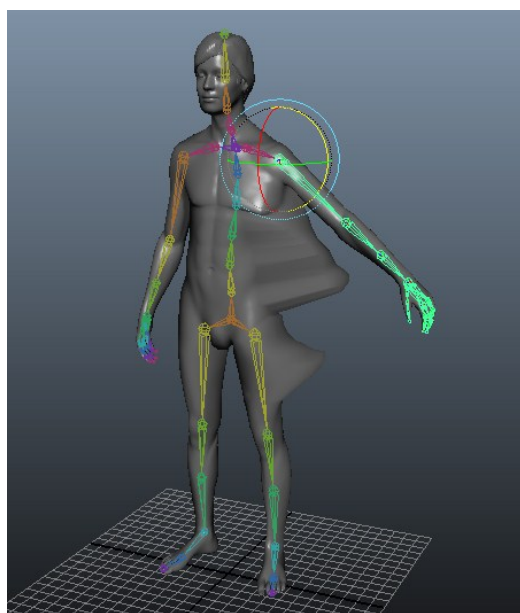


Figure 6.13: Default skin weighting

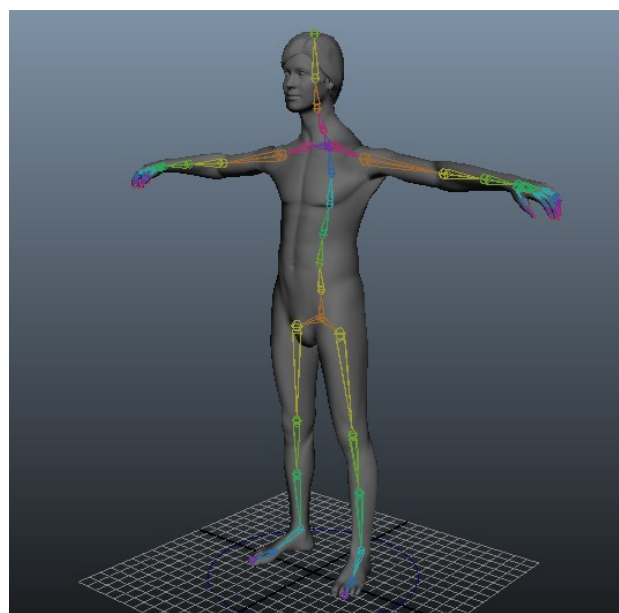


Figure 6.14: Adjusted skin weighting

Once the skin weighting was complete, the character was set in a T-pose and a master node was added to allow the character to be scaled and moved between software without problem; Autodesk's MotionBuilder, which is used to apply the captured motion data, uses metre units as opposed to decimetres which Maya uses.

The mesh, skeleton hierarchy and master node was grouped accordingly and exported to .fbx file format, which can be imported into MotionBuilder.

6.4 Animating the Character

Within MotionBuilder, the rigged mesh was characterised to a biped character template, which is as simple as dragging and dropping the template onto the avatar since the naming convention was followed earlier. The new character appears in the Navigator section of the software and can be named accordingly. A pre-recorded motion capture file was then imported into the scene from .bvh file format. This brings a skeleton into the scene defined by the header section of the .bvh file. In order for the .bvh file to drive the animation of the

avatar, the skeleton associated with the .bvh motion capture file also needed to be characterised. To do this, the joints need to be set to zero rotation values and the arms need raising so the skeleton is in a similar T-pose to the avatar. A biped character template can then be dropped onto it, and the character can be named in the navigator.

Under the character settings for the avatar, the input type can now be changed to 'character' and the input source can be defined as the .bvh character. This associates the animation from the captured motion data within the .bvh file to the avatar. The results of the motion data driven avatar can be seen in figure 6.15.



Figure 6.15: Avatar driven by dance capture

The animation can then be plotted to the joints within the avatar in order for it to be taken from MotionBuilder and back into Maya without the necessity of the .bvh file being present.

6.5 Conclusion

The above investigation describes the workflow used to create a virtual character, which accurately represents the form of a scanned subject. This avatar can then be animated using motion recorded from the same subject using the IGS-190 motion capture suit and viewed in real-time within a virtual environment.

It has been shown that a proportionally accurate character avatar with clean topology suitable for animation can be created using depth sensor body scanning.

6.6 Summary

A template character mesh was sized according to measurements of a subject calculated by the [TC]² KX-16 software. This mesh was then cleaned up for animation using MEL scripting. A joint hierarchy was placed within the mesh combining a Python script, which identified and placed joints at locations taken from the body scanner, and manual rigging methods. The character mesh was then bound to the skeleton and geometry deformations were controlled by manual skin weighting methods. The skin weighting profile was saved to a data file for use in future avatar development. The rigged character was then animated within a virtual environment using inertial motion capture of a human performer.

7 Analysis of Recorded Character Motion

This chapter provides an explanation of the necessary theory for mathematical methods of analysing the data which is recorded during a motion capture session. It serves as a foundation for error detection and evaluation of alignment of a specified joint in order for knowledge of performance to be attained so that augmented feedback can be provided. The composition of matrices which are used to store translational information within Maya is described, and a Python script is developed to decompose these matrices and output values specific to the orientation of a named joint.

For reference, an explanation of vectors and matrices can be found in appendix 11.1 and 11.2 respectively.

7.1 Matrix Composition in Maya

In Maya, any object within a scene has transform information that describes its scale, shear, rotation and translation. The transformation information for the node is represented as a 4x4 transformation matrix. A transformation matrix is composed of the following components:

[Sp]	Scale pivot point	point around which scales are performed
[S]	Scale	scaling about x, y, z axes
[Sh]	Shear	shearing in xy, xz, yx
[St]	Scale pivot translation	translation introduced to preserve existing scale transformations when moving pivot. This is used to prevent the object from moving when the objects pivot point is not at the origin and a non-unit scale is applied to the object
[Rp]	Rotate pivot point	point about which rotations are performed
[Ro]	Rotation orientation	rotation to orient local rotation space
[R]	Rotation	rotation
[Rt]	Rotate pivot translation	translation introduced to preserve existing rotate transformations when moving pivot. This is used to prevent the object from moving when the objects pivot point is not at the origin and the pivot is moved
[T]	Translate	translation in x, y, z axes

Note that the default rotation order is kXYZ.

The matrices are post-multiplied in Maya. For example, to transform a point P from object-space to world-space (P') you would need to post-multiply by the world matrix. ($P' = P \times WM$).

The transformation matrix is then constructed as follows:

$$[Sp]^{-1} \times [S] \times [Sh] \times [Sp] \times [St] \times [Rp]^{-1} \times [Ro] \times [R] \times [Rp] \times [Rt] \times [T]$$

where 'x' denotes matrix multiplication and '-1' denotes matrix inversion.

Sp =	1	0	0	0
	0	1	0	0
	0	0	1	0
	spx	spy	spz	1

S =	sx	0	0	0
	0	sy	0	0
	0	0	sz	0
	0	0	0	0

Sh =	1	0	0	0
	shxy	1	0	0
	shxz	shyz	1	0
	0	0	0	1

St =	1	0	0	0
	0	1	0	0
	0	0	1	0
	sptx	spty	sptz	1

Rp =	1	0	0	0
	0	1	0	0
	0	0	1	0
	rpx	rpy	rpz	1

Rt =	1	0	0	0
	0	1	0	0
	0	0	1	0
	rptx	rpty	rptz	1

$$Ro = AX * AY * AZ$$

AX =	1	0	0	0
	0	cx	sx	0
	0	-sx	cx	0
	0	0	0	1

AY =	cy	0	-sy	0
	0	1	0	0
	sy	0	cy	0
	0	0	0	1

AZ =	cz	sz	0	0
	-sz	cz	0	0
	0	0	1	0
	0	0	0	1

$$sx = \sin(rax), cx = \cos(rax)$$

$$sy = \sin(ray), cy = \cos(ray)$$

$$sz = \sin(raz), cz = \cos(raz)$$

$$R = RX * RY * RZ \text{ (Note: order is determined by rotate order)}$$

RX =	1	0	0	0
	0	cx	sx	0
	0	-sx	cx	0
	0	0	0	1

RY =	cy	0	-sy	0
	0	1	0	0
	sy	0	cy	0
	0	0	0	1

RZ =	cz	sz	0	0
	-sz	cz	0	0
	0	0	1	0
	0	0	0	1

sx = sin(rx), cx = cos(rx)

sy = sin(ry), cy = cos(ry)

sz = sin(rz), cz = cos(rz)

T =	1	0	0	0
	0	1	0	0
	0	0	1	0
	tx	ty	tz	1

7.2 Rotations and Matrices

Determination of Euler angles is sometimes a necessary step in computer graphics, vision, robotics, and kinematics. We start with the standard definition of the rotations about the three principle axes.

A rotation of ψ radians about the X-axis is defined as:

$$R_x(\psi) = \begin{bmatrix} 1 & 0 & 0 \\ 0 & \cos \psi & \sin \psi \\ 0 & -\sin \psi & \cos \psi \end{bmatrix}$$

Similarly, a rotation of θ radians about the Y-axis is defined as:

$$R_y(\theta) = \begin{bmatrix} \cos \theta & 0 & -\sin \theta \\ 0 & 1 & 0 \\ \sin \theta & 0 & \cos \theta \end{bmatrix}$$

Finally, a rotation of φ radians about the Z-axis is defined as:

$$R_z(\varphi) = \begin{bmatrix} \cos \varphi & \sin \varphi & 0 \\ -\sin \varphi & \cos \varphi & 0 \\ 0 & 0 & 1 \end{bmatrix}$$

The angles ψ , θ , and φ are the Euler angles.

Using the Maya documentation, we find that the rotation matrix is the result of multiplying three different matrices together; one for X, one for Y and one for Z. The order in which these matrices are multiplied together is the rotation order.

The above are the individual matrices for the X rotation, the Y rotation and the Z rotation represented as angles. To get the rotation matrix for a transform with XYZ rotation order, you multiply these matrices together in that order.

$$R = Rx(\psi)Ry(\theta)Rz(\varphi)$$

The fact that they get multiplied in this order comes from the fact that a row-major convention is being used. If a column-major convention were being used then the order of the matrix multiplication here would be reversed.

$$= \begin{bmatrix} \cos \varphi \cos \theta & \sin \varphi \cos \psi + \cos \varphi \sin \theta \sin \psi & \sin \varphi \sin \psi - \cos \varphi \sin \theta \cos \psi \\ -\sin \varphi \cos \theta & \cos \varphi \cos \psi - \sin \varphi \sin \theta \sin \psi & \cos \varphi \sin \psi + \sin \varphi \sin \theta \cos \psi \\ \sin \theta & -\cos \theta \sin \psi & \cos \theta \cos \psi \end{bmatrix}$$

This process makes it quite easy to get the rotation matrix from the Euler rotation angles carried out in whichever order they are applied; in this case XYZ. Simply calculate the cos and sin for the X, Y and Z angles, and work them into the equation above.

Converting from the matrix to Euler angles however, is a little more complicated.

$$\text{Given the rotation matrix } R = \begin{bmatrix} R_{11} & R_{12} & R_{13} \\ R_{21} & R_{22} & R_{23} \\ R_{31} & R_{32} & R_{33} \end{bmatrix}, \text{ we can compute the Euler angles by}$$

equating each element in R , with the corresponding element in the matrix product $Rz(\varphi)Ry(\theta)Rx(\psi)$. Notice this time that the order for decomposition is ZYX. This is a mirror of the composition order due to matrix multiplication being non-commutative. This results in nine equations that can be used to find the Euler angles.

$$\begin{bmatrix} \cos \theta \cos \varphi & \cos \theta \sin \varphi & -\sin \theta \\ \sin \psi \sin \theta \cos \varphi - \cos \psi \sin \varphi & \sin \psi \sin \theta \sin \varphi + \cos \psi \cos \varphi & \sin \psi \cos \theta \\ \cos \psi \sin \theta \cos \varphi + \sin \psi \sin \varphi & \cos \psi \sin \theta \sin \varphi - \sin \psi \cos \varphi & \cos \psi \cos \theta \end{bmatrix} =$$

$$Rz(\varphi)Ry(\theta)Rx(\psi) = R$$

Starting with R_{13} , we find

$$R_{13} = -\sin \theta \quad \text{Equation 1}$$

which can be inverted to yield $\theta = -\sin^{-1}(R_{13})$

However, one must be careful in interpreting this equation. Since $\sin(\pi - \theta) = \sin(\theta)$ there are actually two distinct values (for $R_{13} \neq \pm 1$) of θ that satisfy equation 1. Therefore, both equations 2 and 3 are valid solutions.

$$\theta_1 = -\sin^{-1}(R_{13}) \quad \text{Equation 2}$$

$$\theta_2 = \pi - \theta_1 = \pi + \sin^{-1}(R_{13}) \quad \text{Equation 3}$$

To find the values for ψ , we observe that $\frac{R_{23}}{R_{33}} = \frac{\sin \psi \cos \theta}{\cos \psi \cos \theta} = \tan \psi$

We use this equation to solve for ψ , as

$$\psi = \arctan 2(R_{23}, R_{33}) \quad \text{Equation 4}$$

Where $\arctan 2(y, x)$ is arc tangent of the two variables x and y . It is similar to calculating the arc tangent of y/x , except that the signs of both arguments are used to determine the quadrant of the result, which lies in the range $[-\pi, \pi]$. One must be careful interpreting equation 4 as if $\cos \theta > 0$, then $\psi = \arctan 2(R_{23}, R_{33})$. However, when $\cos \theta < 0$, then $\psi = \arctan 2(-R_{23}, -R_{33})$. A simple way to handle this is to use equation 5 to compute ψ .

$$\psi = \arctan 2\left(\frac{R_{23}}{\cos \theta}, \frac{R_{33}}{\cos \theta}\right) \quad \text{Equation 5}$$

Equation 5 is valid for all cases except when $\cos \theta = 0$. For each value of θ , we compute a corresponding value of ψ using equation 5, yielding

$$\psi_1 = \arctan 2\left(\frac{R_{23}}{\cos \theta_1}, \frac{R_{33}}{\cos \theta_1}\right)$$

$$\psi_2 = \arctan 2\left(\frac{R_{23}}{\cos \theta_2}, \frac{R_{33}}{\cos \theta_2}\right)$$

A similar analysis holds for finding φ . We observe that $\frac{R_{12}}{R_{11}} = \tan \varphi$

We solve for φ the equation

$$\varphi = \arctan 2 \left(\frac{R_{12}}{\cos \theta}, \frac{R_{11}}{\cos \theta} \right) \quad \text{Equation 6}$$

Again, this equation is valid for all cases except when $\cos \theta = 0$. For each value of θ , we compute a corresponding value of φ using equation 6, yielding

$$\varphi_1 = \arctan 2 \left(\frac{R_{12}}{\cos \theta_1}, \frac{R_{11}}{\cos \theta_1} \right)$$

$$\varphi_2 = \arctan 2 \left(\frac{R_{12}}{\cos \theta_2}, \frac{R_{11}}{\cos \theta_2} \right)$$

For the case of $\cos \theta \neq 0$, we now have two triplets of Euler angles that reproduce the rotation

matrix, namely $(\psi_1, \theta_1, \varphi_1)$ and $(\psi_2, \theta_2, \varphi_2)$. Both of these solutions will be valid.

This technique described above does not work if the R_{13} element of the rotation matrix is 1 or -1, which corresponds to $\theta = \frac{-\pi}{2}$ or $\theta = \frac{\pi}{2}$ respectively, and to $\cos \theta = 0$. When we try to solve for the values of ψ and φ using the above technique, problems will occur since the elements R_{11}, R_{12}, R_{23} , and R_{33} will all be zero, and therefore Equations 5 and 6 will become

$$\psi = \arctan 2 \left(\frac{0}{0}, \frac{0}{0} \right)$$

$$\varphi = \arctan 2 \left(\frac{0}{0}, \frac{0}{0} \right)$$

In this case, R_{11}, R_{12}, R_{23} , and R_{33} do not constrain the values of ψ and φ . Therefore, we must use different elements of the rotation matrix to compute the values of ψ and φ .

Consider the case when $\theta = \frac{\pi}{2}$, for which:

$$R_{21} = \sin \psi \cos \varphi - \cos \psi \sin \varphi = \sin(\psi - \varphi)$$

$$R_{31} = \cos \psi \cos \varphi + \sin \psi \sin \varphi = \cos(\psi - \varphi)$$

$$R_{22} = \sin \psi \sin \varphi + \cos \psi \cos \varphi = \cos(\psi - \varphi) = R_{31}$$

$$R_{32} = \cos \psi \sin \varphi - \sin \psi \cos \varphi = -\sin(\psi - \varphi) = -R_{21}$$

Any ψ and φ that satisfy these equations will be a valid solution. Using the equations for R_{21} and R_{31} we find that

$$(\psi - \varphi) = \arctan 2(R_{21}, R_{31})$$

$$\psi = \varphi + \arctan 2(R_{21}, R_{31})$$

Not surprisingly, a similar result holds for the case when $\theta = \frac{-\pi}{2}$, for which

$$R_{21} = -\sin \psi \cos \varphi - \cos \psi \sin \varphi = -\sin(\psi + \varphi)$$

$$R_{31} = -\cos \psi \cos \varphi + \sin \psi \sin \varphi = -\cos(\psi + \varphi)$$

$$R_{22} = -\sin \psi \sin \varphi + \cos \psi \cos \varphi = \cos(\psi + \varphi) = -R_{31}$$

$$R_{32} = -\cos \psi \sin \varphi - \sin \psi \cos \varphi = -\sin(\psi + \varphi) = R_{21}$$

Again using the equations for R_{21} and R_{31} we find that

$$(\psi + \varphi) = \arctan 2(R_{21}, R_{31})$$

$$\psi = -\varphi + \arctan 2(R_{21}, R_{31})$$

In both the $\theta = \frac{\pi}{2}$ and $\theta = \frac{-\pi}{2}$ cases, it is found that ψ and φ are linked. This phenomenon is called Gimbal Lock. Although in this case, there are an infinite number of solutions to the problem, in practice one is often interested in finding one solution. For this task, it is convenient to set $\varphi = 0$ and compute $\psi = \arctan 2(R_{21}, R_{31})$.

A Python script has been written to implement the said theory in order to extract Euler angles from a transformation matrix in Maya. An extract from this script to return the Euler angles in XYZ rotation order, as in the theory example, is given below.

```
easy = self[0][2]
if easy == 1:
    z = math.pi
    y = -math.pi / 2.0
    x = -z + atan2( -self[1][0], -self[2][0] )
elif easy == -1:
```

```

        z = math.pi
        y = math.pi / 2.0
        x = z + atan2( self[1][0], self[2][0] )
    else:
        y = -asin( easy )
        cosY = cos( y )

        x = atan2( self[1][2] * cosY, self[2][2] * cosY )
        z = atan2( self[0][1] * cosY, self[0][0] * cosY )

    angles = x, y, z

    if degrees:
        return map( math.degrees, angles )

    return angles

```

7.3 Summary

This chapter has provided an introduction to the concept of vectors and matrices and their use within Maya. The composition and decomposition of transformation matrices has been explained and a Python script has been developed so that the orientation values for a specific joint can be output from the software. The next chapter shall use this script to evaluate the performance of a subject.

8 Fault Analysis and Isolation

Results written in this chapter validate the theories and scripts developed in previous chapters, to deliver analysis of human motion in performance. The extraction of data for analysis is carried out on the direct import of recorded .bvh file data, and then on the virtual character avatar animated using the motion data from the same file source. The results of both methods, and the workflows involved, are evaluated and discussed.

8.1 Methods

To import a .bvh motion capture file to Maya without any application to a character, it first needs to be applied to a skeleton within MotionBuilder and exported to a readable file format. When a .bvh motion file is imported into MotionBuilder it places joints using the hierarchical and offset data specified in the header section of the .bvh file (see figures 8.1 and 8.2).

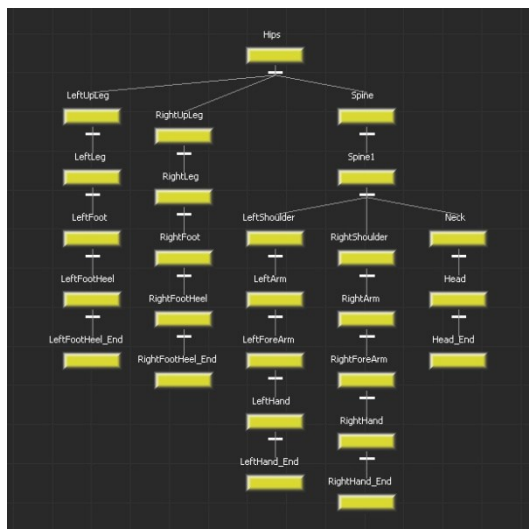


Figure 8.1: Hierarchical joint nodes in schematic view

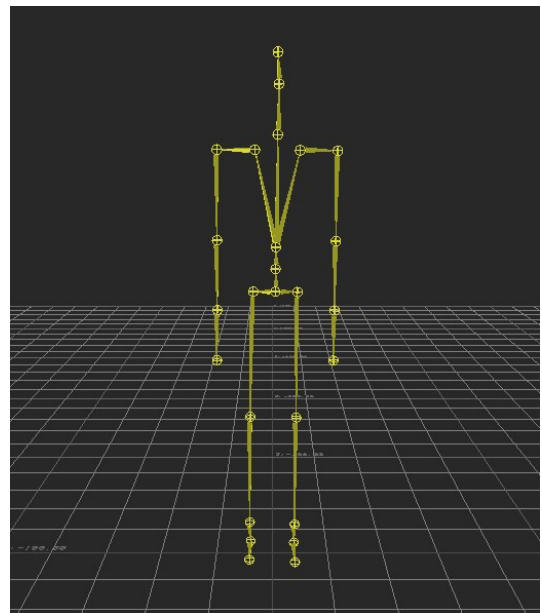


Figure 8.2: Hierarchical joint nodes in perspective view

Without any amendment, this file can now be saved as an .fbx binary file that will directly import into Maya. One difficulty exporting between MotionBuilder and Maya is the difference in scaling units; when this .fbx file is imported into Maya with the default scaling units of centimetres, it is unusually large within the scene (see figure 8.3).

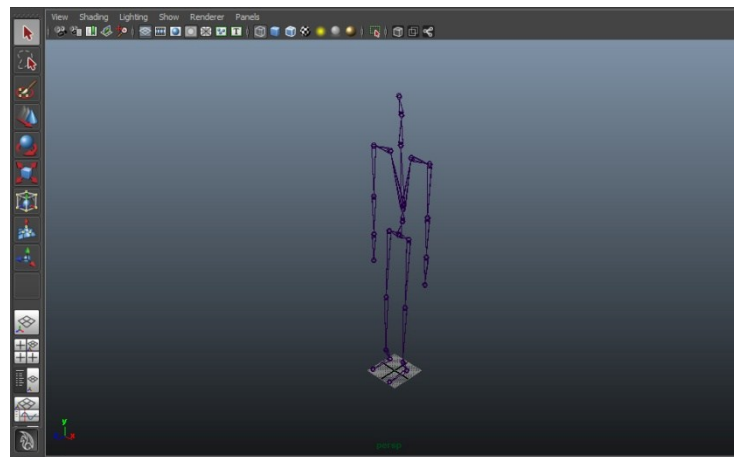


Figure 8.3: Direct .fbx import to Maya

For the skeleton to import into the scene at a logical working size, the file units on import need to be converted to decimetres. However, this causes problems in that the joint sizes display unexpectedly; most notably the hip joint that is illustrated in figure 8.4. This is because on import with the unit conversion only the hip joint is scaled, as it is the root joint of the skeleton. The scale of the hips joint is set to 0.1 as opposed to 1, though the draw radius for the joint remains at the default of 3. In order to change the draw size to match that of the other joints, the draw radius needs to be manually adjusted to 0.3; however, this then affects the display of the bone as shown in figure 8.5.

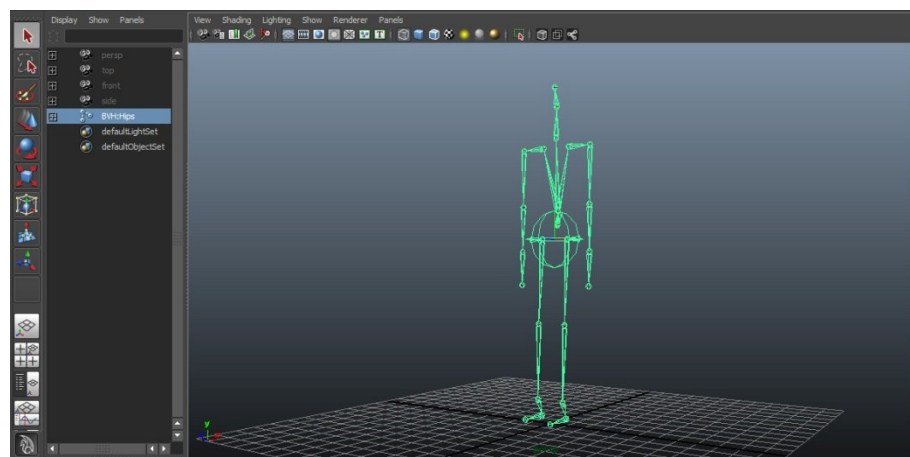


Figure 8.4: Joint display when converted to decimetres on import

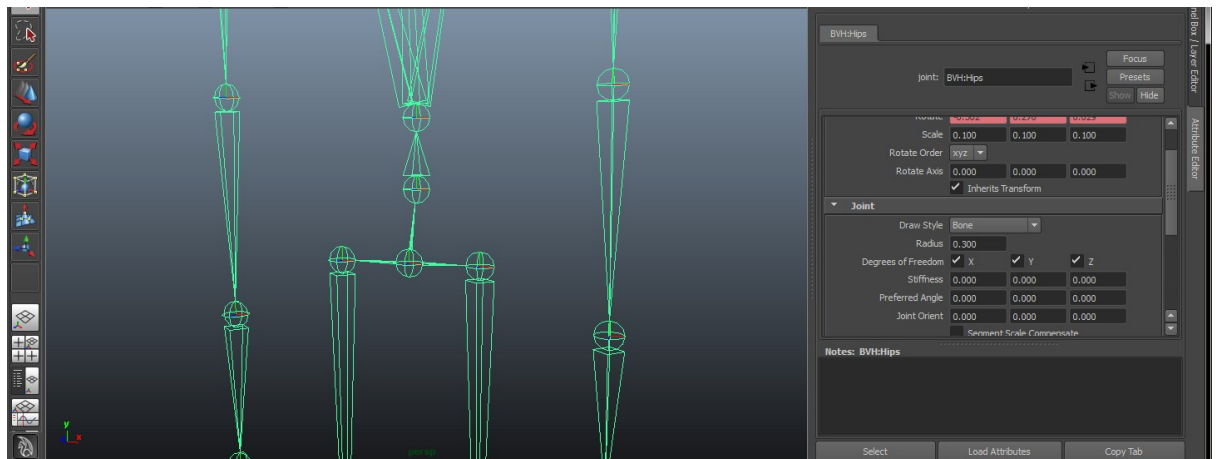


Figure 8.5: Scale 0.1 Joint Radius 0.3

In order for the imported skeleton to be converted to a good working size and also display consistent joint radius, when importing the motion file to Motion Builder a reference node needs to be created. This can be done automatically by ensuring that the 'Create Reference Node' checkbox is selected (see figure 8.6). This creates a locator at the world origin that acts as a master node to the skeleton hierarchy and, once imported to Maya, can be then scaled to control the overall size of the skeleton. This can be scaled most efficiently using a small MEL script which selects the locator, scales it and then returns the scale attributes back to 1:

```
select -r Fbx_Root;
scale 0.1 0.1 0.1;
FreezeTransformations;
select -clear;
```

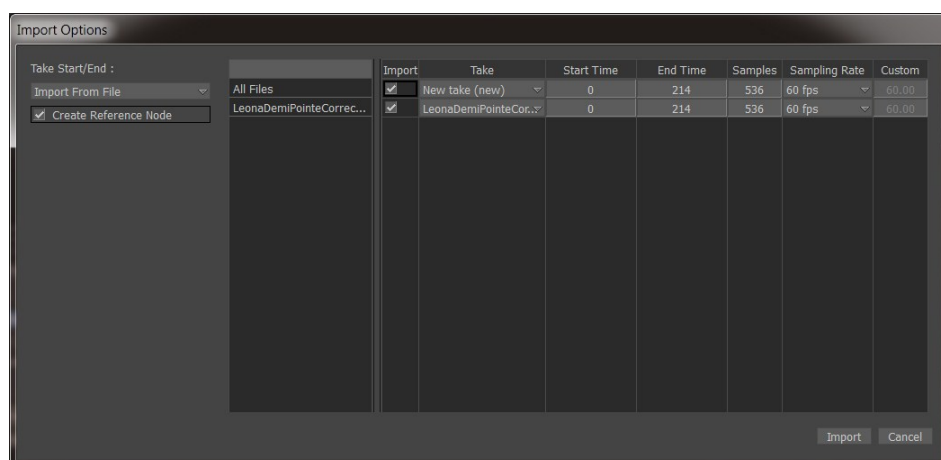


Figure 8.6: Create Reference Node

When the skeleton with applied motion data was imported into Maya, it was also noted that the local axis of the joints were uniformly positioned and following the direction of the world axis (see figure 8.7).

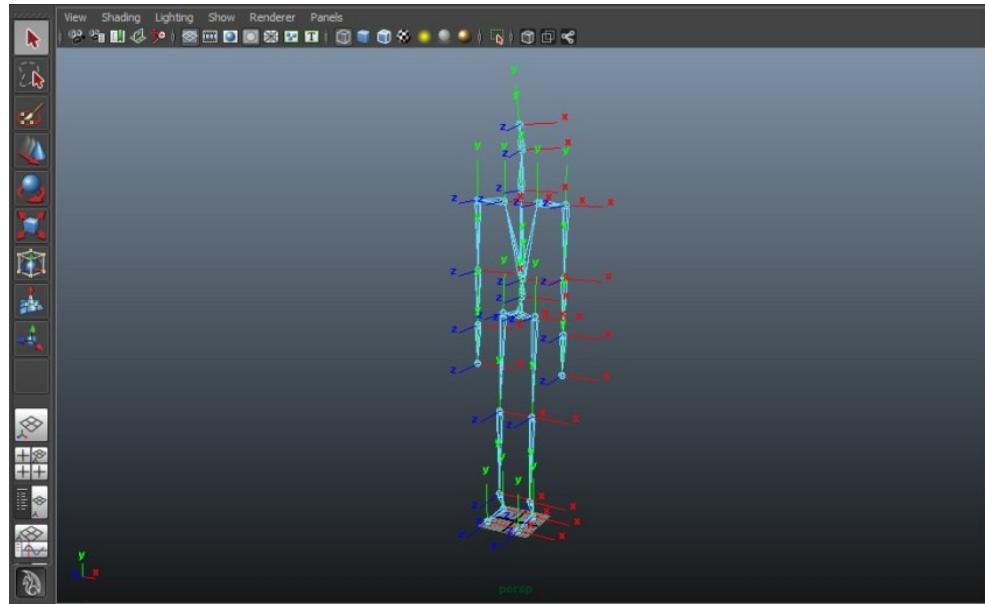


Figure 8.7: Local rotation axis

This was unusual to see as generally when creating a skeleton in Maya, the local X-axis will follow the flow of the joints (see figure 8.8), as is conventional in manual animation techniques. This will affect the fault detection in the sense that it will be the Z-axis rotations, as opposed to the X-axis rotations, which will determine the side-to-side movement of the joint associated with sickle or winged alignment.

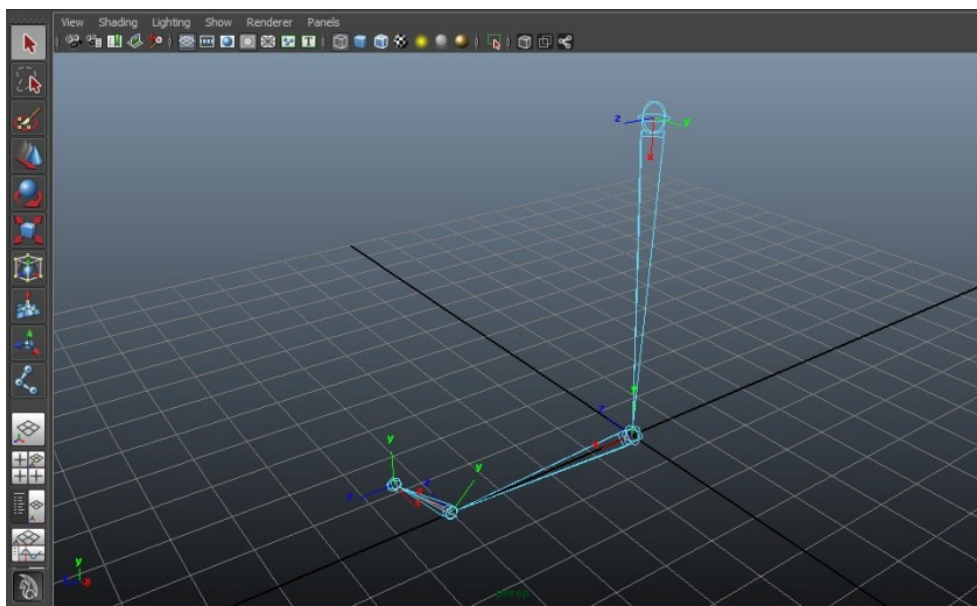


Figure 8.8: Default local axis orientation on joint creation

The animation curves for each individual joint are accessible through the Maya graph editor. Figure 8.9 shows the rotateX, rotateY and rotateZ plots for the right ankle joint.

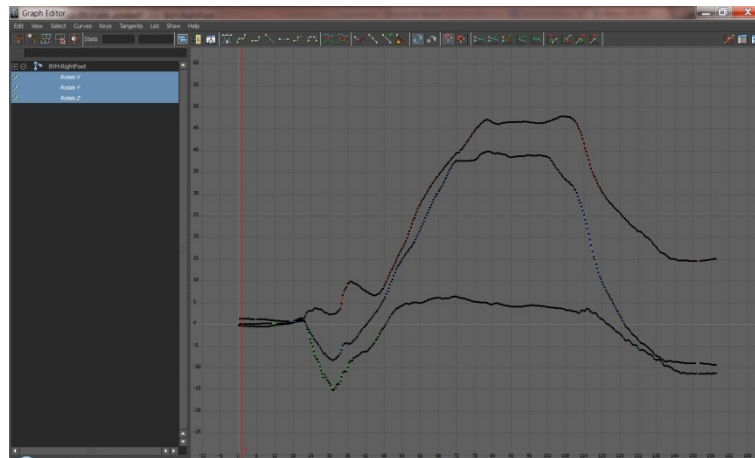


Figure 8.9: Maya graph editor

Although these plot curves give us an indication as to whether there is misalignment of a joint when compared to an exemplar performance as shown in our earlier experiment, in order to evaluate the alignment of a specific joint without comparison to an exemplar performance (which in itself has the potential to be in some degree of fault) and return a calculated degree of fault, the joint rotation values must be compared with its surrounding joints. For example, if the foot were required to be in direct alignment with the lower leg, with no inward or outward twist, the rotation axis would need to be the same for both joints (see figure 8.10).

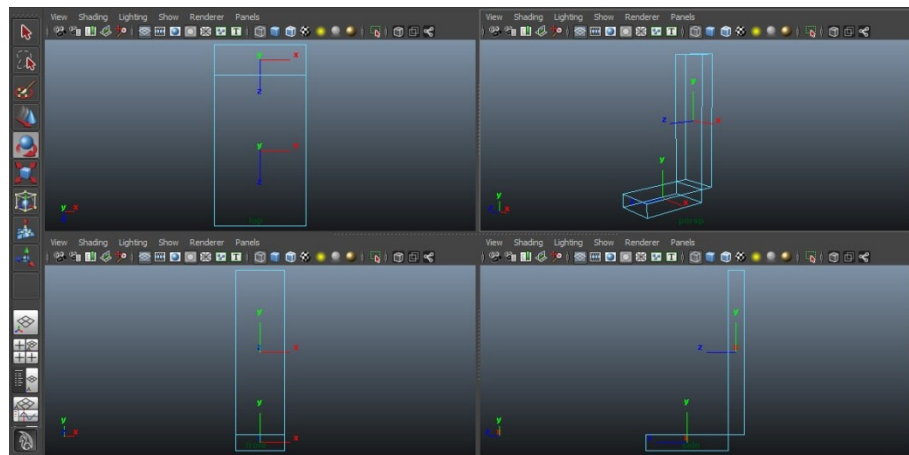


Figure 8.10: Example alignment of lower leg joints

If there was a twist of the foot, it would be indicated by difference in rotation around a specific axis; in the example shown in figure 8.11, a rotation around the Z-axis of -10° :

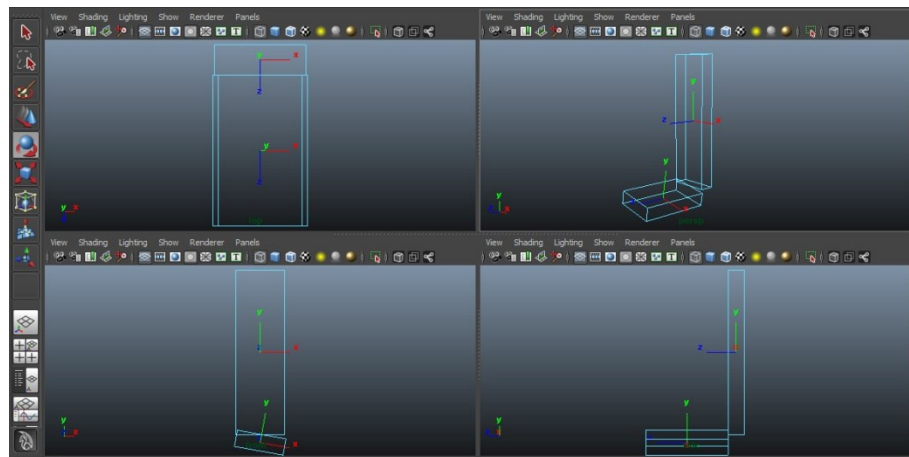


Figure 8.11: Example misalignment of lower leg joints

The same principle applies to the rotation values of the joints in the motion data. Whether the foot is aligned with the ankle, or whether the ankle is aligned with the knee can be identified by the difference in the rotation around a specific axis. Figure 8.12 shows a similar rotation of -10° on the Z-axis on the subject's right foot.

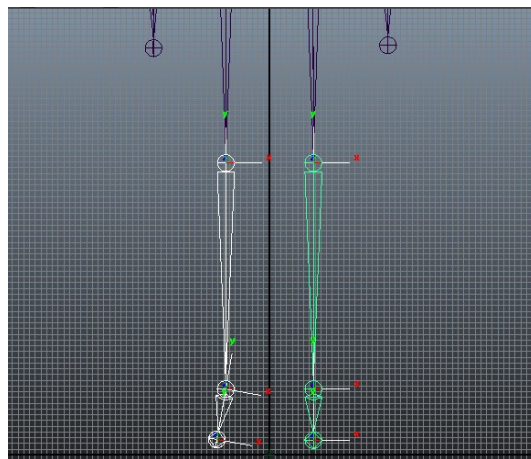


Figure 8.12: Motion data example of misalignment on Z-axis

The value of the rotation of a joint in Maya is held in the transformation matrix, so in order to define the rotation of a joint around a specific axis, this matrix must be decomposed and converted to Euler angles as described in the previous chapter.

In Maya, there are two transformation matrices held for each node; the world transformation matrix and the local transformation matrix. The world transformation matrix describes the nodes transformation values in relation to the world axis, which is fixed. The local transformation matrix describes the nodes transformation values in relation to its parent node. The two matrices are directly related in that the world matrix is the sum of the multiplication of the local matrices of the nodes parents. For example, considering a simple 3

joint chain with the root joint being jntA, the child of that joint being jntB and the child of that joint being jntC, in order to find the world matrix of jntC we would multiply the local matrices in the order $\text{jntC} * \text{jntB} * \text{jntA}$, or as the world matrix of jntB would be calculated by $\text{jntB} * \text{jntA}$ we could simplify $\text{jntC} = \text{jntC} * \text{jntB}$. As is the case with matrix multiplication, the order of multiplication is important, as it is non-commutative. In order to find the local matrix of a node, the calculation is done using the inverse of the parent joint, therefore, the local matrix of jntC would equal the world matrix of jntC multiplied by the inverse of the world matrix of jntB; $\text{jntC} = \text{jntC} * \text{jntB}^{-1}$. When working in Maya, the software caches the world matrix for each transform so either matrix can be returned through a query.

In order for the ankle joint to be compared with the knee joint, to ascertain whether the foot is aligned with the lower leg or there is a degree of fault, the local rotation values must be used. The local rotation values for the ankle joint will show the difference in rotation when compared to the knee joint (its parent joint) and therefore, the Euler angle for the Z-axis rotation will provide us with our calculated degree of fault.

Utilising the script from the previous chapter which decomposes the transformation matrix and converts the rotation part to Euler angles, the following script has been written to return the Euler angles for both the left and right ankle joint.

```
import maya.cmds as cmd
from vectors import Matrix

localHips = Matrix( cmd.getAttr( 'BVH:Hips.matrix' ) )

RightUpLeg = Matrix( cmd.getAttr( 'BVH:RightUpLeg.matrix' ) )
RightLeg = Matrix( cmd.getAttr( 'BVH:RightLeg.matrix' ) )
RightFoot = Matrix( cmd.getAttr( 'BVH:RightFoot.matrix' ) )
RightHeel = Matrix( cmd.getAttr( 'BVH:RightFootHeel.matrix' ) )
RightEnd = Matrix( cmd.getAttr( 'BVH:RightFootHeel_End.matrix' ) )

LeftUpLeg = Matrix( cmd.getAttr( 'BVH:LeftUpLeg.matrix' ) )
LeftLeg = Matrix( cmd.getAttr( 'BVH:LeftLeg.matrix' ) )
LeftFoot = Matrix( cmd.getAttr( 'BVH:LeftFoot.matrix' ) )
LeftHeel = Matrix( cmd.getAttr( 'BVH:LeftFootHeel.matrix' ) )
LeftEnd = Matrix( cmd.getAttr( 'BVH:LeftFootHeel_End.matrix' ) )

RightFootXYZ = RightFoot.ToEulerXYZ( degrees=True )
```

```
LeftFootXYZ = LeftFoot.ToEulerXYZ( degrees=True )

print RightFootXYZ
print LeftFootXYZ
```

The script returns Euler angles in the XYZ rotation order in the following format:

```
[32.42082595825196, 2.9826929569244376, 19.45307540893555]
[34.906620025634773, -11.722748756408693, 2.6220684051513676]
```

8.2 Results from Direct Analysis of Motion Data

In order to validate both the matrix decomposition method and the ballet gesture fault detection experiment, the script was run at several frames throughout the motion recordings and the output Euler angles were noted. The foot alignment that shows fault in either sickle or winged position can be seen in the rotation of the Z-axis; see figure 8.13.

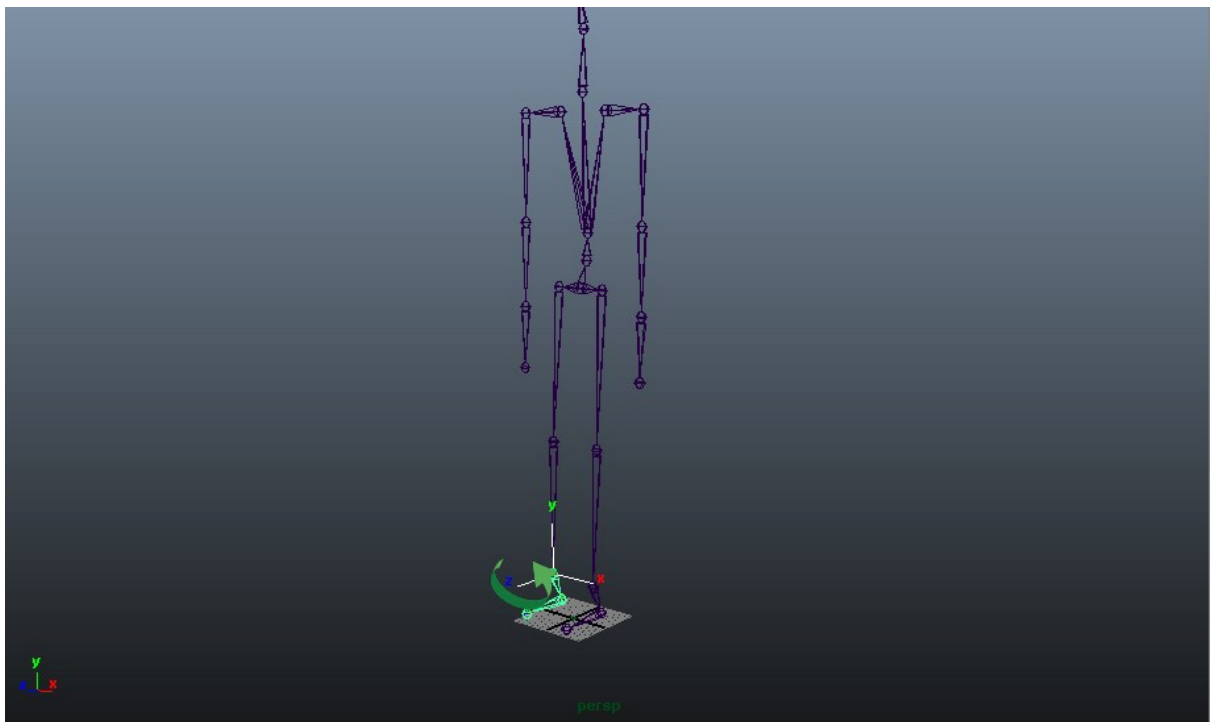


Figure 8.13: Fault in foot alignment shown on the Z-axis rotation

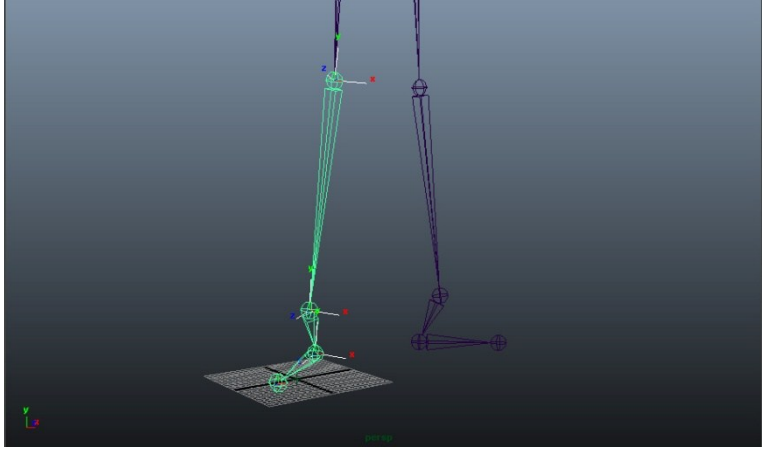
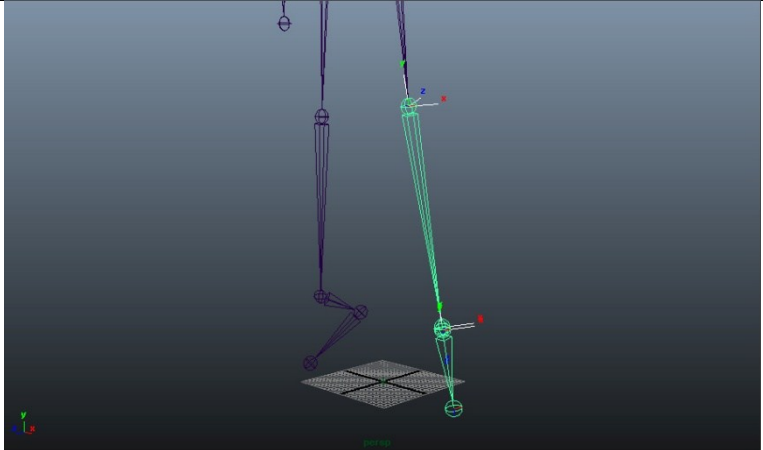
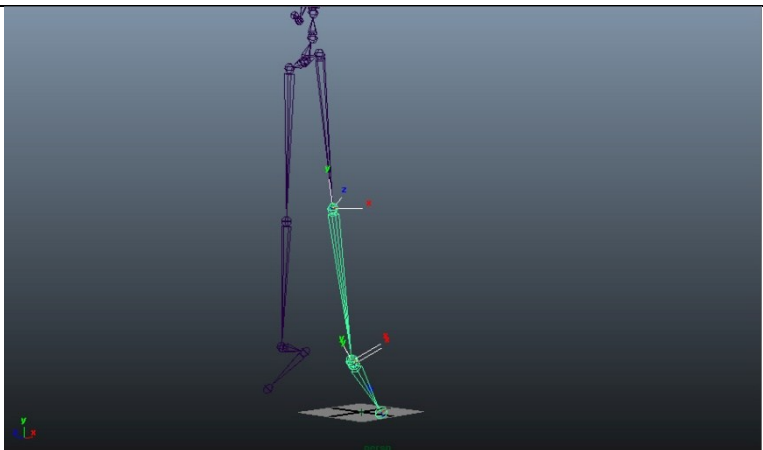
Table 8.1 shows results for the 9 motion recordings of the 3 examples of gesture in correct position, sickle position and winged position for both feet. It can be observed that for the right foot, as the foot enters sickled position, the angle in the Z-axis is greater than when in correct position and when the foot enters winged position, the angle in the Z-axis is less than when in correct position. The same is true with the left foot, although with inverse values, with the exception of the en pointe gesture. This could be explained by a mistake by the dancer when

demonstrating the gesture. The en pointe gesture is the most physically difficult gesture and as such, would be more difficult to hold; especially when in a fault position which could cause physical discomfort. The dancer used for this experiment, although familiar with the gestures and correct technique, would not be regarded as an expert and, as such, the imperfect results might be a reflection of imperfect technique of the performer.

		Right foot (X, Y, Z)	Left foot (X, Y, Z)
First position	Correct	8.089659570923553, -7.1246470579741645, 0.30448006832249608	7.1551825021085635, 3.3825616369674889, -4.0752506558191239
	Sickle	-5.6357387116638717, -3.2596796157525358, 19.256563540355714	11.61707192845634, -10.617930231300642, -13.544522765764873
	Winged	11.955315589904789, -7.8588919639587429, -7.0570243837216449	2.7515323162078862, 9.949186325073244, 10.548957824707033
Demi-pointe	Correct	53.976455688476562, 0.40929716825485424, 33.208576202392578	58.000831604003906, -22.998432159423835, -0.52777254581451583
	Sickle	46.556430816650398, 4.322926998138426, 39.026115417480476	54.287475585937507, -23.76622200012207, -7.7322049140930211
	Winged	53.852802981960068, -4.996121865029945, 12.721874410619051	43.580731864232135, -13.449856500781703, 23.241144776491399
Pointe	Correct	58.944753872874607, -15.901755999993869, 49.829689264098661	60.358521940414796, -20.532869096169041, 23.724507951791715
	Sickle	56.945885395460301, -13.296491767899383, 53.404483181426862	68.43795825825238, -14.546177108965589, 10.518937326516268
	Winged	72.996665017142988, -8.5493385572813434, 17.261944707308263	63.019453001558418, -13.18864845285086, 20.94848102216385

Table 8.1: Euler XYZ values from gesture examples

When these results are viewed alongside the position of the foot, it is clear to see that they correlate with the foot being in or out of alignment and that the Z-axis rotation is the telling axis of fault in either sickle or winged position. Table 8.2 shows examples comparing the visual reconstruction of the joints to the output Euler angles.

<p>8.1618187071934507, -6.9429793685873777, 0.22883278514260808</p>	
<p>58.22472858563571, -23.13083427156764, -0.58238911416686578</p>	
<p>60.422221379777028, -20.16009756208447, 23.702952413615833</p>	

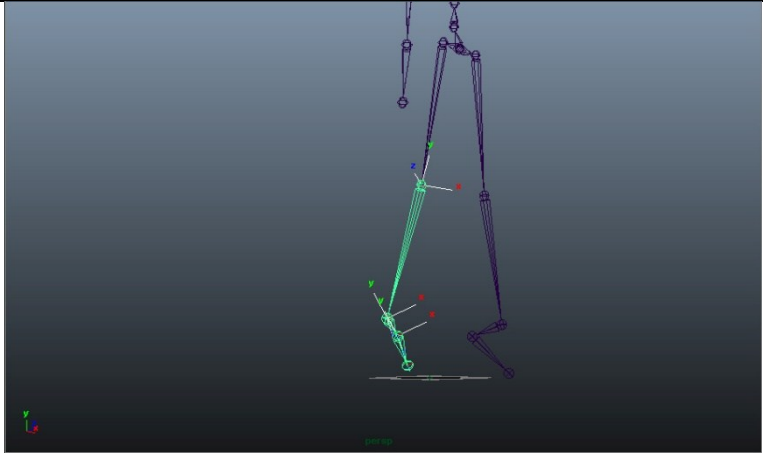
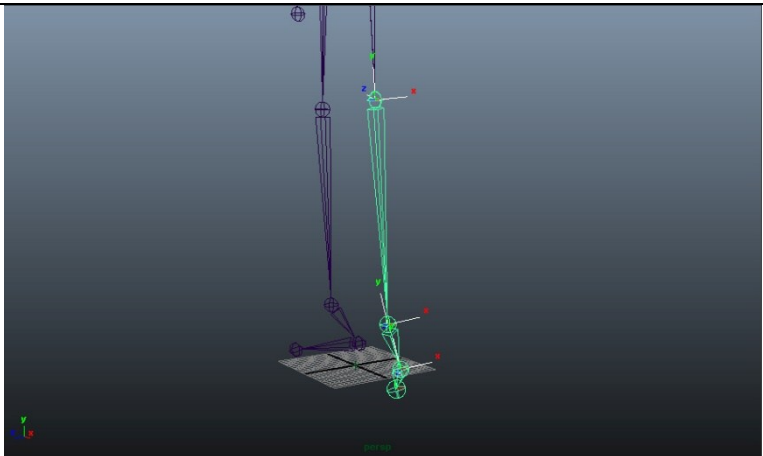
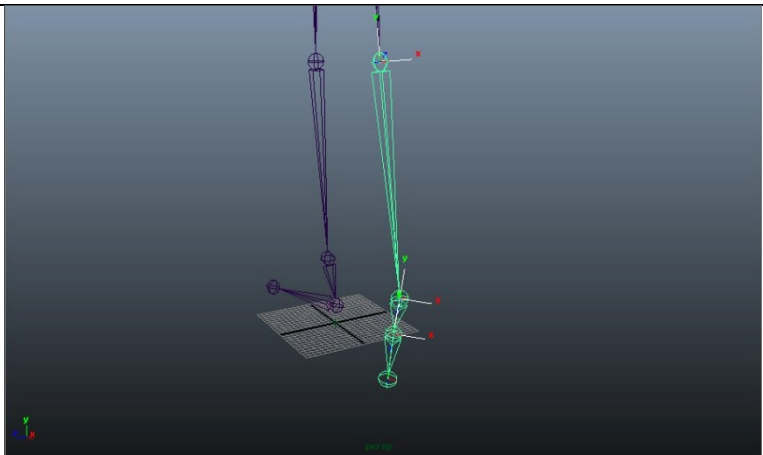
46.423892974853516, 4.3914442062377921, 38.875656127929702	
2.7213550325616565, 9.6625669866335553, 10.240813581142948	
11.72716790330103, -10.527695997908079, -13.754865019374094	

Table 8.2: Examples comparing visual representation with the output Euler angles

As well as the experiments that were set up to purposefully show gestures in fault, the same script was used to examine foot alignment technique in the original dance capture with the experienced dancers from the Northern Ballet School. The results shown in table 8.3 were again in correlation with what could be seen by eye.

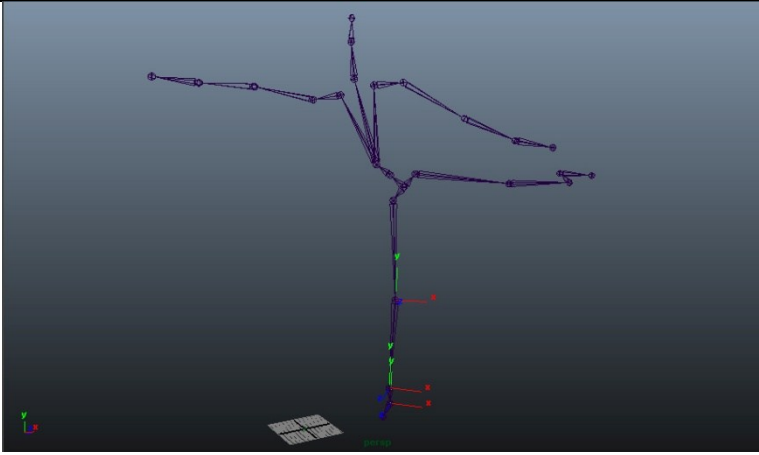
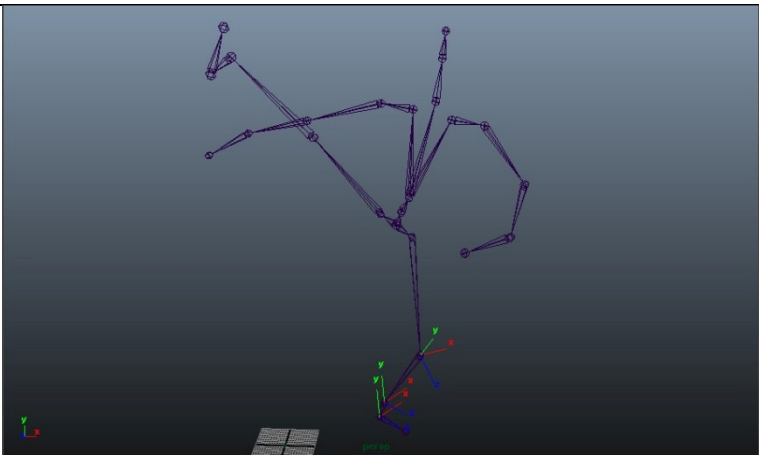
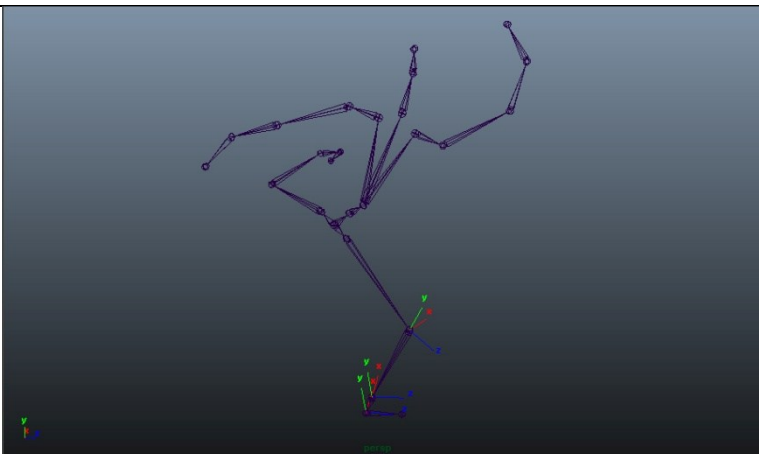
<p>7.1950831413269052, -19.754835128784183, -0.090389907360076863</p>	
<p>-36.184291839599609, 15.249855995178221, -0.53434365987777654</p>	
<p>-29.604055404663079, 26.921581268310543, 0.14203189313411743</p>	

Table 8.3: Examples comparing visual representation of highly skilled dancer with the output Euler angles

It is both interesting and significant that the alignment in the foot of the dancer from the dance school is noticeably closer to direct alignment more frequently and when demonstrating more technically difficult positions. This would indicate that the more accomplished dancer has better technique and further proves the reliability of the fault detection methods.

8.3 Discussion on Direct Analysis of Motion Data

Following validation of results of the matrix decomposition script, the script was developed to provide analysis of every frame of the recorded motion during the capture session. The following script runs the matrix to Euler angle conversion for every frame in the playback range and writes the Euler angles for each ankle joint to an .xml file. This data can then be graphed to show the joint alignment throughout the performance.

```
import maya.cmds as cmd
from xml.dom.minidom import Document
from vectors import Matrix

#create xml
xmlDoc = Document()

root = xmlDoc.createElement('graph')
xmlDoc.appendChild(root)

#get times
start = int(cmd.playbackOptions(q=True, minTime=True))
end = int(cmd.playbackOptions(q=True, maxTime=True))

for i in range(start, (end + 1)):

    cmd.currentTime(i)

    localHips = Matrix( cmd.getAttr( 'BVH:Hips.matrix' ) )

    RightUpLeg = Matrix( cmd.getAttr( 'BVH:RightUpLeg.matrix' ) )
    RightLeg = Matrix( cmd.getAttr( 'BVH:RightLeg.matrix' ) )
    RightFoot = Matrix( cmd.getAttr( 'BVH:RightFoot.matrix' ) )
    RightHeel = Matrix( cmd.getAttr( 'BVH:RightFootHeel.matrix' ) )
    RightEnd = Matrix( cmd.getAttr( 'BVH:RightFootHeel_End.matrix' ) )

    LeftUpLeg = Matrix( cmd.getAttr( 'BVH:LeftUpLeg.matrix' ) )
    LeftLeg = Matrix( cmd.getAttr( 'BVH:LeftLeg.matrix' ) )
    LeftFoot = Matrix( cmd.getAttr( 'BVH:LeftFoot.matrix' ) )
    LeftHeel = Matrix( cmd.getAttr( 'BVH:LeftFootHeel.matrix' ) )
    LeftEnd = Matrix( cmd.getAttr( 'BVH:LeftFootHeel_End.matrix' ) )
```

```
RightFootXYZ = RightFoot.ToEulerXYZ( degrees=True )
RightEulerX = RightFootXYZ[0]
RightEulerY = RightFootXYZ[1]
RightEulerZ = RightFootXYZ[2]

LeftFootXYZ = LeftFoot.ToEulerXYZ( degrees=True )
LeftEulerX = LeftFootXYZ[0]
LeftEulerY = LeftFootXYZ[1]
LeftEulerZ = LeftFootXYZ[2]

keyFrame = xmlDoc.createElement('frame')
keyFrame.setAttribute('index', str(i))
keyFrame.setAttribute('rightX', str(RightEulerX))
keyFrame.setAttribute('rightY', str(RightEulerY))
keyFrame.setAttribute('rightZ', str(RightEulerZ))
keyFrame.setAttribute('leftX', str(LeftEulerX))
keyFrame.setAttribute('leftY', str(LeftEulerY))
keyFrame.setAttribute('leftZ', str(LeftEulerZ))
root.appendChild(keyFrame)

file = open('H:/filename.xml', 'w+')
file.write(xmlDoc.toprettyxml())
file.close()
```

Figure 8.14 shows the plotted results in first position for the right foot, and figure 8.15 shows the same for the left foot.

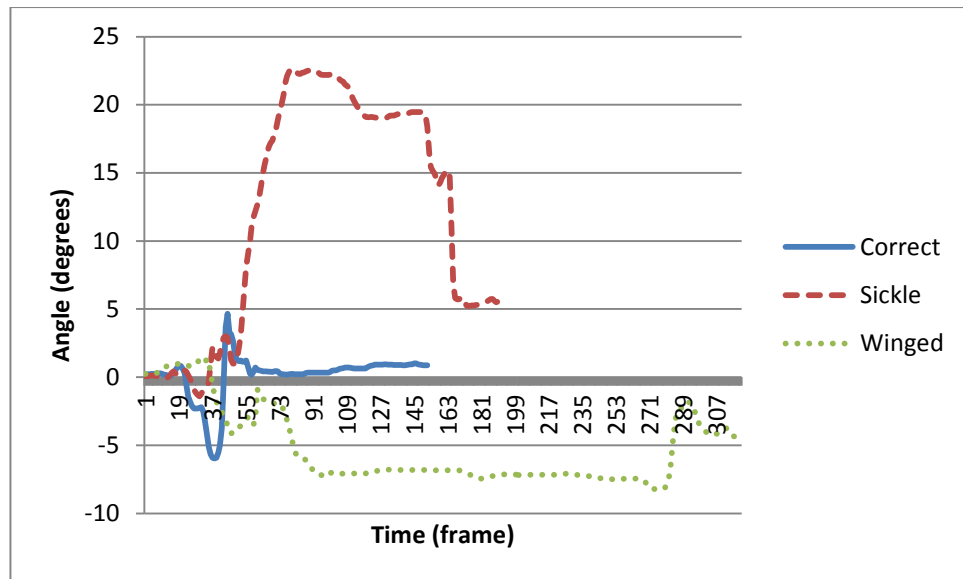


Figure 8.14: First Position - Right Foot

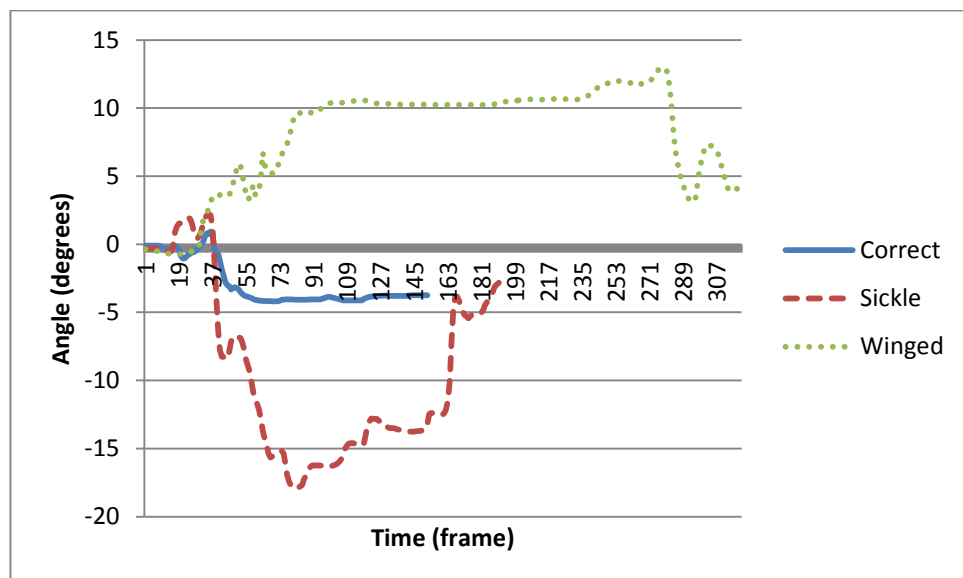


Figure 8.15: First Position - Left Foot

It can be seen from the graphs that the correctly demonstrated gesture is closer to the zero line on the angle axis and the angle of fault is represented by a move away from this axis. The degree to sickie is shown by a positive increase for the right foot and a negative increase for the left foot and the degree to winged is shown by the reverse.

The next pair of graphs show the same data for the gesture of demi-pointe; figure 8.16 being for the right foot and figure 8.17 being for the left.

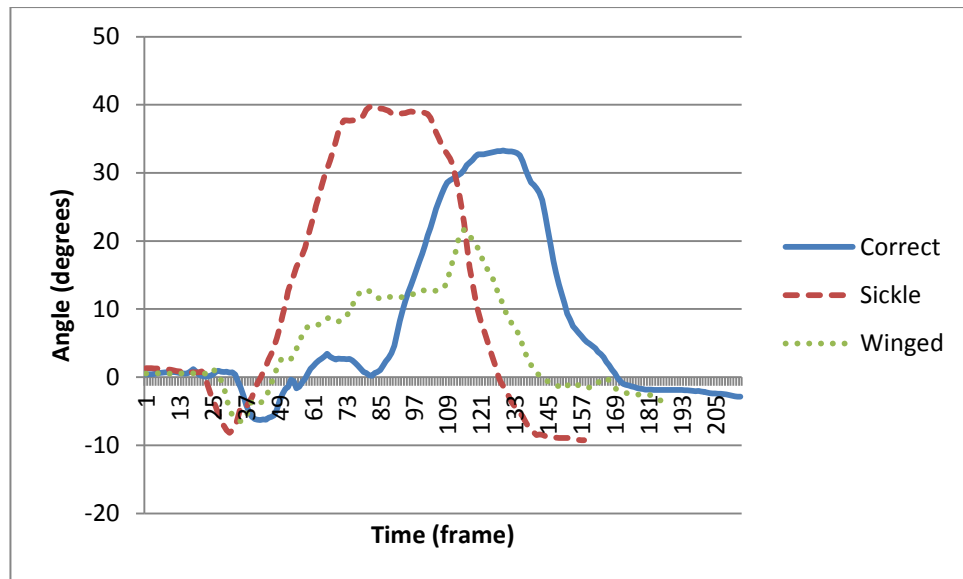


Figure 8.16: Demi-Pointe - Right Foot

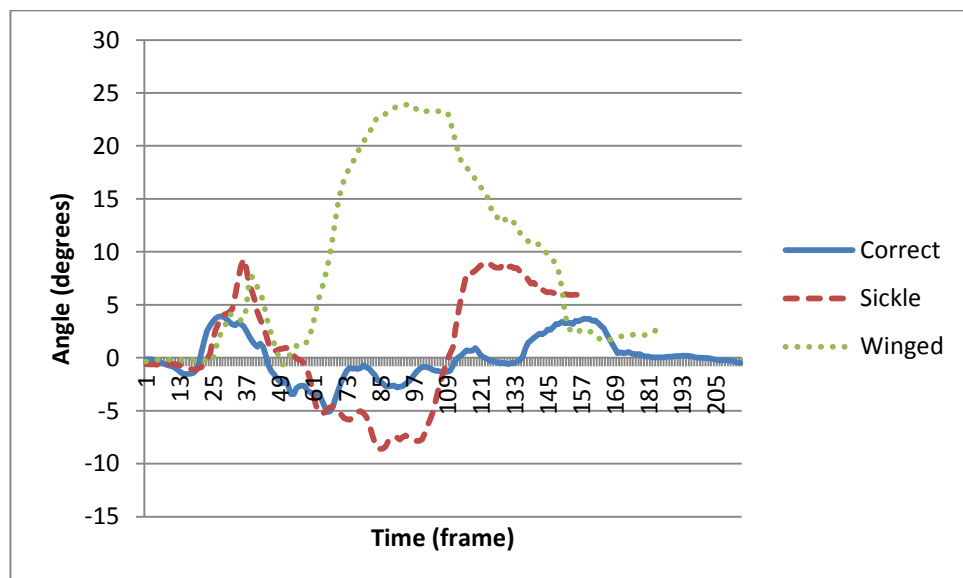


Figure 8.17: Demi-Pointe - Left Foot

Figure 8.16 appears to show that the performer has a natural tendency to sickie as all of the lines are in the positive section of the graph. It does show that the demonstration of sickie position is to the positive, and the demonstration of winged is to the negative of the attempted correct demonstration, which agrees with the theoretical relationship. The example of the left foot in figure 8.17 is a much more controlled example and might suggest that the performer has a stronger left foot than right foot. Alternatively, it might be that the attention of the performer was focussed on demonstrating the position of fault in the left foot with less attention given to the right foot.

Figures 8.18 and 8.19 show the same data for the gesture en-pointe for the right foot and left foot respectively.

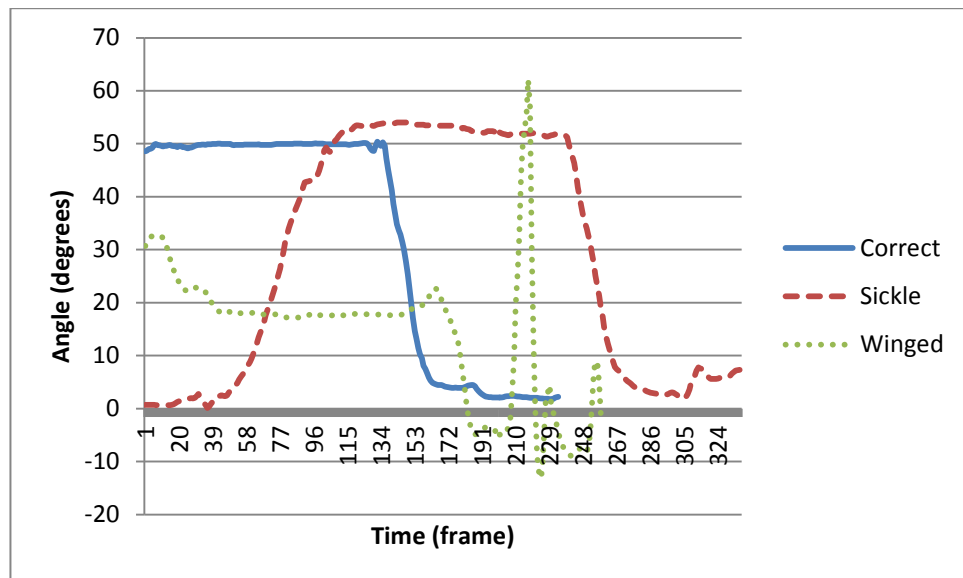


Figure 8.18: En-Pointe - Right Foot

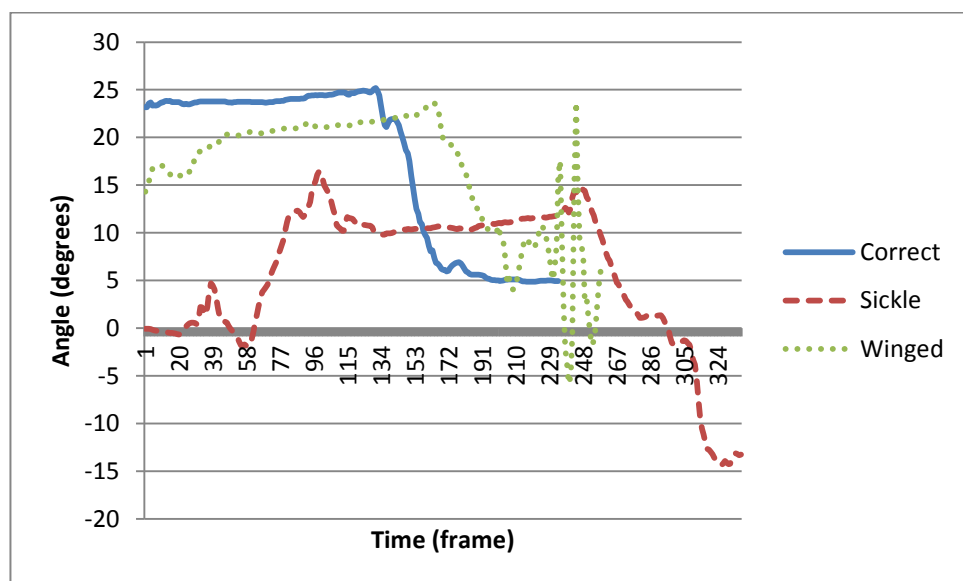


Figure 8.19: En-Pointe - Left Foot

Both examples again show that the performer has a tendency to sickle as the lines for both feet occupy the positive side of the angle axis. Figure 8.18 reiterates the theory that the position of fault to sickle is to the positive side of the attempted correct position, and fault to winged is to the negative. Figure 8.19 however, shows a poor demonstration of the correct position. The sickle and winged examples are as expected with the winged line significantly higher than the sickle line, however, the attempted correct position does not reside between

the two examples of fault. This could be explained by a poor performance on this occasion, poor technique of the left foot whilst en-pointe or a focus of attention on the right foot during demonstration. It can be seen from the full visualisation of the captured motion from this example (see figure 8.20), that the performer uses a prop to the right hand side in order to steady themselves whilst performing the gesture and the left foot is visibly in poor alignment. It could be for this reason that a shift in balance of the performer would explain the poor alignment of the left foot on this occasion.

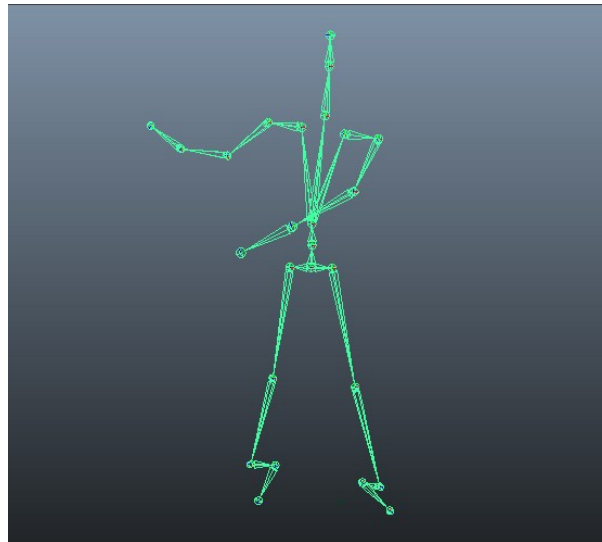


Figure 8.20: Demonstration of En-Pointe in 'correct' position

The collective results show that converting the transform matrices associated with the joints to Euler angles gives an accurate, numerical and coherent analysis of the position of fault of a given joint throughout a performance. Augmented feedback of the performance can be given in a variety of forms including numerical analysis of joint rotations, a visualisation of the joint angles in the form of a representative skeleton or visualisation of the data in the form of graphs. The scripts used to extract the data can be amended very simply to collect information on any specified joint recorded to the .bvh motion capture data file. The workflow could therefore be adapted to provide analysis of critical features of any sport or performance.

8.4 Results and Discussion of Analysis with Avatar Application

When applying the fault analysis methods to the character avatar, rather than the .bvh conversion, the results are less predictable. This is because of the way the skeleton is set up. As mentioned previously, the default local axis alignment when introducing joints in Maya follows XYZ orientation; the X-axis being the first axis will point towards the child joint, the Z-

axis will be aligned with the vector perpendicular to both the first axis (the established X-axis) and the vector from the joint to its parent joint (cross product), the Y-axis will then be aligned according to the right hand rule.

The default local axis orientation for the skeleton created for the avatar rig is shown in figure 8.21.

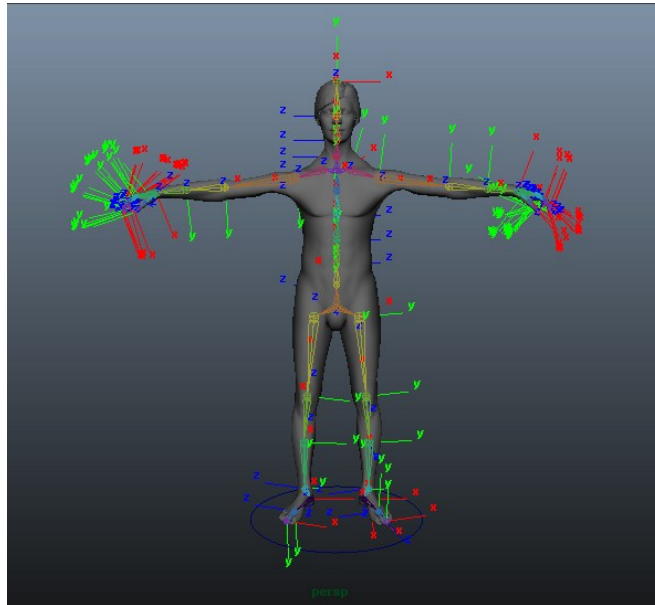


Figure 8.21: Default joint orientation

The sporadic orientation of the local axis throughout the skeleton makes it very difficult to compare alignment of joints. Once the skeleton has been drawn to fit the geometry, it can be rebuilt using a script that sets all local rotation axes to the same orientation as the world axes. The script is shown below.

```
import maya.cmds as cmd

def jgReSkel():

    #get root as selection
    jgRoot = cmd.ls(sl=1)

    #get all children
    jgSkel = cmd.listRelatives(ad=1, type='joint')
    #add root to list
    jgSkel.extend(jgRoot)
```

```

#new joint list
jgNewSkel = []

#make a new joint for each item in jgSkel
for i, each in enumerate(jgSkel):
    cmd.select(cl=1)
    jgNewJ = cmd.joint(p=cmd.xform(each, q=1, ws=1, rp=1), n=each+'_NEW')
    jgNewSkel.append(jgNewJ)

#find the correct parent for each new joint
for i, each in enumerate(jgNewSkel):
    #get parent of each original joint
    jgParent = cmd.listRelatives(jgSkel[i], p=1)

    #check to make sure returned parent is not None
    if jgParent is not None:
        #refer to new joint
        jgNewParent = jgParent[0].split(':')[0]+'_NEW'
        cmd.parent(each, jgNewParent)

cmd.select(jgNewSkel[len(jgNewSkel)-1])

```

The result of the script is shown in figure 8.22. The fault analysis of joint alignment is now more predictable, however, as the pose of the skeleton differs from the initial pose of the .bvh skeleton, this leads to irregularities in the results. At the same frame of the motion capture demonstration of a gesture, the resulting alignment analysis of the newly created avatar skeleton was compared with the .bvh skeleton giving the results shown in table 8.4.

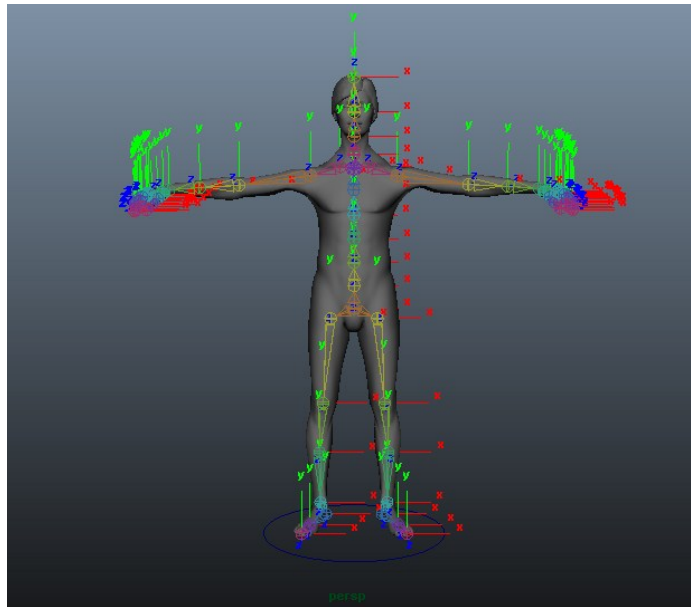


Figure 8.22: World joint orientation

	.bvh skeleton	Character avatar
Right Foot (X, Y, Z)	8.162040710449217, -6.9529504776000968, 0.22964794933795932	9.2075725227513274, -6.4872535774182021, -3.141114048074233
Left Foot (X, Y, Z)	7.1450514793395987, 3.5062937736511226, -4.0447068214416513	7.2906751632690439, 3.1704368591308589, -1.4186139106750488

Table 8.4: Motion data comparison with world orientation avatar

As can be seen, there is a difference in the results, most notably on the Z-axis, due to the difference of foot alignment in the initial poses of the two skeletons.

Another way of setting up the local rotation axis is using the traditional manual animation approach whereby the Y-axis of the horizontal joint chains point upwards and the Z-axis of the vertical joint chains point to the side of the character. This can be achieved using the above script to recreate the skeleton and a combination of the following MEL commands on the appropriate section start joints:

```
joint -e -ch -oj xyz -sao yup
joint -e -ch -oj xyz -sao ydown
joint -e -ch -oj xyz -sao zup
joint -e -ch -oj xyz -sao ydown
```

The joints were oriented as in figure 8.23.

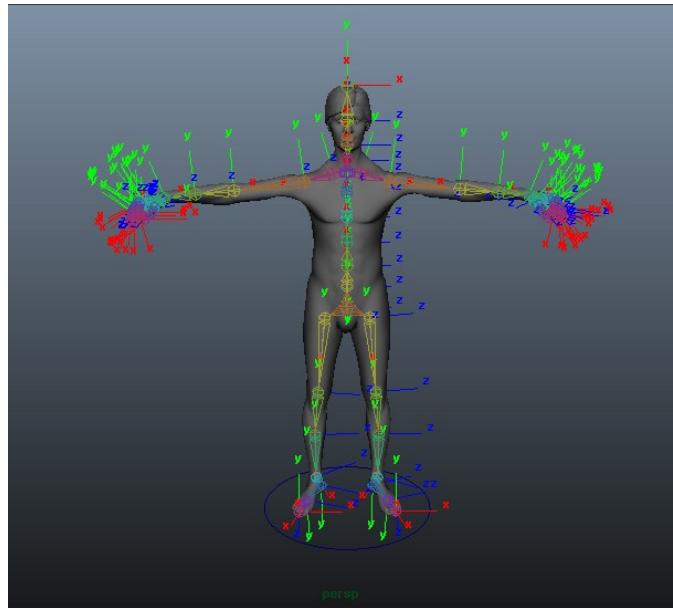


Figure 8.23: Manual animation joint orientation

Again, the resulting alignment analysis of the newly created avatar skeleton was compared with the .bvh skeleton at the same frame of a motion capture demonstration giving the results shown in table 8.5.

	.bvh skeleton	Character avatar
Right Foot (X, Y, Z)	8.1616111624521448, -6.9879957392913861, 0.22376915892845739	-2.880567643962705, -19.611037884203903, 33.046066063891033
Left Foot (X, Y, Z)	7.1553171096962256, 3.4186576741666301, -4.0663992801970394	7.4179503042734485, 18.646808978512929, 33.359651379108072

Table 8.5: Motion data comparison with avatar oriented for manual animation

The results in this case are much further from the direct motion analysis and can be explained by the less uniform joint axis orientation.

8.5 Summary

It can be concluded from the results that fault detection using the avatar representation model of the subject can be considered less reliable than fault detection using analysis of the motion data directly and should be used solely for visual analysis and aesthetic interest.

The results of analysing the motion data directly from the .bvh file import to Maya, using the Python script developed to convert the transformation matrices to Euler angles, are clearly validated by comparison of the output angles with the skeletal visualisation. A full performance can be analysed with accurate orientation values on a frame by frame basis by running the script at any given time of the animation, or can be output and seen as a full graphical representation whereby any deviation from the central axis represents a degree of fault.

9 Conclusion of Thesis and Contribution to Knowledge

It has been established that there is a strong link between technique and the quality of a performance. The consequences of poor technique, and thus a poor quality performance, have been proven to result in both immediate and long-term injury such as sprains, anterior cruciate ligament injury, and stress fractures. There is a recognised desire to utilise motion capture technology to visualise and give feedback on movement within sports and performance in order to develop good technique and contribute to performance enhancement.

Difficulties have been reported in previously tested methods of motion capture for the acquisition of accurate and reliable data for both performance analysis and reproduction; these difficulties are common and vary dependant on the technology and methodologies used.

- The development of motion capture methods to produce accurate data for the classification and analysis of human motion, and a visually pleasing representation of motion in a virtual environment, has been demonstrated in this thesis and therefore provides a clear contribution to existing knowledge.
- A workflow has been established and validated to detect misalignments in ankle position whilst performing gestures of relevé in ballet.
- Results show that subtle variations in joint rotation can be clearly measured and used for fault detection, improved performance and injury prevention.
- Augmented feedback has been shown to encourage practice and participation of skill learning and technology-based feedback is becoming increasingly popular.
- Motion capture methods described in this thesis have shown that the extreme movements that occur in the performance of ballet can be recorded and analysed in detail.

Objective, accurate and pertinent data on performance is essential to provide learners with the feedback necessary for skill learning and performance enhancement. Knowledge of performance should be provided to the performer in a way that scaffolds the learning process without becoming essential to the learner. As instantaneous feedback has been revealed to result in dependence upon feedback and low retention rates of a skill, enough time should be allowed before providing feedback. In this way, it facilitates the discovery of critical sources of intrinsic feedback that are essential to controlling performance when feedback is not presented. The methods of data analysis described within this report only allow performance to be evaluated post performance, although a representation of the performance can be visually observed in real-time. This allows time for the learner to self-evaluate before

knowledge of performance is provided. This sequence of performance, self-evaluation and augmented feedback would benefit the learning process without leading to dependence. Implementing a bandwidth to the desired, or undesired, movement may also offer a way to assist coaches and practitioners gradually lower the frequency of feedback to further avoid dependence.

It has also been confirmed in the report that there is much interest in the use of motion capture technologies for use in augmented performance and virtual reality.

- A workflow describing the production of a virtual character using depth sensor body scanning, which accurately represents the form of a scanned subject, has been presented.
- This character avatar can then be rigged with assistance from customised scripts, and animated using motion recorded from the same subject using the IGS-190 motion capture suit and viewed in real-time within a virtual environment.

The application of the unadulterated captured motion to a virtual character was well received by audiences at two international exhibitions and signs of the ‘uncanny valley’ phenomenon were not evident. It can therefore be accepted that the method of character production described would be suitable for use in both augmented performance applications and for the visualisation of a virtual performance for analysis.

9.1 Further Work and Application

As the performance analysis methods described in this thesis requires a working knowledge of various complex pieces of software, a more usable workflow may need to be developed to facilitate the analysis of performance by a wider user group; this might include coaches and physiotherapists, or individual performers wishing to analyse their own performance. There may be several ways to go about this.

Autodesk’s Maya and MotionBuilder are open and extensible products. The Application Programmer Interface (API) is a C++ API that provides internal access to both Maya and MotionBuilder. This API can be used to implement plug-ins that extend the functionality of the programmes, or develop stand-alone console applications. A programme could therefore be developed to make use of the functionality of MotionBuilder and the computational efficiency of Maya in order to directly deal with the motion data. Through doing this, it may be possible to produce an interface that allows the user to select a joint, or collection of joints, for analysis and calculate the deviation from a desirable orientation.

An alternative approach may involve using the motion capture hardware (the IGS-190) as an input to a real-time rendering application such as UNREAL, Unity, or Panda3D games engines. Animazoo advertise that they offer real-time driver packages allowing the live visualization of data on characters, although there is little evidence to suggest that this has been formally demonstrated. It might be possible that, should the IGS-190 be able to serve as an input device into such a real-time games engine, 'on the fly' analysis can be incorporated into the programme. A bandwidth KR method might also be implemented in the form of a traffic light system where green shows safe alignment, red being alignment causing immediate danger of injury, and amber being a non-immediate risk but with risk of longer term injury.

In order to gain a more comprehensive insight into combining motion capture technologies with virtual characters and environments to deliver augmented performances, further formalised feedback would need to be documented. This could come in many forms, in a number of different scenarios. Live theatrical performances involving virtual environments as a set for the production, and virtual characters featuring as part of the performance may be one way of setting up an experiment. The audience could be asked a number of open-ended questions about the experience, and the success of the production could be established. Similarly, the user of performance analysis software described above might also be able to give valuable feedback on the comfort felt whilst viewing a virtual representation of themselves in a virtual environment.

The further work suggested here would be a development of the research carried out within this thesis, and would add to the knowledge surrounding the subject as a whole.

10 References

1. ADAMS, J. A. 1968. Response Feedback and Learning. *Psychological Bulletin*, 70, 486-504.
2. ADAMS, J. A. 1971. A Closed-Loop Theory of Motor Learning. *Journal of Motor Behavior*, 3, 111-150.
3. ADAMS, J. A. & DIJKSTRA, S. 1966. Short-term memory for motor responses. *Journal of Experimental Psychology*, 71, 314-318.
4. ADRIAN, M. J. & COOPER, J. M. 1995. *Biomechanics of Human Movement*, Dubuque, Iowa, Brown & Benchmark.
5. AGUINALDO, A. L. & CHAMBERS, H. 2009. Correlation of Throwing Mechanics With Elbow Valgus Load in Adult Baseball Pitchers. *The American Journal of Sports Medicine*, 37, 2043 - 2048.
6. ANDERSON, D. I., MAGILL, M. A. & SEKIYA, H. 2001. Motor learning as a function of KR schedule and characteristics of task-intrinsic feedback. *Journal of Motor Behavior*, 33, 59-66.
7. ANDERSON, D. I., MAGILL, M. A., SEKIYA, H. & RYAN, G. 2005. Support for an explanation of the guidance effect in motor skill learning. *Journal of Motor Behavior*, 37, 231-238.
8. ANDERSON, D. I., MAGILL, R. A. & SEKIYA, H. 1994. A reconsideration of the trials-delay of knowledge of results paradigm in motor skill learning. *Research Quarterly for Exercise and Sport*, 65, 286-290.
9. ANDREADIS, A., HEMERY, A., ANTONAKAKIS, A., GOURDOGLOU, G., MAURIDIS, P., CHRISTOPOULOS, D. & KARIGIANNIS, J. N. 2010. Real-Time Motion Capture Technology on a Live Theatrical Performance with Computer Generated Scenery. 14th Panhellenic Conference on Informatics, 10-12 Sept 2010, Tripoli, Greece. pp.148 - 152.
10. ANNETT, J. 1961. The role of knowledge of results in learning: A survey. Port Washington, LI, New York: US Naval Training Device Center.
11. ANNETT, J. & KAY, H. 1957. Knowledge of results and "skilled performance". *Occupational Psychology*, 31.
12. ARMOUR, K. 2011. *Sport Pedagogy: an introduction for teaching and coaching*, Essex, UK, Pearson Education.
13. ARMSTRONG, T. R. 1970. Feedback and perceptual-motor skill learning: A review of information feedback and manual guidance training techniques. Ann Arbor, Michigan: Human Performance Center.

14. AZUMA, R., BAILLOT, Y., BEHRINGER, R., FEINER, S., JULIER, S. & MACINTYRE, B. 2001. Recent Advances in Augmented Reality. *IEEE Computer Graphics and Applications*, 21 (6), 34-47.
15. BARLETT, R. 1999. Sports Biomechanics: reducing injury and improving performance, London, E & FN Spon.
16. BAUDRY, L., LEROY, D., THOUVARECQ, R. & CHOLLET, D. 2006. Auditory concurrent feedback benefits on the circle performed in gymnastics. *Journal of Sports Sciences*, 24, 149-156.
17. BECKERMAN, H. 2003. *Animation: The Whole Story*, New York, Allworth Press.
18. BENNETT, K. & CAVANAUGH, R. A. 1998. Effects of immediate self-correction, delayed self-correction, and no correction on the acquisition and maintenance of multiplication facts by a fourth-grade student with learning disabilities. *Journal of Applied Behaviour Analysis*, 31 (2), 303 - 306.
19. BERTRAM, C. P., MARTENIUK, R. G. & GUADAGNOLI, M. A. 2007. On the use and misuse of video analysis. *International Journal of Sports Science & Coaching*, 2, 37-46.
20. BILODEAU, E. A. & BILODEAU, I. M. 1958. Variable frequency of knowledge of results and the learning of a simple skill. *Journal of Experimental Psychology*, 55, 379-383.
21. BILODEAU, E. A., BILODEAU, I. M. & SCHUMSKY, D. A. 1959. Some effects of introducing and withdrawing knowledge of results early and late in practice. *Journal of Experimental Psychology*, 58, 142-144.
22. BLANDIN, Y., TOUSSAINT, L. & SHEA, C. H. 2008. Specificity of practice: Interaction between concurrent sensory information and terminal feedback. *Journal of Experimental Psychology: Learning, Memory and Cognition*, 34, 994-1000.
23. BRANFIELD, J. R. & BELL, H. W. 1970. *Matrices and their Applications*, London, Macmillan.
24. BRISSON, T. A. & ALAIN, C. 1996. Should common optimal movement patterns be identified as the certain to be achieved? *Journal of Motor Behavior*, 28, 211-223.
25. BRISSON, T. A. & ALAIN, C. 1997. A comparison of two references for using knowledge of performance in learning a motor task. *Journal of Motor Behavior*, 29, 339-350.
26. BRODIE, M., WALMSLEY, A. & PAGE, W. 2008. Fusion motion capture: a prototype system using inertial measurement units and GPS for the biomechanical analysis of ski racing. *Sports Technology*, 1, 17 - 28.
27. CHAMBERS, K. L. & VICKERS, J. N. 2006. Effects of bandwidth feedback and questioning on the performance of competitive swimmers. *The Sport Psychologist*, 20 (2), 184-197.

28. CHOLLET, D., MADANI, M. & MICALLEF, J. P. 1992. Effects of two types of biomechanical bio-feedback on crawl performance. *In: LEES, A., MACLAREN, D. & REILLY, T. (eds.) Biomechanics and medicine in swimming: Swimming science V1*. London: Spon Press.
29. CORAZZA, S., MÜNDERMANN, L., CHAUDHARI, A. M., DEMATTIO, T., COBELLI, C. & ANDRIACCHI, T. P. 2006. A Markerless Motion Capture System to Study Musculoskeletal Biomechanics: Visual Hull and Simulated Annealing Approach. *Annals of Biomedical Engineering*, 34 (6), 1019–1029.
30. DIXON, E. 2005. The mind/body connection and the practice of classical ballet. *Research in Dance Education*, 6, 75-96.
31. DOI, J., SHIMIZU, K. & SATO, W. 2007. High-Density Scanning for Virtual Heritage and Archeology: Reproduction and Restoration. 3DTV Conference, 7-9 May 2007, Kos, Greece. pp.1 - 4.
32. ERIKSSON, M., HALVORSEN, K. A. & GULLSTRAND, L. 2011. Immediate effect of visual and auditory feedback to control the running mechanics of well-trained athletes. *Journal of Sports Sciences*, 29 (3), 253-262.
33. FANTINO, E. & LOGAN, C. A. 1979. The experimental analysis of behaviour: A biological perspective, San Francisco, Freeman.
34. FELTZ, D. L., SHORT, S. E. & SINGLETON, D. A. 2008. The effect of self-modelling on shooting performance and self-efficacy with intercollegiate hockey players. *In: SIMMONS, M. P. & FOSTER, L. A. (eds.) Sport and exercise psychology research advances*. New York: Nova Science.
35. FINKBEINER, D. T. 1966. Introduction to Matrices and Linear Transformations: Second Edition, San Francisco, US, Freeman.
36. FITTS, P. M. & POSNER, M. I. 1967. *Human performance*, California, Brooks/Cole Pub. Co.
37. FLEISCHER, M. 1917. *Method of producing moving picture cartoons*. United States of America patent application. 09/10/1917.
38. FLEISIG, G., BARRANTINE, S. W., ZHENG, N., ESCAMILLIA, R. F. & ANDREWS, J. R. 1999. Kinematic and Kinetic Comparison of Baseball Pitching Among Various Levels of Development. *Journal of Biomechanics*, 32, 1371-1375.
39. FRYAR, C. D., GU, Q. & OGDEN, C. L. 2012. Anthropometric reference data for children and adults 2007-2010. *In: STATISTICS, V. H. (ed.)*. United States: National Center for Health Statistics.
40. HAAG, J. 2009. Inertial Motion Capture and Live Performance (with a Focus on Dance). *Dance Dialogues: Conversations across cultures, artforms and practices*.

41. HATTIE, J. & TIMPERLEY, H. 2007. The Power of Feedback. *Review of Educational Research*, 77 (1), 81 - 112.
42. HAY, J. G. & REID, G. 1988. *Anatomy, Mechanics and Human Motion*, Englewood Cliffs, New Jersey, Prentice-Hall.
43. HELMER, R. J. N., FARROW, D., LUCAS, S. R., HIGGERSON, G. J. & BLANCHONETTE, I. 2010. Can interactive textiles influence a novice's throwing technique? *Procedia Engineering*, 2 (2), 2985-2990.
44. HILLER, C. E., REFSHAUGE, K. M. & BEARD, D. 2004. Sensory Motor Control Is Impaired in Dancers With Functional Ankle Instability. *The American Journal of Sports Medicine*, 32, 216 - 223.
45. HO, C.-C. & MACDORMAN, K. F. 2010. Revisiting the uncanny valley theory: Developing and validating an alternative to the Godspeed indices. *Computers in Human Behavior*, 26, 1508 - 1518.
46. HOGAN, J. C. & YANOWITZ, B. A. 1978. The role of verbal estimates of movement error in ballistic skill acquisition. *Journal of Motor Behavior*, 10, 133-138.
47. HUCKLEMEMKES, J. 1992. Model Technique for the Womens 100-Meter Hurdles. *Track Technique*, 118, 3759-3766.
48. HUGHES, M. & FRANKS, I. 2004. *Notational Analysis of Sport: Systems for Better Coaching and Performance in Sport*, Routledge.
49. IMAMURA, R. & JOHNSON, B. 2003. A kinematic analysis of a judo leg sweep: Major outer leg reap-osto-gari. *Journal of Sports Biomechanics*, 2 (2), 191-201.
50. KADEL, N. J. 2006. Foot and Ankle Injuries in Dance. *Physical Medicine and Rehabilitation Clinics of North America*, 17 (4), 813-826.
51. KANG, J., WRIGHT, D. K., QIN, S. F. & ZHAO, Y. 2005. Modelling human behaviours and reactions under dangerous environment. *Biomedical Sciences Instrumentation*, 41, 265 - 270.
52. KIRYATI, N., RAVIV, T. R., IVANCHENKO, Y. & ROCHEL, S. 2008. Real-time Abnormal Motion Detection in Surveillance Video. *19th International Conference on Pattern Recognition*, 1-4.
53. KNUDSON, D. V. & MORRISON, C. S. 2002. *Qualitative Analysis of Human Movement*, Champaign, Illinois, Human Kinetics.
54. KOH, M. & TAN, J. 2006. *Understanding Biomechanics: for physical education and sports*, Singapore, McGraw-Hill.

55. KONTTINEN, N., MONONEN, K., VIITASALO, J. T. & METS, T. 2004. The effects of augmented auditory feedback on psychomotor skill learning in precision shooting. *Journal of Sport & Exercise Psychology*, 26, 306-316.
56. KULIK, J. A. & KULIK, C.-L. C. 1988. Timing of Feedback and Verbal Learning. *Review of Educational Research*, 58 (1), 79 - 97.
57. LAVERY, J. J. 1962. Retention of simple motor skills as a function of type of knowledge of results. *Canadian Journal of Psychology*, 16, 300-311.
58. LAZOUKIS, A. The "Science Center To Go" project. In: LAZOUKIS, A., SALMI, H. & SOTIRIOU, S., eds. *Augmented Reality in Education*, October 27-29 2011, Athens, Greece.
59. LEES, A. 1999. *Technique Analysis*, Leeds, National Coaching Foundation.
60. LEES, A. 2002. Technique analysis in sports: A critical review. *Journal of Sports Sciences*, 20, 813-828.
61. LEES, A. 2013. Biomechanics applied to soccer skills. In: WILLIAMS, A. M. (ed.) *Science and Soccer: Developing Elite Performers*. Oxon: Routledge.
62. LI, X. & LI, X. 2010. Human Body Dimensions Extraction From 3D Scan Data. *International Conference on Intelligent Computation Technology and Automation*. Changsha, China.
63. LIEDERBACH, M., DILGEN, F. E. & ROSE, D. J. 2008. Incidence of Anterior Cruciate Ligament Injuries Among Elite Ballet and Modern Dancers. *The American Journal of Sports Medicine*, 36 (9), 1779-1788.
64. LINDEN, J. V. D., SCHOONDERWALDT, E., BIRD, J. & JOHNSON, R. 2011. MusicJacket - Combining Motion Capture and Vibrotactile Feedback to Teach Violin Bowing. *IEEE Transactions on Instrumentation and Measurement*, 60, 104 - 113.
65. LINTERN, G. 1980. Transfer of landing skill after training with supplementary visual cues. *Human Factors*, 22, 81-88.
66. LIU, J. & WRISBERG, C. A. 1997. The effect of knowledge of results delay and the subjective estimation of movement form on the acquisition and retention of a motor skill. *Research Quarterly for Exercise and Sport*, 68, 145-151.
67. LOKER, S., ASHDOWN, S. & SHOENFELDER, K. 2005. Size-Specific Analysis of Body Scan Data to Improve Apparel Fit. *Journal of Textile and Apparel, Technology and Management*, 4 (3), 1 - 15.
68. LORGE, I. & THORNDIKE, E. L. 1935. The influence of delay in the after-effect of a connection. *Journal of Experimental Psychology*, 18, 186-194.
69. LUFT, A. R. & BUITRAGO, M. M. 2005. Stages of Motor Skill Learning. *Molecular Neurobiology*, 32 (3), 205 - 216.

70. MA, R., CHABLAT, D., BENNIS, F. & MA, L. 2011. A framework of motion capture system based human behaviours simulation for ergonomic analysis. *14th International Conference on Human-Computer Interaction*.
71. MAGILL, R. A. & ANDERSON, D. I. 2012. The roles and uses of augmented feedback in motor skill acquisition. In: HODGES, N. J. & WILLIAMS, A. M. (eds.) *Skill Acquisition in Sport: Research, Theory and Practice*. Oxon: Routledge.
72. MAREY, E. J. 1879. *Animal Mechanism: A treatise on terrestrial and aerial locomotion*, New York, Appleton and Co.
73. MASLOVAT, D., BRUNKE, K. M., CHUA, R. & FRANKS, I. M. 2009. Feedback effects on learning a novel bimanual coordination pattern: Support for the guidance hypothesis. *Journal of Motor Behavior*, 41, 45-54.
74. MCLEAN, S. G., SU, A. & BOGERT, A. J. V. D. 2003. Development and validation of a 3-D model to predict knee joint loading during dynamic movement. *Journal of Biomechanical Engineering*, 125 (6), 864 - 874.
75. MCPHERSON, M. 1990. A Systematic Approach to Skill Analysis. *Sports Science Periodical on Research Technology in Sports*, 11 (1), 1 - 10.
76. MEADOR, W. S., ROGERS, T. J., O'NEAL, K., KURT, E. & CUNNINGHAM, C. 2004. Mixing Dance Realities: Collaborative Development of Live-Motion Capture In a Performing Arts Environment. *Computers in Entertainment*, 2, 12.
77. MENACHE, A. 2000. *Understanding Motion Capture for Computer Animation and Video Games*, San Francisco, Morgan Kaufmann.
78. MONONEN, K., VIITASALO, J. T., KONTTINEN, N. & ERA, P. 2003. The effects of augmented kinematic feedback on motor skill learning in rifle shooting. *Journal of Sports Sciences*, 21 (10), 867-876.
79. MORI, M. 1970. The Uncanny Valley (Bukimi No Tani). *Energy*, 7, 33 - 35.
80. MOTTA-VALENCIA, K. 2006. Dance-Related Injury. *Physical Medicine and Rehabilitation Clinics of North America*, 17, 697 - 723.
81. MYER, G. D., FORD, K. R., MCLEAN, S. G. & HEWETT, T. E. 2006. The Effects of Plyometric Versus Dynamic Stabilization and Balance Training on Lower Extremity Biomechanics. *The American Journal of Sports Medicine*, 34 (3), 445-455.
82. NICHOLLS, R., FLEISIG, G., ELLIOT, B., LYMAN, S. & OSINSKI, E. 2003. Accuracy of Qualitative Analysis for Assessment of Skilled Baseball Pitching Technique. *Journal of Sports Biomechanics*, 11 (1), 1-10.

83. NOURRIT, D., DELIGNIÈRES, D., CAILLOU, N., DESCHAMPS, T. & LAURIOT, B. 2003. On discontinuities in motor learning: A longitudinal study of complex skill acquisition on a ski simulator. *Journal of Motor Behavior*, 35, 151-170.
84. O'ROURKE, M. 2003. Principles of three-dimensional computer animation: modelling, rendering, and animating with 3D computer graphics, New York, Norton and Co.
85. OHGI, Y. 2006. MEMS Sensor Application for the Motion Analysis in Sports Science. *ABCM Symposium Series in Mechatronics*, 2, 501 - 508.
86. OKADA, R., STENGER, B., IKE, T. & KONDOH, N. 2006. Virtual Fashion Show Using Real-Time Markerless Motion Capture. *Asian Conference on Computer Vision*. Berlin, Heidelberg: Springer-Verlag.
87. ORR, J. F. & SHELTON, J. C. 1997. *Optical Measurement Methods in Biomechanics*, London, Chapman & Hall.
88. PARENT, R. 2008. *Computer Animation - Algorithms & Techniques*. Waltham, MA: Morgan Kaufmann.
89. PATTERSON, J. T. & CARTER, M. 2010. Learner regulated knowledge of results during the acquisition of multiple timing goals. *Human Movement Science*, 29, 214-227.
90. RACHLIN, H. 1976. *Introduction to Modern Behaviourism*, San Francisco, W. H. Freeman and Company.
91. ROSENHAHN, B., KLETTE, R. & METAXAS, D. N. 2008. *Human Motion: understanding, modeling, capture and animation*, Springer.
92. RUCCI, J. A. & TOMPOROWSKI, P. D. 2010. Three types of kinematic feedback and the execution of the hang power clean. *Journal of Strength and Conditioning Research*, 24 (3), 771-778.
93. SALMONI, A. W., SCHMIDT, R. A. & WALTER, C. B. 1984. Knowledge of results and motor learning: A review and critical reappraisal. *Psychological Bulletin*, 95, 355-386.
94. SAVION-LEMIEUX, T. & PENHUNE, V. B. 2005. The effects of practice and delay on motor skill learning and retention. *Experimental Brain Research*, 161 (4), 423 - 431.
95. SCHMIDT, R. A. 1975. A schema theory of discrete motor skill learning. *Psychological Review*, 82, 225-260.
96. SCHMIDT, R. A. & LEE, T. D. 1999. *Motor control and learning: a behavioral emphasis*, Champaign, Illinois, Human Kinetics.
97. SCHMIDT, R. A. & WRISBERG, C. A. 2008. *Motor Learning and Performance: A Situation-based Learning Approach*, Champaign, Illinois, Human Kinetics.
98. SHERWOOD, D. E. 1988. Effect of bandwidth knowledge of results on movement consistency. *Perceptual and Motor Skills*, 66, 535-542.

99. SKINNER, B. F. 1974. *About Behaviourism*, London, Jonathan Cape Ltd.
100. SMITH, R. M. & LOSCHNER, C. 2002. Biomechanics feedback for rowing. *Journal of Sports Sciences*, 20, 783-791.
101. SPARACINO, F. 2004. Scenographies of the past and museums of the future: from the wunderkammer to body-driven interactive narrative spaces. *Proceedings of the 12th annual ACM international conference on Multimedia*. New York, NY, USA: ACM.
102. SPINKS, W. L. & SMITH, R. M. 1994. The effects of kinetic information feedback on maximal rowing performance. *Journal of Human Movement Studies*, 27, 17-35.
103. STEINBERG, N., SIEV-NER, I., PELEG, S., DAR, G., MASHARAWI, Y., ZEEV, A. & HERSHKOVITZ, I. 2012. Extrinsic and intrinsic risk factors associated with injuries in young dancers aged 8-16 years. *Journal of Sports Sciences*, 30 (5), 485-495.
104. STILLMAN, J. D. B. & MUYBRIDGE, E. 1882. *The Horse in Motion: As shown by instantaneous photography with a study on animal mechanics*, Boston, Osgood and Co.
105. SWINNEN, S. P., SCHMIDT, R. A., NICHOLSON, D. E. & SHAPIRO, D. C. 1990. Information feedback for skill acquisition: Instantaneous knowledge of results degrades learning. *Journal of Experimental Psychology: Learning, Memory and Cognition*, 16, 706-716.
106. TAKEI, Y., DUNN, H. & BLUCKER, E. 2003. Techniques used in high-scoring and low-scoring 'roche' vaults performed by elite male gymnasts. *Journal of Sports Biomechanics*, 2 (2), 141-162.
107. TARPY, R. M. & SAWABINI, F. L. 1974. Reinforcement delay: A selective review of the last decade. *Psychological Bulletin*, 81, 984-997.
108. THOMAS, F. & JOHNSTON, O. 1981. *The Illusion of Life: Disney Animation*, New York, Disney Editions.
109. THORNDIKE, E. L. 1914. *Educational Psychology*, New York, Columbia University.
110. THORNDIKE, E. L. 1927. The Law of Effect. *American Journal of Psychology*, 39, 212-222.
111. THORNDIKE, E. L. 1932. *The Fundamentals of Learning*, New York, Teachers College.
112. TIDOW, G. 1990. Models for Teaching Techniques and Assessing Movements in Athletics: The Long Jump. *Track Technique*, 113, 3607-3615.
113. TONG, J., ZHOU, J., LIU, L., PAN, Z. & YAN, H. 2012. Scanning 3D Full Human Bodies Using Kinects. *IEEE Transactions on Visualization and Computer Graphics*, 18 (4), 643 - 650.
114. TROWBRIDGE, M. H. & CASON, H. 1932. An experimental study of Thorndike's theory of learning. *Journal of General Psychology*, 7, 245 - 258.
115. TYLER, D., MITCHELL, A. & GILL, S. 2012. Recent advances in garment manufacturing technology: joining techniques, 3D body scanning and garment design. *In: SHISHOO, R.*

- (ed.) *The global textile and clothing industry: Technological advances and future challenges*. Cambridge, UK: Woodhead Publishing.
116. VANDER-LINDEN, D. W., CAURAUGH, J. H. & GREENE, T. A. 1993. The effect of frequency of kinetic feedback on learning an isometric force production task in nondisabled subjects. *Physical Therapy*, 73, 79-87.
 117. WATERS, J. K. 2003. *Blobitecture: waveform architecture and digital design*, Massachusetts, Rockport Publishers.
 118. WEBSTER, C. 2005. *Animation: The Mechanics of Motion*, Oxford, Elsevier.
 119. WEEKS, D. L. & KORDUS, R. N. 1998. Relative frequency of knowledge of performance and motor skill learning. *Research Quarterly for Exercise and Sport*, 69, 224-230.
 120. WINCHESTER, J. B., PORTER, J. M. & MCBRIDE, J. M. 2009. Changes in bar path kinematics and kinetics through use of summary feedback in power snatch training. *Journal of Strength and Conditioning Research*, 23 (2), 444-454.
 121. WINSTEIN, C. J. & SCHMIDT, R. A. 1990. Reduced frequency of knowledge of results enhances motor skill learning. *Journal of Experimental Psychology: Learning, Memory and Cognition*, 16, 677-691.
 122. WORTHEN, L. & HAMILL, J. 1997. Biomechanical issues in ballet: Ankle alignment in pointe shoes. 15th Annual Symposium on Medical Problems of Musicians and Dancers, 1997 Denver, Colorado.
 123. WREN, P. A. G., S. 2010. Industry Fit Practices and Their Variation. Textile Institute 100th World Conference, 2 - 3 November 2010. Manchester, UK.
 124. WULF, G. & SHEA, C. H. 2004. Understanding the role of augmented feedback: The good, the bad and the ugly. In: WILLIAMS, A. M. & HODGES, N. J. (eds.) *Skill Acquisition in Sport: Research, Theory, and Practice*. London: Routledge.
 125. XU, B., HUANG, Y., YU, W. & CHEN, T. 2002. Body Scanning and Modeling for Custom Fit Garments. *Journal of Textile and Apparel, Technology and Management*, 2 (2), 1 - 11.
 126. YOUNG, D. E. & SCHMIDT, R. A. 1992. Augmented feedback for enhanced skill acquisition. In: STELMACH, G. E. & REQUIN, J. (eds.) *Tutorials in Motor Behaviour II*. Amsterdam: Elsevier.
 127. ZELLER, J. 2009. Teaching through Time: Tracing Ballet's Pedagogical Lineage in the Work of Maggie Black. *Dance Chronicle*, 32 (1), 57-88.

11 Appendices

11.1 Vectors

In mathematics, physics, and engineering, an *Euclidean vector* (sometimes called a *geometric vector*, or referred to simply as a *vector*) is a geometric object that has magnitude (or length) and direction and can be added to other vectors according to vector algebra. An Euclidean vector is frequently represented by a line segment with a definite direction, or graphically as an arrow, connecting an *initial point* A with a *terminal point* B , and denoted by \overrightarrow{AB} .

It is important to distinguish Euclidean vectors from the more general concept in linear algebra of vectors as elements of a vector space. A vector space is a mathematical structure formed by a collection of vectors, which may be added together and multiplied (scaled) by numbers, called scalars in this context. Scalars are often taken to be real numbers, but there are also vector spaces with scalar multiplication by complex numbers, rational numbers, or generally any field (any set of elements that satisfies the field axioms for both addition and multiplication and is a commutative division algebra). The concept of a Euclidean space encompasses Euclidean plane and the three-dimensional space of Euclidean geometry as spaces of dimensions 2 and 3 respectively. Euclidean spaces also generalise these ideas to higher dimensions.

Classical Greek geometry defined the Euclidean plane and Euclidean three-dimensional space using certain axioms (statements or propositions regarded as being established, accepted, or self-evidently true), while the other properties of these spaces were deduced as theorems. As algebra and mathematical analysis have developed, it is now more common to define Euclidean space using Cartesian coordinates (a system that specifies each point uniquely by an ordered list of numerical coordinates that relate to mutually perpendicular planes) and the ideas of analytic geometry. It means that points of the space are specified with collections of real numbers and geometric shapes are defined as equations and inequalities. This approach brings the tools of algebra and calculus to bear on questions of geometry, and has the advantage that it generalises easily to Euclidean spaces of more than three dimensions.

As the environment for which this research is carried out is based in three-dimensional Euclidean space, specifically Autodesk's Maya and MotionBuilder software, Euclidean vectors shall be used throughout this chapter.

In mathematics, the *standard basis* (also called *natural basis* or *canonical basis*) for a Euclidean space consists of one unit vector pointing in the direction of each axis of the Cartesian coordinate system. For example, the standard basis for the Euclidean plane are the vectors

$$e_x = (1, 0), \quad e_y = (0, 1)$$

and the standard basis for three-dimensional space are the vectors

$$e_x = (1, 0, 0), \quad e_y = (0, 1, 0), \quad e_z = (0, 0, 1)$$

Here the vector e_x points in the x direction, the vector e_y points in the y direction, and the vector e_z points in the z direction. There are several common notations for these vectors, including (e_x, e_y, e_z) , (e_1, e_2, e_3) , $(\hat{i}, \hat{j}, \hat{k})$, and $(\hat{x}, \hat{y}, \hat{z})$.

These vectors are a basis in the sense that any other vector can be expressed uniquely as a linear combination of these. For example, every vector V in three-dimensional space can be written uniquely as

$$V = v_x e_x + v_y e_y + v_z e_z$$

the scalars v_x, v_y, v_z being the scalar components of the vector V .

In n -dimensional Euclidean space, the standard basis consists of n distinct vectors

$$\{e_i : 1 \leq i \leq n\}$$

where e_i denotes the vector with a 1 in the i th coordinate and 0's elsewhere.

The *length* or *magnitude* or *norm* of the vector a is denoted by $\|a\|$ or, less commonly, $|a|$ which is not to be confused with the absolute value (a scalar "norm").

The length of the vector a can be computed with the Euclidean norm, where a_1 represents the first axis in three-dimensional space, a_2 the second and a_3 the third.

$$\|a\| = \sqrt{a_1^2 + a_2^2 + a_3^2}$$

This length formula is a consequence of the Pythagorean theorem since the basis vectors e_x, e_y and e_z are orthogonal unit vectors. Euclidean vectors, in geometry, are orthogonal if they are perpendicular. A line is said to be perpendicular to another line if the two lines intersect at a right angle, a line is said to be perpendicular to a plane if it is perpendicular to every line in

the plane that it intersects, and two planes are said to be perpendicular if the dihedral angle (the angle formed by two intersecting planes) is a right angle (for example see figure 7.1).

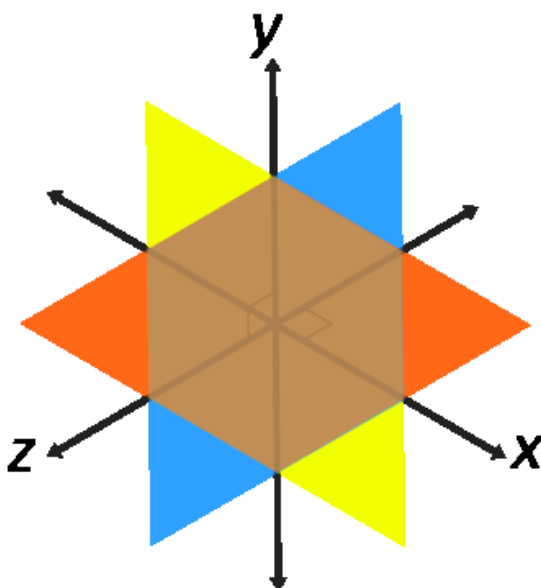


Figure 7.1: Perpendicular axes and planes

This happens to be equal to the square root of the dot product (discussed below) of the vector with itself:

$$\|a\| = \sqrt{a \cdot a}$$

The *dot product* of two vectors a and b (sometimes called the *inner product*, or, since its result is a scalar, the *scalar product*) is denoted by $a \cdot b$ and is defined as:

$$a \cdot b = \|a\| \|b\| \cos \theta$$

where θ is the measure of the angle between a and b . Geometrically, this means that a and b are drawn with a common start point and then the length of a is multiplied with the length of that component of b that points in the same direction as a (see figure 7.2).

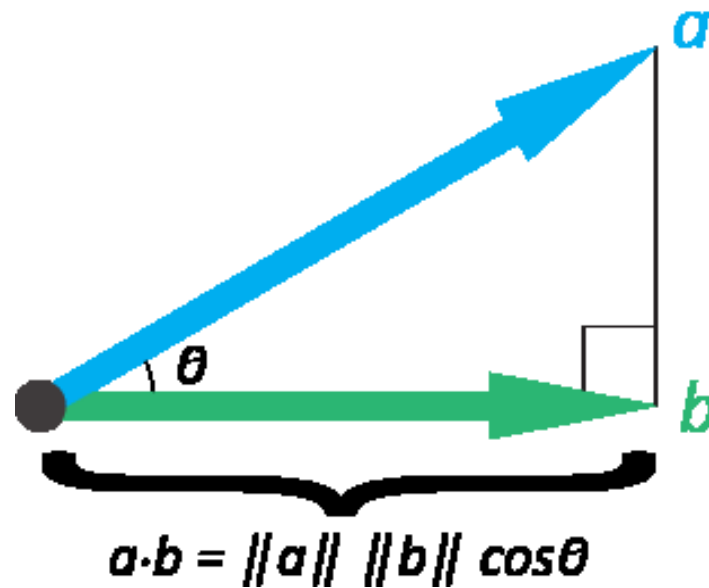


Figure 7.2: Visual explanation of the dot product

The dot product can also be defined as the sum of the products of the components of each vector as

$$\mathbf{a} \cdot \mathbf{b} = a_1 b_1 + a_2 b_2 + a_3 b_3$$

A *unit vector* is any vector with a length of one; normally unit vectors are used simply to indicate direction. A vector of arbitrary length can be divided by its length to create a unit vector. This is known as *normalizing* a vector. A unit vector is often indicated with a circumflex; as in \hat{a} .

To normalize a vector $\mathbf{a} = [a_1, a_2, a_3]$, scale the vector by the reciprocal of its length $\|\mathbf{a}\|$. That is:

$$\hat{\mathbf{a}} = \frac{\mathbf{a}}{\|\mathbf{a}\|} = \frac{a_1}{\|\mathbf{a}\|} \mathbf{e}_1 + \frac{a_2}{\|\mathbf{a}\|} \mathbf{e}_2 + \frac{a_3}{\|\mathbf{a}\|} \mathbf{e}_3$$

11.2 Matrices

Matrices are a quite general concept and are made up of a rectangular array of numbers, symbols, or expressions arranged in *rows* and *columns*. They are widely used in applications that need to represent 3D transformations programmatically. The individual items in a matrix are called its *elements* or *entries*. Some applications use *row major*, others use *column major*

for their transformations; Autodesk's Maya is row major and is the one we shall use in this chapter. One is the transpose of the other, i.e. the elements are reflected along the main diagonal resulting in the rows of a row major matrix being the columns of a column major matrix.

$$\text{Row major} \quad p = [P_x \ P_y \ P_z] \begin{bmatrix} X_x & X_y & X_z \\ Y_x & Y_y & Y_z \\ Z_x & Z_y & Z_z \end{bmatrix}$$

$$\text{Column major} \quad p = \begin{bmatrix} X_x & Y_x & Z_x \\ X_y & Y_y & Z_y \\ X_z & Y_z & Z_z \end{bmatrix} \begin{bmatrix} P_x \\ P_y \\ P_z \end{bmatrix}$$

If an object is rotated by 90 degrees around the Y axis, then that object's basis vectors would be:

$$x = \langle 0, 0, -1 \rangle$$

$$y = \langle 0, 1, 0 \rangle$$

$$z = \langle 1, 0, 0 \rangle$$

In the example described above and shown in figure 7.3, you would see the object's X axis facing down the negative Z of the world, the Y axis pointing in the direction of the world Y and the Z axis pointing in the direction of the world X.

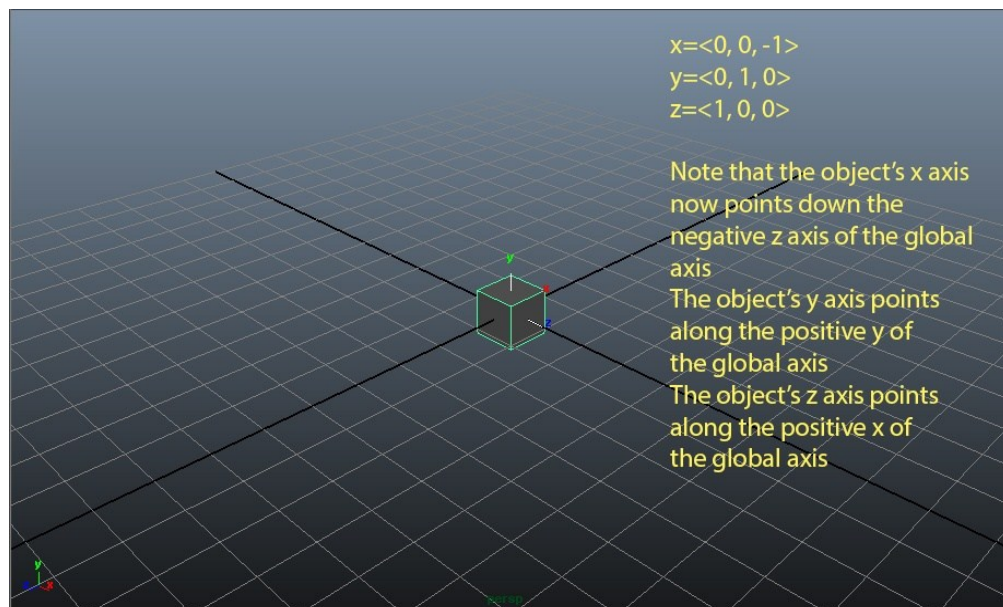


Figure 7.3: an object rotated by 90 degrees around the Y axis

These are the basis vectors for the transform in world space and if you have basis vectors for the transform, you have enough information to solve the rotation; i.e. from the above three vectors, you could figure out that the rotation was 90 degrees around the Y-axis. The reverse, converting a matrix into rotations, will be covered later.

Transformation matrices are quite interesting because they have an anatomy. Understanding this anatomy enormously helps clear away the confusion surrounding matrices. Taking the rotation from the example above (i.e. $r = 0, 90, 0$), the resulting matrix would be:

```
0  0  -1  0
0  1   0  0
1  0   0  0
0  0   0  1
```

This is the matrix for an object sitting at origin rotated 90 degrees around the Y-axis. As can be seen, the top-left 3x3 part of the matrix is just the basis vectors from the above example and this is generally true for all transformation matrices; the top left 3x3 part of the matrix contains the basis vectors for the transform. This 3x3 part of the matrix is the rotation matrix because it completely describes the rotation. For the matrix to be a proper rotation matrix, it must be true that the vectors are both orthogonal to one another and are normalised (converted to unit vectors).

The position of a transform is stored in the first three items of the last row. If we wanted to have our transform in the above example positioned at $\langle 1, 2, 3 \rangle$ in XYZ, our transformation matrix would look like this:

```
0  0  -1  0
0  1   0  0
1  0   0  0
1  2   3  1
```

Scale is slightly different, as it does not have a clear spot in the matrix. Technically it is impossible to extract scale and rotation from a general transformation matrix, as a general transformation matrix can have shear (a transformation in which all points along a given line remain fixed while other points are shifted parallel to it by a distance proportional to their perpendicular distance) and scale (changing an objects dimensions) as well as rotation, and all three of these pieces of data live in the upper 3x3 quadrant of the matrix. However, if it

is known you are just working with rotations, translations and scale (which is the case in most 3D modelling applications) then it is not only possible, but also relatively straightforward.

A scale matrix by itself is simple; it is a diagonal matrix with the s_x , s_y and s_z values along the diagonal. A diagonal matrix has all zeros except for its diagonal; i.e. a scale of 1.5, 1.1, 2.5 would look like this:

$$\begin{bmatrix} 1.5 & 0 & 0 \\ 0 & 1.1 & 0 \\ 0 & 0 & 2.5 \end{bmatrix}$$

The above is a simple scale matrix by itself and to get the resulting transformation matrix it needs to be multiplied with the rotation matrix.

The product C of two matrices A and B is defined as

$$\begin{bmatrix} c_{11} & c_{12} & \cdots & & & & \cdots \\ c_{21} & c_{22} & \cdots & & & & \cdots \\ \vdots & \vdots & \ddots & \vdots & \vdots & \vdots & \ddots \\ c_{n1} & c_{n2} & \cdots & & & & \cdots \end{bmatrix}$$

where

$$\begin{aligned} c_{11} &= a_{11}b_{11} + a_{12}b_{21} + \dots & 1 \\ c_{12} &= a_{11}b_{12} + a_{12}b_{22} + \dots & 2 \\ c_{1p} &= a_{11}b_{1p} + a_{12}b_{2p} + \dots & p \\ c_{21} &= a_{21}b_{11} + a_{22}b_{21} + \dots & 1 \\ c_{22} &= a_{21}b_{12} + a_{22}b_{22} + \dots & 2 \\ c_{2p} &= a_{21}b_{1p} + a_{22}b_{2p} + \dots & p \\ c_{n1} &= a_{n1}b_{11} + a_{n2}b_{21} + \dots & 1 \\ c_{n2} &= a_{n1}b_{12} + a_{n2}b_{22} + \dots & 2 \\ c_{np} &= a_{n1}b_{1p} + a_{n2}b_{2p} + \dots & p \end{aligned}$$

To get to our transformation matrix, we'll call the scale matrix S and using the rotation matrix from earlier calling it R , our transformation matrix is SR . Doing so gives us this:

$$\begin{bmatrix} 1.5 & 0 & 0 \\ 0 & 1.1 & 0 \\ 0 & 0 & 2.5 \end{bmatrix} \begin{bmatrix} 0 & 0 & -1 \\ 0 & 1 & 0 \\ 1 & 0 & 0 \end{bmatrix} = \begin{bmatrix} 0 & 0 & -1.5 \\ 0 & 1.1 & 0 \\ 2.5 & 0 & 0 \end{bmatrix}$$

One thing to note here is that scale comes first in the equation. The order of multiplication is important in matrix multiplication, as it is non-commutative and in the case of Maya we must look at the documentation to determine which order the transform matrices are calculated. This shall be discussed in further detail later. Without knowing in advance the order of calculation, it is still possible to determine it.

$$A = \begin{bmatrix} 1 & 2 \\ 3 & 4 \end{bmatrix}, B = \begin{bmatrix} a & b \\ c & d \end{bmatrix}$$

their matrix products are:

$$AB = \begin{bmatrix} 1 & 2 \\ 3 & 4 \end{bmatrix} \begin{bmatrix} a & b \\ c & d \end{bmatrix} = \begin{bmatrix} a+2c & b+2d \\ 3a+4c & 3b+4d \end{bmatrix}$$

and

$$BA = \begin{bmatrix} a & b \\ c & d \end{bmatrix} \begin{bmatrix} 1 & 2 \\ 3 & 4 \end{bmatrix} = \begin{bmatrix} a+3b & 2a+4b \\ c+3d & 2c+4d \end{bmatrix}$$

If you have a more interesting rotation matrix, the result of multiplying it with the scale matrix can get quite messy, as the values are intertwined. This is what the matrix for a rotation of (35, 24, 18) in XYZ with the above scale looks like:

$$\begin{bmatrix} 1.5 & 0 & 0 \\ 0 & 1.1 & 0 \\ 0 & 0 & 2.5 \end{bmatrix} \begin{bmatrix} 0.87 & -0.03 & 0.5 \\ 0.28 & 0.85 & -0.44 \\ -0.41 & 0.52 & 0.75 \end{bmatrix} = \begin{bmatrix} 1.3 & -0.05 & 0.74 \\ 0.31 & 0.94 & -0.49 \\ -1.0 & 1.31 & 1.87 \end{bmatrix}$$

Factoring out elements of a matrix, such as scale or rotation, is called matrix decomposition. Decomposition will take a single matrix and return a number of other matrices, which when multiplied together will return the original matrix. Therefore, if you had a matrix that had translation, rotation and scale and you wanted to change the rotation in the X-axis, you'd need to decompose the matrix, perform the operation on the rotation matrix and then put it all back together.

To do this we first need to understand what a matrix inverse is. A matrix inverse restores the results of a matrix to its original state.

For example, a matrix scaling by factor k would be written:

$$\begin{bmatrix} k & 0 & 0 \\ 0 & k & 0 \\ 0 & 0 & k \end{bmatrix}$$

A matrix that would 'un-do' this scaling would be:

$$\begin{bmatrix} 1/k & 0 & 0 \\ 0 & 1/k & 0 \\ 0 & 0 & 1/k \end{bmatrix}$$

We can verify this by multiplying the scale by the inverse:

$$\begin{bmatrix} k & 0 & 0 \\ 0 & k & 0 \\ 0 & 0 & k \end{bmatrix} \begin{bmatrix} 1/k & 0 & 0 \\ 0 & 1/k & 0 \\ 0 & 0 & 1/k \end{bmatrix} = \begin{bmatrix} 1 & 0 & 0 \\ 0 & 1 & 0 \\ 0 & 0 & 1 \end{bmatrix}$$

To find the inverse of the general 2 x 2 matrix $A = \begin{bmatrix} a & b \\ c & d \end{bmatrix}$, let the inverse of A be

$$M = \begin{bmatrix} p & q \\ r & s \end{bmatrix} \text{ and it is required to find } p, q, r, s \text{ in terms of } a, b, c, d.$$

$$\text{From } \begin{bmatrix} p & q \\ r & s \end{bmatrix} \begin{bmatrix} a & b \\ c & d \end{bmatrix} = \begin{bmatrix} 1 & 0 \\ 0 & 1 \end{bmatrix} \text{ we obtain}$$

$$ap + qc = 1$$

$$bp + qd = 0$$

$$ra + sc = 0$$

$$rb + sd = 1$$

By solving these equations; $p = \frac{d}{(ad-bc)}$, $q = \frac{-b}{(ad-bc)}$, $r = \frac{-c}{(ad-bc)}$, and

$s = \frac{a}{(ad-bc)}$. The inverse matrix A is thus $\frac{1}{(ad-bc)} \begin{bmatrix} d & -b \\ -c & a \end{bmatrix}$. Note the pattern of the elements.

The expression $(ad-bc)$ is known as the *determinant* of the matrix (Branfield and Bell, 1970). Not all matrices have inverses and it is this determinant that characterises matrices that have, or do not have, an inverse. The inverse matrix only exists if this determinant is non-zero,

for if it is zero then the system of 4 equations set above does not have a solution. Such matrices with zero determinants are called *singular* matrices. They do not have an inverse and geometrically they would represent transformations that cannot be *undone*; as multiple points would be returned to the same point.

A is $\begin{bmatrix} a & b \\ c & d \end{bmatrix}$ and its determinant is denoted by $\det(A)$, $\det A$, or $|A|$. Its value $(ad - bc)$ is

found by multiplying the entries in the principal, or leading, diagonal and subtracting the product of the entries in the other diagonal. In the case where the matrix entries are written out in full, the determinant is denoted by surrounding the matrix entries by vertical bars instead of the brackets or parentheses of the matrix. For instance, the determinant of the matrix

$\begin{bmatrix} a & b & c \\ d & e & f \\ g & h & i \end{bmatrix}$ is written $\begin{vmatrix} a & b & c \\ d & e & f \\ g & h & i \end{vmatrix}$ and has the value $aei + bfg + cdh - ceg - bdi - afh$.

One of the most useful properties of the determinant function is that it provides a simple characterisation of *non-singular* matrices ($n \times n$) (Finkbeiner, 1966). Furthermore, the cofactors of a non-singular matrix can be used to calculate its inverse by a method which is quite easy with matrices where $n \leq 4$.

For Matrix $A = \begin{bmatrix} a_{11} & a_{12} & a_{13} \\ a_{21} & a_{22} & a_{23} \\ a_{31} & a_{32} & a_{33} \end{bmatrix}$

the inverse would be:

$$A^{-1} = \frac{1}{|A|} \begin{bmatrix} \begin{vmatrix} a_{22} & a_{23} \\ a_{32} & a_{33} \end{vmatrix} & \begin{vmatrix} a_{13} & a_{12} \\ a_{33} & a_{32} \end{vmatrix} & \begin{vmatrix} a_{12} & a_{13} \\ a_{22} & a_{23} \end{vmatrix} \\ \begin{vmatrix} a_{23} & a_{21} \\ a_{33} & a_{31} \end{vmatrix} & \begin{vmatrix} a_{11} & a_{13} \\ a_{31} & a_{33} \end{vmatrix} & \begin{vmatrix} a_{13} & a_{11} \\ a_{23} & a_{21} \end{vmatrix} \\ \begin{vmatrix} a_{21} & a_{22} \\ a_{31} & a_{32} \end{vmatrix} & \begin{vmatrix} a_{12} & a_{11} \\ a_{32} & a_{31} \end{vmatrix} & \begin{vmatrix} a_{11} & a_{12} \\ a_{21} & a_{22} \end{vmatrix} \end{bmatrix}$$

The inverse of a matrix M can be written as M^{-1} such that $MM^{-1}=I$ where I is the identity matrix.

Just like the unit vector, an identity matrix is the matrix equivalent of the number 1. Just as any number multiplied by 1 equals the original number, the same goes for the identity matrix.

When you scale a transform, the basis vectors that make up the matrix are also scaled. Therefore, if you have a transformation matrix scaled by 2 in X, then the X basis vector has a length of 2. So now, it becomes easy to extract the scale matrix from our transformation:

$$\begin{matrix} scaleX & 0 & 0 \\ 0 & scaleY & 0 \\ 0 & 0 & scaleZ \end{matrix}$$

Now we know from before that the transform matrix is equal to the scale matrix multiplied by the rotation matrix, or to put it another way:

$$M = SR$$

$$\begin{bmatrix} 0 & 0 & -2 \\ 0 & 1 & 0 \\ 1 & 0 & 0 \end{bmatrix} = \begin{bmatrix} 2 & 0 & 0 \\ 0 & 1 & 0 \\ 0 & 0 & 1 \end{bmatrix} \begin{bmatrix} 0 & 0 & -1 \\ 0 & 1 & 0 \\ 1 & 0 & 0 \end{bmatrix}$$

Using a bit of matrix algebra, we get this:

$$S^{-1}M = R$$

$$\begin{bmatrix} 0.5 & 0 & 0 \\ 0 & 1 & 0 \\ 0 & 0 & 1 \end{bmatrix} \begin{bmatrix} 0 & 0 & -2 \\ 0 & 1 & 0 \\ 1 & 0 & 0 \end{bmatrix} = \begin{bmatrix} 0 & 0 & -1 \\ 0 & 1 & 0 \\ 1 & 0 & 0 \end{bmatrix}$$

Moreover, that is how the scale matrix is decomposed from the rotation matrix.